# PHASE SEPARATION PHENOMENA IN CELLULOSE ACETATE SOLUTIONS IN RELATION TO ASYMMETRIC MEMBRANE FORMATION

## PROEFSCHRIFT

ter verkrijging van de graad van doctor
in de technische wetenschappen
aan de Technische Hogeschool Twente,
op gezag van de rector magnificus,
prof.dr.ir. H.H. van den Kroonenberg,
volgens besluit van het College van Dekanen
in het openbaar te verdedigen op
donderdag 14 januari 1982 te 16.00 uur

door

**FRANCISCUS WILLIBRORDUS ALTENA**

geboren op 23 juli 1953 te Bloemendaal

Dit proefschrift is goedgekeurd door de promotor
prof.dr. C.A. Smolders

Aan Lidy

# VOORWOORD

Het onderzoek naar het vormingsmechanisme van asymmetrische membranen, dat in dit proefschrift beschreven wordt, is uitgevoerd binnen de werkgroep Membraanfiltratie bij de vakgroep Macromoleculaire Chemie en Materiaalkunde, afdeling Chemische Technologie, T.H.Twente.

In deze groep, onder leiding van Kees Smolders, vond ik de voedingsbodem en samenwerking die voor het tot stand komen van onderzoek noodzakelijk zijn. Als natuurkundige eend in een vreemde chemische bijt, heb ik mij altijd gesteund geweten door alle andere medewerkers van de werkgroep.

Stimulerende discussies en samenwerking met aanvankelijk Dick Koenhen en Lute Broens en later met Rik Bokhorst en Hans Wijmans, heb ik zeer gewaardeerd. Derk Bargeman, Hans van de Berg, G. van de Ridder en Piet Bast stonden mij steeds met raad en daad terzijde. De langdurige technische en experimentele ondersteuning door Henk Koetsier heb ik erg op prijs gesteld. M.A. de Jongh heeft ondersteuning gegeven met de raster elektronenmikroskoop, waarvoor ik zeer erkentelijk ben.

Een wezenlijke bijdrage aan het onderzoek werd door studenten geleverd: Jaap Smid tijdens zijn doctoraalonderzoek en Klaas van Gelder tijdens zijn baccalaureaatsopdracht, Marcel Postel, Janneke Bastiaans, Harry Knoef en René Mossel tijdens hun HTS afstudeeropdracht en Rob van Hulst en Jan Schröder tijdens hun HBO-A stage. Aan allen mijn hartelijke dank.

Marcel Mulder dank ik voor het scheppen van het woud van groen op onze gedeelde kamer en voor het kritisch doorlezen van het manuscript.

De figuren in dit proefschrift werden getekend door mijn broer Tom, Henri Heskamp en Richard Arends en de omslagfoto werd vervaardigd door Henk Wassink (Wafilin b.v.), waarvoor dank. Ik ben de heer H. van Baars zeer erkentelijk voor de korrekties van het Engels taalgebruik.
Het typewerk werd met zorg uitgevoerd door Lidy.

Verder dank ik allen die mij hielpen en hier ongenoemd blijven.

**CONTENTS**

## 3. PHASE SEPARATION PHENOMENA IN SOLUTIONS OF CELLULOSE ACETATE. I. DIFFERENTIAL SCANNING CALORIMETRY OF CELLULOSE ACETATE IN MIXTURES OF DIOXANE AND WATER



## 4. PHASE SEPARATION PHENOMENA IN SOLUTIONS OF CELLULOSE ACETATE. II. MELTING POINTS OF THERMOREVERSIBLE GELS OF CELLULOSE ACETATE IN MIXTURES OF DIOXANE AND WATER

## 6. THERMODYNAMIC PROPERTIES OF CELLULOSE ACETATE IN SOLVENT/NONSOLVENT MIXTURES STUDIED BY OSMOMETRY

## 7. DIFFUSION DURING MEMBRANE FORMATION

# 1. INTRODUCTION

## 1.1 MEMBRANE FILTRATION

A membrane (from Latin membrana: skin of body) can be defined as a selective barrier to transport between two phases (see Figure 1). A fluid solution (feed) under pressure is brought into contact with the membrane. The (synthetic) membrane is a thin solid layer of a suitable polymer. The properties of the membrane are such that one or more components of the solution can pass through the membrane whereas others are rejected. An ideal membrane rejects completely the component to be removed from the solution.

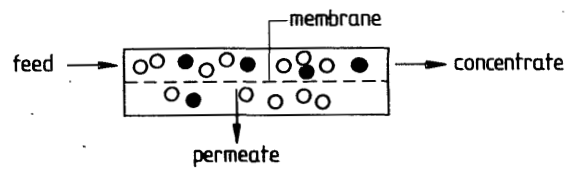


FIG.1. Membrane filtration.

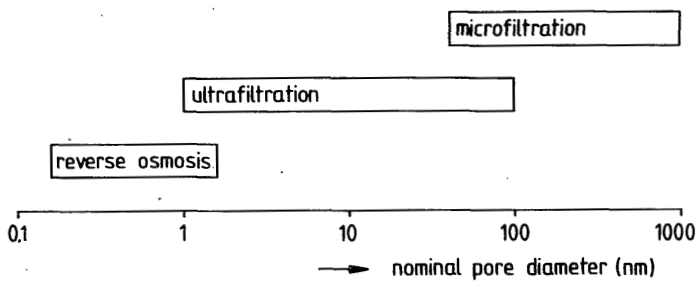


FIG.2 Classification of membrane according to nominal pore diameter.

Several membrane filtration processes can be distinguished. These can be classified on the basis of the size of the "particles" to be separated (Figure 2) or of the applied pressure (Table 1).[1] Microfiltration is applied in filtration of suspensions and sterile filtration of biological solutions. Rather large particles can be removed from the solution. Ultrafiltration is a membrane process for filtration of high molecular weight solutions, e.g. protein solutions. For separation in systems with low molecular weight components reverse osmosis (or hyperfiltration) is used.

| | particle diameter (nm) | pressure (bar) | specific flux ($m^3/m^2$.day.bar) |
|---|---|---|---|
| microfiltration | >50 | 0.2-4 | >1 |
| ultrafiltration | 1-100 | 2-7 | 0.1-0.5 |
| reverse osmosis | 0.2-1 | 7-100 | <0.05 |

Table 1: Classification of membrane filtration according to applied pressure and specific flux.

In Figure 3 (by courtesy of H.Heskamp) the principle of reverse osmosis (or hyperfiltration) is given. In low molecular weight systems the osmotic pressure can be very high, e.g. seawater has an osmotic pressure of about 27 bar.

A larger pressure than the osmotic pressure has to be exerted on the salt solution to obtain a pure water product flux through the membrane.

In fact the membranes mentioned in Figure 1 form a continuum in properties, ranging from coarse filters with well-defined pore diameters to essentially non-porous membranes. The latter perform a separation on the basis of the physico-chemical properties of the permeants and the membrane material rather than on the size of the permeants.

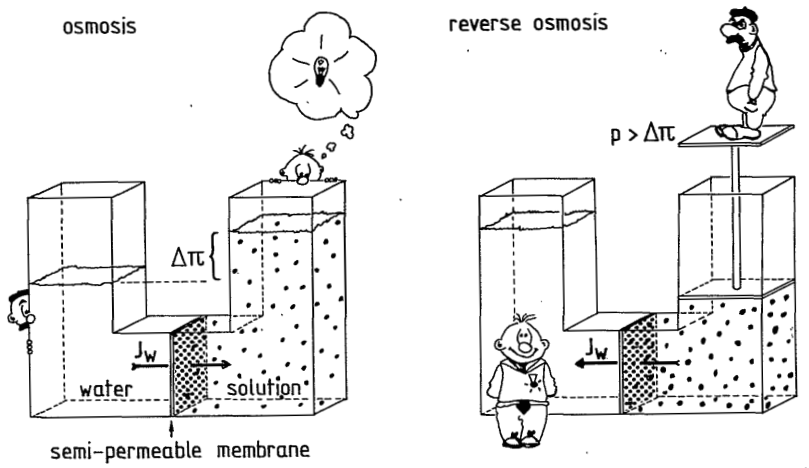


FIG.3. Principle of reverse osmosis.

Membrane filtration has been applied on an increasingly wider scale in recent years to purify water and to recover valuable materials from aqueous solutions.

Some typical examples of industrial applications in The Netherlands are:

- production of process water for greenhouses from brackish ground water, or potable water;
- concentration and separation of product streams in the food industry: raw milk, skimmed milk and whey;
- recovery of indigo dye from waste water;
- concentration and fractionation of starches and proteins;
- treatment of oil/water emulsions.

Advantages of membrane filtration are:

- it is a relatively simple technique, and works at ambient temperature;
- only a small amount of energy is required;
- continuous upscaling is feasible.

In the near future we might expect application of membrane filtration on an industrial scale in the field of gas separation, separation in non-aqueous systems and ethanol-water separation.

The three types of membranes mentioned above are usually produced by a very similar process. A film of a concentrated polymer solution (the casting solution) is cast on a supporting surface and is precipitated by a nonsolvent in a controlled way. With microfiltration membranes precipitation is achieved by imbition of water from a humid atmosphere. This process is rather slow and a rather open porous symmetric structure will result (see Chapter 2, the membrane formation process operative is liquid-liquid phase separation).

In the Loeb-Sourirajan process[2], which is generally used in the preparation of reverse osmosis or ultrafiltration membranes, precipitation occurs through immersion of the film in a nonsolvent bath. Precipitation is quite rapid. In a number of cases, depending on the choice of the polymer/solvent/nonsolvent system, the result is a membrane with a so-called asymmetric structure: a very thin (0.2-0.5 µm) and relatively dense toplayer or "skin", supported by a sponge-like substructure (thickness>100 µm) (Figure 4).

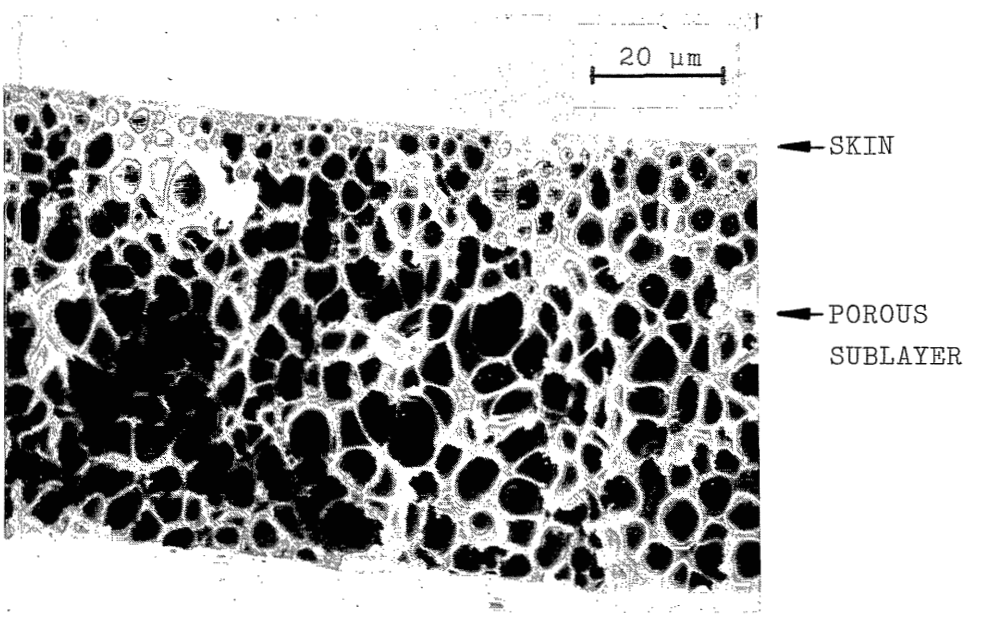


FIG.4. Cross-section of an asymmetric membrane.

The toplayer determines the degree of permselectivity, defined by the degree of salt rejection at a given water

flux for desalting membranes. The porous sublayer does not contribute to the selectivity of the membrane, but it is important because of the mechanical strength necessary to withstand high pressures.

## 1.2 ASYMMETRIC MEMBRANES AND THEIR CHARACTERIZATION

The asymmetry of the membrane can be shown by electron-microscope photographs (as the built-up of two layers) as well as in the transport properties of the membrane. One can show the asymmetry in the transport properties by placing the membrane upside down in reverse osmosis operation. Because of the high internal concentration polarization (the accumulation of salt in the porous sublayer) the rejection of the membrane then becomes very small, and shows a maximum as a function of the volume flux. This is a proof of the existence of asymmetry.[3]

Not only is the dense toplayer responsible for the permselectivity of the membrane, it is also the main barrier for water transport. Up to this moment it is still very difficult to characterize the skin properly in terms of its structure and thickness and the relation of these properties with transport properties. Although the existence of the asymmetry can be shown by electron-microscopy no reliable estimate of the skin thickness can be deduced with this technique.

Many authors have found that the toplayer of ultrafiltration and reverse osmosis membranes consists of a so-called nodular morphology, which is a packing of more or less spherical particles, each of at least 20 nm in diameter. An example is to be found in Chapter 2 (Figure 5). Some authors claim that this structure is the desired morphology for effective membranes.[4] Nodules of cellulose acetate (CA) with a diameter of 20 nm would incorporate about 100 coils with $\bar{M}_n$ = 40.000.

Interpretation of the electron-microscope photographs

can lead to the conclusion that the nodules are hard spheres. This might be a good interpretation for ultrafiltration membranes, generally consisting of more hydrophobic polymeric materials. In this way Bargeman et al.[5] could give estimates of the skin thickness of poly(2,6-dimethyl-1,4-phenylene oxide) membranes from a combined observation of transport behaviour, size of the nodules from scanning electron-microscopy and pore radii obtained from gas adsorption measurements.

For reverse osmosis membranes interpretation in terms of hard spheres seems less likely. The pore radii calculated from electron-microscopy are much too high (2 nm). The nominal pore radii calculated from transport measurements are comparable to the segmental cross section of the polymer molecule (< 1 nm for CA).
Clearly one cannot apply Poiseuille's law in this region as a fixed pore is not very likely.[6]

For reverse osmosis membranes it is probably better to visualize the nodular structure as a layer with a more or less regular distribution of segments with regions of low and high order and without a fixed pore structure. A point which should be stressed here is that no systematic study has appeared in the literature in which variation in the nodular structure (e.g. size of the nodules) has been correlated with concurrently obtained differences in transport properties.

## 1.3 SEPARATION MECHANISM OF REVERSE OSMOSIS MEMBRANES

Before we come to the subject described in this thesis we would like to devote a few words to another very basic problem: the mechanism of selectivity of reverse osmosis (here: salt rejecting) membranes.

The problem of a good characterization of the toplayer (structure and thickness of the skin) is closely related to uncertainties about the precise separation mechanism of re-

verse osmosis membranes. Possible structures in membranes found with electron-microscopy are illustrated in Figure 5. The structures can be observed in the toplayer in the case of asymmetric membranes or in the whole membrane cross-section in the case of symmetric membranes.

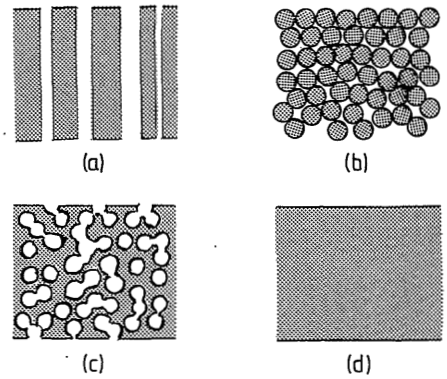


FIG.5. Schematic representation of the cross-section of different membrane structures: (a) cylindrical pore membrane; (b) nodular structure; (c) spongelike structure; (d) nonporous membrane.

Concerning the separation mechanism there are several schools of thought of which we give two examples:

a. Preferential sorption-capillary flow (PSCF) model.
Sourirajan[7] suggested that water is preferentially adsorbed onto the membrane pore walls. In this water layer, with a thickness of several monolayers, hydrated salt-ions are excluded. In the toplayer of the membrane pores may then exist through which salt-ions can move when the pore diameter is more than twice the thickness of the preferentially adsorbed water layer. If only pores are present with a diameter smaller than this value, selective permeation of water and therefore a positive salt rejection will result.
The effective pore radius is assumed to be about 2 nm in diameter. The model has not been proved experimentally, as has been remarked quite correctly by Belfort[8]: "There is

no direct evidence to support PSCF for solute separation".

b. Solution-diffusion model.[9]

In this (black box) description the transport properties are determined by large differences in permeability of water and solute. The permeability is determined by two factors, diffusion and solubility. These two factors are not independent; a high solubility (i.e. swelling) for water favours also the diffusion of dissolved materials. Lonsdale et al.[9] state that the transport properties of the toplayer of a reverse osmosis membrane can be compared with those of a homogeneous film, obtained by evaporation of the solvent, of the same membrane material. The basic transport relations are given below.

The driving force for permeation of water is the net pressure difference, $\Delta p - \Delta\pi$, where $\Delta p$ is the applied pressure difference and $\Delta\pi$ is the osmotic pressure difference. The waterflux can be represented by[9]:

$$J_w = \frac{D_w C_w \bar{v}_w (\Delta p - \Delta\pi)}{RT\ \Delta X} \qquad (1)$$

where $D_w$ is the diffusion coefficient of water and $C_w$ is the solubility of water in the membrane, $\bar{v}_w$ is the partial molar volume of water in the feed solution, and $\Delta X$ is the effective membrane thickness. The water/membrane solution is assumed to obey (ideal) dilute solution laws.

The driving force for salt permeation is the concentration difference $\Delta c_s$ across the membrane:

$$J_s = \frac{D_s K\ \Delta c_s}{\Delta X} \qquad (2)$$

where K is the membrane solution partition coefficient for salt, and $D_s$ is the diffusion coefficient of salt in the membrane matrix. The standard index for the membrane selectivity is the degree of salt rejection, R, defined as:

$$R = \Delta c_s / c_{feed} \qquad (3)$$

where $c_{feed}$ refers to the salt concentration in the feed. Substitution of equations (1) and (2) into equation (3) gives:

$$R = \frac{J_w \Delta c_s}{J_w \Delta c_s + J_s} = \left[ 1 + \frac{D_s K R T}{D_w C_w \bar{v}_w (\Delta p - \Delta \pi)} \right]^{-1} \qquad (4)$$

The salt rejection increases with increasing pressure difference. From equation (4) it follows that the salt rejection approaches unity for $\Delta p \to \infty$. However, at very large pressure the assumption underlying equation (2), i.e. $\bar{v}_s \Delta p << RT\Delta(\ln c_s)$, is no longer fulfilled; $\bar{v}_s$ is the partial molar volume of salt in the solution. For $\Delta p \to \infty$ one obtaines:

$$R_{max} = 1 - \left( \frac{c_{permeate}}{c_{feed}} \right)_{\Delta p \to \infty} = 1 - \frac{K \bar{D}_s \bar{v}_s}{C_w \bar{D}_w \bar{v}_w} \qquad (5)$$

Equation (5) gives the expected maximum degree of salt rejection for a given membrane.

For the determination of the various parameters the model makes use of the supposition that the transport properties of the toplayer of an asymmetric membrane and those of a homogeneous dense film of the same polymer material are very similar. The solution-diffusion model gives a good phenomenological description of the reverse osmosis process. If intrinsic transport properties for the polymer are known (solubilities and diffusion coefficients of water and dissolved salts) one can estimate water- and salt flux from equations (1) and (2) for asymmetric reverse osmosis membranes with a skin of a certain thickness.

What is lacking however is a bridge between the thermodynamic and kinetic coefficients used in the model and the molecular transport process in the membrane. What we would like to have is a precise description of the toplayer, its

structure characteristics in relation to the formation process of the membrane and the ultimate transport properties. A homogeneous model such as the solution-diffusion model does not give a satisfactory understanding of the effect of changing the process variables during membrane formation. For instance, one can drastically change the transport properties, even of homogeneous films, by varying the solvent of the solution from which the membrane is cast[9] (see also Chapter 6). By using additives to the casting solution one can obtain a membrane with a waterflux of more than 0.15 $m^3/m^2$.day.bar (a factor five higher than without the additive) though with a salt rejection of only 70%.[10] These values cannot be understood with the help of equations (1)-(4) unless $D_w$, $C_w$, $D_s$ and K are made empirical quantities, varying for membranes prepared from the same polymer.

Our view is that the toplayer of a reverse osmosis membrane is a moderately swollen fine mazed gel of randomly entangled and crosslinked chains. Locally there are regions with low and regions with higher polymer order, the latter probably of a crystalline nature. The chains between crosslink points are flexible enough so that chain segments take part as osmotically active components in the Brownian motion in the system. Such a membrane has no fixed pore structure and flow takes place in the membrane matrix. The friction for molecular transport depends on the rigidity or flexibility of the chains between crosslinks.

## 1.4 DESIRED PROPERTIES OF REVERSE OSMOSIS MEMBRANE MATERIALS

In the past the search for membrane materials with favourable transport properties has largely been based on empirical research. This situation is still continuing. Unfortunately there are only vague correlations available between physico-chemical properties of the polymer and the reverse osomosis transport properties.

There is only little pertinent material which may be of help to us. Two groups of polymers which are mostly used are cellulose acetates (CA; degree of substitution 2.4-2.8) and polyamides.

a. degree of hydrophylicity:
Both materials are moderately hydrophylic. Cellulose acetate sorbs 10-15% water at saturated water vapour pressure. Polyamides adsorb two to three times as much, see Table 2.

b. differences in salt and water diffusion coefficients:
Values are given in Table 2. The permeability to NaCl ($D_sK$) is at least three orders of magnitude lower than that of water ($D_wC_w$). The salt diffusivity of the polyamides is lower, which may be due to a stiffer backbone of the molecule.

c. waterclustering:
The best membrane materials adsorb water without clustering. Large aqueous domains, which could dissolve salt, must be avoided.[12-14]

The number of papers on the intrinsic transport properties of reverse osmosis membrane materials is very limited. We would like to argue here that a logical step in the development of new reverse osmosis membranes is to determine beforehand whether a polymer has suitable permselective properties. The next step is to prepare an effective asymmetric membrane or to use this polymer as a toplayer for a composite membrane.

In Table 2 also values for the product flux and the degree of rejection are given calculated from equations (1) and (4). We have assumed a skin thickness of 0.1 μm. The degree of rejection is a limiting value, under the prevailing experimental conditions, for a toplayer free of imperfections. Imperfections considerably reduce the rejection value, but not the waterflux. The waterflux through the toplayer is assumed to have the same value as that of a dense

Table 2: Intrinsic transport properties of some important reverse osmosis membrane materials.[1)]

| | $D_w \cdot 10^6$ ($cm^2 s^{-1}$) | $C_w$ (g $cm^{-3}$) | $D_w C_w \cdot 10^7$ (g $cm^{-1} s^{-1}$) | $D_s \cdot 10^{10}$ ($cm^2 s^{-1}$) | K | $D_s K \cdot 10^{11}$ ($cm^2 s^{-1}$) | $J^{a)}$ ($cm h^{-1}$) | R (%) |
|---|---|---|---|---|---|---|---|---|
| cellulose triacetate (CTA)[9)c)] | 1.3 | 0.12 | 1.5 | 2.2 | 0.015 | 0.33 | 1.4 | 99.9 |
| cellulose diacetate (CA)[9)d)] | 1.6 | 0.16 | 2.6 | 9.4 | 0.039 | 3.4 | 2.7 | 99.6 |
| polyamide (CA)[11)e)] | 1.6 | 0.35[b)] | 5.6 | 1.3 | 0.2 | 2.6 | 5.8 | 99.8 |

a) $\Delta p - \Delta \pi$ = 40 bar; 3.5 wt-% NaCl; 25°C; (1 cm/h ≃ 0.25 $m^3/m^2$.day ≃ 5.8 gal/$ft^2$.day)
b) mean value
c) acetyl content 43.2%
d) acetyl content 39.8%
e) nomex® ; aromatic polyamide

film of the same membrane material obtained by evaporation. Only by reducing the thickness of the toplayer a higher product flux at the same rejection value might be expected. Changing the structure of the toplayer in some way might result in a higher flux but inevitably has also a diminishing effect on the degree of rejection.

## 1.5 OBJECT OF THIS THESIS

Although successful developments in the field of composite membranes take place there is still a need for new, preferably more resistant, asymmetric membranes. Two separate developments have been followed in the past. On the one hand one tries to prepare asymmetric membranes with a skin as thin as possible, i.e. optimizing the flux at a given salt rejection value. The second approach is to optimize membrane surface area per unit of volume by preparing membranes which can be packed densely in the equipment used. The latter membranes are usually in the form of hollow fibres, which have a relatively low water flux, 0.1 $m^3/m^2$.day or less, compared to 1 $m^3/m^2$.day for flat membranes (sea water desalination at 60 bar; rejection > 99%).

This thesis tries to give a contribution to the explanation and, if possible, the prediction of the formation of the asymmetric structure of reverse osmosis (and ultrafiltration) membranes. We shall investigate the thermodynamics and the kinetics of the demixing process of membrane materials in solution and the relation between the conditions of the preparation process and the resulting structure of the membrane.

In order to make the thermodynamic description of the membrane forming system not too complex we study primarily ternary systems consisting of polymer/solvent/nonsolvent. The membranes prepared have no optimal flux and rejection properties. For effective membrane preparation usually extra components are added to the casting solution (e.g. formami-

de, inorganic salts or carboxylic acids to solutions of CA in solvents such as acetone or dioxane). In our research approach this means studying the influence of these additives on the thermodynamics and the kinetics of the demixing processes.

In this thesis the experimental work has been concentrated on cellulose acetate, a widely used membrane material. Little is known, however, about the demixing processes and their quantative description.

Improvement of CA membranes is still possible and desirable. We mention three possible improvements which can be the result of fundamental studies, like the present one:

a. wet-dry reversibility.
Normal CA membranes have to be stored wet. Air drying causes irreversible deterioration of the transport properties. This is probably due to collapse of the polymer matrix in an intermediate layer between skin and porous sublayer containing small, irregular pores. One might achieve improvements by trying to enlarge the pore diameter in this intermediate layer. One way to achieve this is to control liquid-liquid phase separation, the process responsible for the formation of the porous sublayer, as will be shown in Chapter 2.

b. pressure retarded osmosis.
A possible way of gaining energy from a gradient in salt concentration is the application of membranes in pressure retarded osmosis. In this process a salt solution is brought into contact with a solution which has a lower salt concentration. Osmosis through the membrane results in an osmotic pressure built-up which is converted to electric power by a turbine. From the study of Lee et al.[15] it appears that CA membranes offer a comparatively good perspective, because of the relatively porous sublayer which keeps the internal concentration polarisation within reasonable limits. To make the process economically feasible considerable progress

should be achieved in the quality of the membranes. The desired properties are:

- sufficient high rejection for salt, about 90%;
- high water flux, of about one order of magnitude higher than membranes which are available today: more than 50 cm/h ($0.17 m^3/m^2.day.atm$ at 70 bar and 3.5 wt% NaCl);
- a very porous sublayer. This is in principle possible with membranes prepared from dioxane-based casting solutions (cp. Chapter 3, section 3.5).

c. improvement of reproducibility in membrane preparation. The approach followed in this thesis might result in a better understanding of factors which influence reproducibility. Such factors are:

- presence of water in the casting solution or in the casting atmosphere;
- evaporation time before coagulation;
- effect of changing coagulation temperature;
- influence of additives to the casting solution;
- explanation of the presence of finger-like cavities (macro voids), which possibly may cause pinhole (= leak) formation when high pressures are applied.

## 1.6 LITERATURE SURVEY

An analysis of different approaches in the literature for the formation of the asymmetry of the membrane shows that phase separation processes and diffusion during coagulation should be studied in detail.

Three views on the formation of the toplayer of asymmetric membrane are:

a. The asymmetry is already present in the cast film of the concentrated polymer solution before precipitation takes place. Further steps in the preparation process, such as coagulation and heat treatment, will only fix the already

existing asymmetry. Representatives of this approach are Panar[4] (nodular morphology) and Tanny.[16]

b. The skin is formed through evaporation from the upper layer of the cast film. The duration and the conditions of the evaporation step determine to a great extent the resulting properties of the membrane. This approach is followed by Sourirajan[17] and Kunst[18] (solution structure-evaporation rate concept), Kesting[19] and Anderson.[20]

c. The coagulation process is responsible for the formation of the asymmetry. Skin formation and formation of the porous sublayer are the result of a complex interplay of phase separation and diffusional processes. Authors who have made important contributions are Frommer[21], Strathmann[22] and Koenhen.[23]

We do not agree that solvent evaporation in general is a necessary step to induce the formation of the asymmetric structure. The following objections can be made:

- One can prepare excellent asymmetric membranes from polymer/solvent/nonsolvent systems in which evaporation of the solvent is negligible, e.g. polysulfone/DMF/water and cellulose acetate/dioxane/water.
- Also systems with a volatile solvent (CA/acetone-formamide/water) cast and coagulated under circumstances that the atmosphere is saturated with the solvent acetone give excellent asymmetric membranes (Sarbolouki[24]).
- Asymmetric hollow fibres with a skin at the interior can be made which have had no contact with air during the preparation (Strathmann[25]).

However, in order to prepare an effective membrane it might be very useful to allow for evaporation in specific systems. Most of the experiments in this thesis have been performed using a CA system in which the solvent is dioxane, which has a negligible evaporation.

The degree of structure formation in the casting solution depends on the thermodynamics of the system at hand: a polymer in a solvent/nonsolvent mixture. It is known that a number of membrane forming polymers (CA,PSn,PPO) crystallize at higher polymer concentration (see e.g. Chapter 2). We might expect that at lower polymer concentrations, in the casting solution , a certain degree of association is present, since we assume that the interaction forces do not differ from those at high polymer concentration.

In our opinion the effect of nonsolvent of this structure formation cannot be ignored, as has been done by Kunst. Structurization can strongly be influenced by adding nonsolvent to polymer solutions. An example is to be found in the work of McKay et al.[26] for the system polyacrylonitrile/DMF/water, an ultrafiltration membrane forming system. The gelpoint in this system is about 5% water at a polymer concentration of 10%. Adding a much smaller amount to a solution of PAN in DMF gives already large changes in the rheological behaviour on the solution, probably caused by some kind of network formation in the solution.

At this point we conclude that basic information on the formation of the asymmetric structure should originate from studies of the processes taking place during the coagulation step of the membrane formation process.

## 1.7 HYPOTHESIS ON THE FORMATION MECHANISM OF ASYMMETRIC MEMBRANES

In Chapter 2 we will deal extensively with the general picture of the formation of asymmetric membranes. Here we only review what is needed to understand the structure of this thesis.

Following Koenhen et al.[23] we hypothesize that two distinctly different demixing processes determine the formation of the asymmetry of the membrane. These are illustrated in Figure 6.

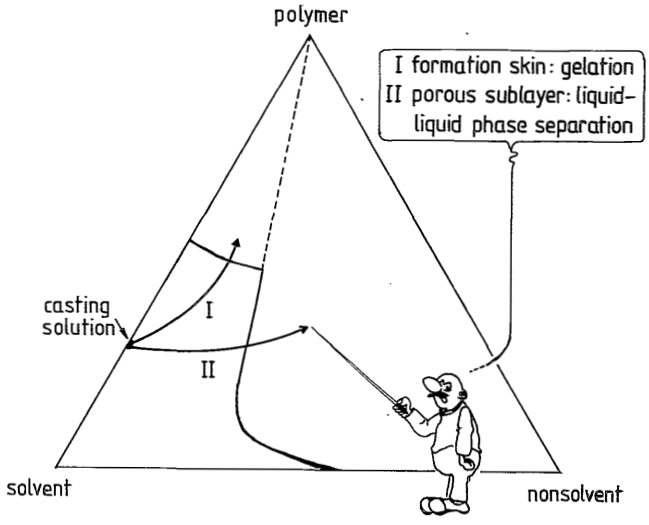


FIG.6. Formation of asymmetric membranes.

I. After immersing the cast film in a nonsolvent bath a large amount of solvent exchanges with a relatively small amount of nonsolvent in the upper layer of the film. The local composition enters the region where gelation takes place, probably through local crystallization, and the skin layer is being formed.

II. Further processes in the polymer film below the skin take place at polymer concentrations much less enhanced than in the skin. By diffusion of nonsolvent from the coagulation bath through the initially formed skin into the sublayer, the composition changes continuously and reaches the critical value needed for liquid-liquid phase separation. Through nucleation and growth of the dilute phase pores are formed in the sublayer. The growth of droplets of the dilute phase is limited by gelation of the surrounding polymer rich phase. Partial coalescence of the droplets gives a structure of connected open pores.

This thesis will give evidence of this hypothesis by trying to establish the occurrence of these separate processes and to give a thermodynamic description for them. The

next step is to gather information about the kinetic aspects. The kinetics of the processes determine which of them is favoured most (cp. Chapter 2). We assume that the main driving force for gelation is the polymer concentration (supersaturation) whereas the driving force for liquid-liquid phase separation is the nonsolvent content of the system (penetration in the miscibility gap at constant polymer concentration).

At this stage we might take a look at the possibility of liquid-liquid phase separation by spinodal decomposition as the leading process for the structure formation in the toplayer instead of the nucleation and growth mechanism or of crystallization (gelation). Through the very fast loss of solvent in the toplayer liquid-liquid phase separation is not very probable: The system would enter the demixing gap at a high polymer concentration. Penetration of large quantities of nonsolvent (in order to enter quickly into the spinodal region) will not be probable. There will be very little time to effect liquid-liquid (l-l) phase separation before a highly viscous gel has been formed. Concentration fluctuations are likely to be damped by specific interactions (like crystallization) and the separation of a polymer-rich and a nonsolvent rich phase is hindered. We conclude that gelation (crystallization) is far more likely. The resulting gel is more or less homogeneous with domains of high and low order, but on a very small geometric scale.

## 1.8 STRUCTURE OF THIS THESIS

For our experimental research we have chosen the system CA/solvent/water. The major part of this thesis describes the behaviour of the system with dioxane as the solvent. This is a membrane forming system which gives an asymmetric reverse osmosis membrane.

Chapter 2 gives a general picture of membrane forma-

tion of an asymmetric membrane considered to be applicable to formation of ultrafiltration and reverse osmosis membranes of various polymeric materials.

Chapters 3 and 4 give experimental evidence of the occurrence of liquid-liquid phase separation and gelation in the system CA/dioxane/water. The techniques used are turbidimetry, Differential Scanning Calorimetry (DSC) and Pulse Induced Critical Scattering (PICS). Also some kinetic information on these processes has been obtained.

Having established the separate processes experimentally one would like to have a thermodynamic description of the demixing phenoma. Starting from the Gibbs free energy function we calculate from the melting point curves the crystal-liquid transition in the Appendix of Chapter 4 and the binodals of the liquid-liquid phase separation in Chapter 5. In the free energy function interaction parameters appear which account for the non-ideality of the system. It is necessary to have reliable values for these parameters. Using osmometry in a ternary system, values for the interaction parameters are obtained in Chapter 6.

Chapter 7 is concerned with some diffusional aspects of membrane formation, the exchange of solvent and nonsolvent, and the independent determination of diffusion coefficients in CA systems with acetone or dioxane as the solvent. Differences in membranes prepared from casting solutions with acetone and dioxane as the solvents are discussed in relation to gelation and liquid-liquid phase separation in these systems.

The description of the formation process and a good characterization of the resultant membrane present interrelated problems. One would like to have some means of investigating the pore structure of a dense gelled toplayer of the membrane. A gas permeation method published in the literature that seemed at first glance an elegant way to determine a mean pore radius of an ultrafiltration or even a reverse osmosis membrane, is criticized in the Appendix and is considered not to be applicable. Finally, the work presented in this thesis is recapitulated in a summary.

## 1.9 REFERENCES


1. V.T.Stannett, W.J.Koros, D.R.Paul, H.K.Lonsdale, and R.W.Baker, Adv.Polym.Sci., 32,69(1979)
2. S.Loeb and S.Sourirajan, Adv.Chem.Ser., 38,117(1962)
3. W.C.M.Henkens and J.A.M.Smit, Desalination, 28,65(1979)
4. M.Panar, H.H.Hoehn and R.R.Hebert, Macromolecules, 6,777(1973)
5. D.Bargeman, Lecture presented at the Third Symposium on Synthetic Membranes in Science and Technology, Tübingen, Sept 7-9 (1981)
6. P.Meares, Phil.Trans.R.Soc.Lond.B., 278,113(1977)
7. S.Sourirajan, Ind.Eng.Chem.Fund., 2,51(1963)
8. G.Belfort, Desalination, 26,325(1978)
9. H.K.Lonsdale, U.Merten, and R.L.Riley, J.Appl.Polym.Sci., 9,1341(1965) and R.L.Riley, H.K.Lonsdale, and C.R.Lyons, J.Appl.Polym.Sci., 15,1267(1971)
10. R.Bokhorst, F.W.Altena, and C.A.Smolders, Lecture presented at the IDEA Congress Bahrain, Nov 30 - Dec 3 1981, to be published in Desalination
11. M.A.Frommer, J.S.Murday, and R.M.Messalem, Europ.Polym.J., 9,367(1973)
12. B.H.Zimm and J.L.Lundberg, J.Phys.Chem., 60,425(1956) and B.H.Zimm, J.Chem.Phys., 21,934(1953)
13. T.A.Orofino, H.B.Hopfenberg, and V.T.Stannett, J.Macromol.Sci.Phys., B3,777(1969)
14. H.Strathmann and U. von Mylius, Proc. 5th Int.Symp. Fresh Water from the Sea, 4,89(1976)
15. K.L.Lee, R.W.Baker, and H.K.Lonsdale, J.Membr.Sci., 8,141(1981)
16. G.B.Tanny, J.Appl.Polym.Sci., 18,2149(1974)
17. S.Sourirajan and B.Kunst in Synthetic Membranes, S.Sourirajan, Ed., National Research Council Canada, Ottawa, 1977, p.129
18. B.Kunst and Z.Vajnaht, J.Appl.Polym.Sci., 21,2505(1974)
19. R.E.Kesting, Synthetic Polymeric Membranes, McGraw-Hill, New York, 1971, Chap. 5

20. J.E.Anderson and R.Ullman, J.Appl.Phys., 44,4303(1973)
21. M.A.Frommer and D.Lancet, in Reverse Osmosis Membrane Research, H.K.Lonsdale and H.E.Podall, Eds., Plenum Press, New York, 1972, p.85
22. H.Strathmann and K.Kock, Desalination, 21,241(1977)
23. D.M.Koenhen, M.H.V.Mulder, and C.A.Smolders, J.Appl. Polym.Sci., 21,199(1977)
24. M.N.Sarbolouki, J.Polym.Sci.Polym.Lett., 11,753(1973)
25. H.Strathmann, K.Kock, P.Amar, and R.W.Baker, Desalination, 16,179(1975)
26. G.R.McKay, J.Ferguson, and N.E.Hudson, J.Non-Newt.Fluid Mech., 4,89(1978); J.Ferguson, C.Doulgeris and G.R.McKay, ibid., 6,333(1980)

## 2. ASYMMETRIC MEMBRANE STRUCTURES AS A RESULT OF PHASE SEPARATION PHENOMENA*)

L.BROENS, F.W.ALTENA, C.A. SMOLDERS
Twente University of Technology, Department of Chemical Technology, Enschede, The Netherlands.
and D.M. KOENHEN**)
Wafilin Membrane Filtration Systems, Hardenberg, The Netherlands.

### 2.0 ABSTRACT

In this Chapter we give a description of the membrane formation mechanism based on theoretical and experimental knowlegde of phase separation phenomena in concentrated polymer solutions. We demonstrate that different types of phase separation are responsible for the built-up of the dense skin layer and the porous supporting layer in asymmetric membranes of several materials: cellulose acetate, polysulfone, polyacrylonitrile and polydimethylphenyleneoxide. The formation of the porous sublayer will be explained in terms of liquid-liquid phase separation, coalescence and gelation. Special attention will be paid to the formation mechanism of the finger-like cavities in the sublayer. A possible explanation will be given on thermodynamic and kinetic grounds, for the formation of nodular structures in the skin of the membranes.

*) This Chapter has been published in Desalination, 32,33(1980

**) Present address: Promac, Zaltbommel, The Netherlands.

## 2.1 INTRODUCTION

Most of the commercially available membranes are produced by the so-called phase inversion process[1], starting from a polymer solution which is precipitated in a nonsolvent coagulation bath. The resultant membranes prepared in this way have an asymmetric structure, i.e. a very thin, more or less dense skin is supported by a porous sublayer of the same material. The technique of producing membranes by the phase inversion method has reached a high degree of reproducibility. This development has been sustained by many systematic studies of the effect of relevant parameters and by the efforts to elucidate the mechanism of membrane formation.[1-12]

The phase inversion process is of a highly complex character, in which phase equilibria, the kinetics of phase separation and changes in morphological structures in non-dilute systems play a role. Phase separation phenomena in dilute polymer solutions have been studied intensively. This is not the case for concentrated polymer solutions, due to experimental difficulties and the complexity of a quantitative theory. We feel that it would be of great value for the improvement of the membrane preparation process if our knowledge of phase separation phenomena in polymer solutions could be extended to the medium and high concentration region.

In this Chapter we present a description of different types of phase separation phenomena in concentrated polymer solutions. Cloud point curves and calorimetric (DSC) measurements will give indications as to which phenomena can occur in different compositional regimes. The question will be discussed which factors, during the formation of the skin, determine the membrane type: ultrafiltration or hyperfiltration membrane. Cavity formation in the porous sublayer will also receive special attention.

## 2.2 THEORETICAL CONSIDERATIONS ON PHASE SEPARATION IN CONCENTRATED POLYMER SOLUTIONS

The following types of phase separation phenomena in polymer solutions can be distinguished:

- liquid-liquid phase separation
- crystallization of the polymer
- gelation

### 2.2.1 Liquid-Liquid (L-L) phase separation

When a homogeneous solution becomes thermodynamically unstable, e.g. by the introduction of a nonsolvent, the original solution can decrease its free enthalpy of mixing by splitting up into two liquid phases of different composition. In Figure 1 a schematic diagram shows such a free enthalpy surface and following the line A/B/C/D/E one sees that all compositions indicated by points between B' and D' of the phase diagram will split up in two phases of composition B' and D'. This process is called liquid-liquid (L-L) phase separation. There are two kinetic ways for L-L separation to occur: either by nucleation and growth of the second phase or by spinodal decomposition.

Entering the miscibility gap e.g. at the side of B' (this is a concentrated polymer solution with a certain, low, amount of nonsolvent) a nucleus of composition D'(this is a tiny drop of high nonsolvent content with almost no polymer in it) will be formed in the polymer solution. This nucleus together with many other nuclei, will grow in size until they touch each other and coalesce or until their growth stops because of gelation of the surrounding polymer solution.

The second kinetic way to L-L phase separation would occur if one could enter the miscibility gap at point B' so quickly that one would pass the dashed line (the spinodal) before nucleation could take place. For those compositions in the spinodal region the solution is unstable with respect to infinitesimally small concentration fluctuations. The so-

lution then separates spontaneously[13,14] into interconnected regions of high and low polymer concentration ending up in intertwined networks of phases with composition B' and D'. As a matter of fact spinodal decomposition is a highly improbable phenomenon in polymer solutions, since nucleation and growth kinetics are too fast for the homogeneous solution to reach the required composition region.

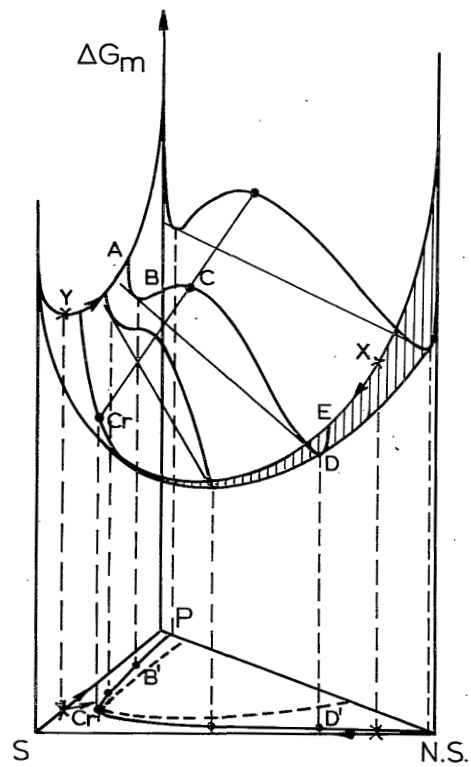


FIG.1. Sketch of $\Delta G_m$ surface and miscibility gap for the system polymer (P), solvent (S), nonsolvent (NS).

Of course it is easy now to draw the connection between L-L phase separation and the genesis of the porous sublayer in membrane formation[11] (see also Section IV). The most interesting question here is, which of the polymer phases will be nucleated when starting with a normal membrane casting solution. In principle two possibilities exist, depending on the composition of the initial polymer solution

with respect to the so-called critical point, point $C_r'$ in Figure 1. For concentrations higher in polymer concentration than $C_r'$ (hence lying on the branch $C_r'B'$) the nuclei will consist of the dilute phase. The reverse is true for initial polymer concentrations below $C_r'$ (branch $C_r'D'$). Now the critical point in polymer solutions is generally located at rather low polymer concentrations ( <10 weight percent in polymer). Since in general membrane forming solutions contain more than 10 weight percent of the polymer one would expect L-L phase separation, with nucleation and growth of the dilute phase to be the rule.

2.2.2 Crystallization and gelation[15]

When the thermodynamic quality of a polymer solution is decreasing, which may occur by loss of solvent, by lowering of the temperature or by the introduction of a nonsolvent, most polymers are able to form ordered agglomerates. In very dilute solutions the polymer molecules can form single crystals of the lamellar type, which are only a few hundred Angströms thick and often many microns in the lateral direction. From solutions of medium concentration more complex morphologies occur i.e. dendrytes or spherulites. These structures may contain appreciable amounts of amorphous polymeric material.

The formation of ordered structures is dependent not only on the thermodynamic quality of the solution but also on the ability of the macromolecules to crystallize in the time available. So if for a certain polymer solution at medium concentration (say about 10 to 20%) crystallization and L-L phase separation are both possible thermodynamically, then the kinetically slower crystallization process would be surpassed by the fast process of L-L phase separation. The sequence of events might well be changed on increasing the polymer concentration. Then, by increase in polymer supersaturation the rate of nucleus formation for crystallization is increased substantially, while that for the L-L phase separation stays essentially the same, being

more dependent on nonsolvent content for its nucleation process.

In Figure 2 we give a schematic representation of the free enthalpy behaviour in the region of high polymer/low nonsolvent content of three component systems, one sees that at higher concentrations the free enthalpy of mixing of the solution can be lowered by the formation of solid, crystalline polymer in equilibrium with a solution of a certain lower polymer content. At a lower (or higher) temperature the $\Delta G_m$ surface will change its shape and the crystalline polymer will be in equilibrium with a solution of lower (or higher) polymer concentration. The so-called melting point curve for a polymer/solvent pair shows this dependence of melting temperature on composition.[11]

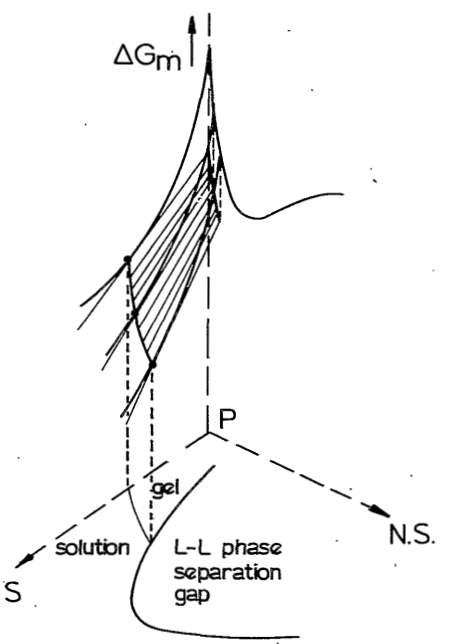


FIG.2. Free enthalpy behaviour at high polymer/low nonsolvent content, explaining the solution-crystal transition.

For crystallization at medium and especially at high concentration, there is a diminished chance to find isolated ordered regions (such as spherulites) which have grown

to microscopically observable size, if time is short. Instead, by the increased rate of nucleation and the limited growth rate, the solution will contain numerous submicroscopical ordered regions, perhaps no larger than the nucleus. These microcrystalline regions act as physical crosslinks in the polymer solution and a thermoreversible polymer gel is formed. Without excluding crosslinks of a different kind to be operative in membrane formation, we think that the type of gelation just described (nonsolvent or temperature induced nucleation at high polymer concentration) could be the leading principle for structure formation in the skin of membranes and for gelation of pore walls in the substructure, after L-L separation.

It is very difficult to demonstrate, using standard diffraction techniques[16], that these gels contain crystalline material. Calorimetric measurements, however, can be used for studying these thermoreversible gels.

## 2.3 EXPERIMENTAL

Materials. The polymers used in this work were Cellulose Acetate(CA), Polyacrylonitrile(PAN), Polysulfone (PSn) and Polydimethylphenyleneoxide (PPO). Membranes were prepared as flat sheets, starting from 10-25 weight % of polymer solutions in solvents which are mentioned in the text. The solutions were cast on a glass-plate and immersed in the coagulation bath.

Cloud point measurements. Cloud points were measured using the method described[17] in Chapter 3.

Optical Microscopy. Following the method first introduced by Epstein[18] the phase separation of polymer solutions was examined with an Olympus E.M. Microscope. A drop of the solution was placed between two microscope slides and by means of a syringe nonsolvent was introduced near the edge.

Scanning Electron Microscopy (SEM). A high resolution

ISI Super III A and Jeol JSM-U3 electron microscope were used. Membrane samples were fractured at liquid nitrogen temperature and sputtered with gold with a Polaron and a Balzer sputter unit. Both cross-sections and upper and lower surfaces of membranes were investigated.

## 2.4 RESULTS AND DISCUSSION

Koenhen et al.[11] were the first to show, in their study of a Polyurethane/DMF/water membrane forming system, that there were two distinctly different types of phase separation operative at different compositions:

- L-L phase separation at low and medium polymer concentration and variable nonsolvent content and
- gelation at high polymer concentration and low nonsolvent content.

Recent work in our group[19] learns that also in the system cellulose acetate/dioxane/water both types of phase separation can be demonstrated. Curve I in Figure 3 shows the cloud points measured at 20°C and curve II shows the solution/gel transition as measured by Differential Scanning Calorimetry (DSC). Curve I represents a true L-L separation phenomenon: up to polymer concentrations of 20% the cloud points are independent of the rate of temperature change. Cloudiness disappears upon direct reheating at the same temperature at which it appeared on cooling. The phase separated solution can not be separated into two liquid layers: the layer concentrated in polymer is gel-like. With DSC measurements no heat effect could be observed during cooling; only after aging at temperatures below the cloud points for some time an endothermic heat effect could be detected upon reheating. This latter effect is ascribed to gelation of the concentrated phase after L-L separation has taken place. Curve II is derived from the presence of DSC melting peaks on reheating samples with high polymer concentration (40-55% CA) and a rather low content of water. These

melting peaks only occur after longer aging times at ambient temperature.

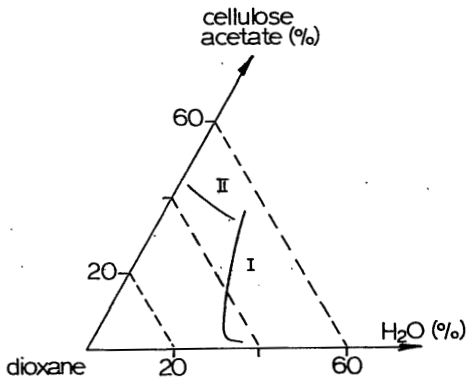


FIG.3. Ternary diagram CA/dioxane/$H_2O$. Curve I:cloud point curve at 20°C; Curve II: solution-gel transition.

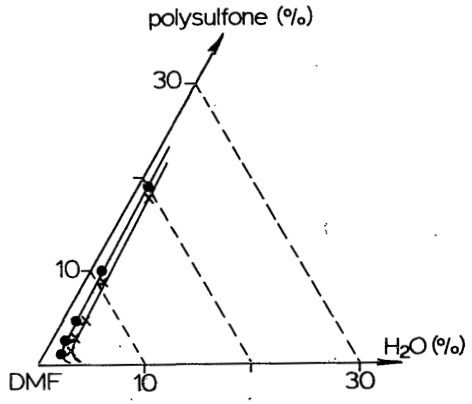


FIG.4. Ternary diagram of PSn/DMF/$H_2O$. Cloud point curves at 20°C (o) and 40°C (x).

Cooling to lower temperatures (e.g.-10°C) or increasing the water content makes the endothermic peaks show up on immediate reheating.

Figure 4 gives some further evidence of the phase separation types found in membrane forming system. In this figure the cloud point curves for Polysulfone/DMF/water are given at 20°C and 40°C. One sees that only a few percent of water in the solution is sufficient to induce L-L separation here. We have no direct measurements on gelation yet, but we observe that a PSn solution in DMF, as used for membrane preparation, when stored at room temperature for some hours under exclusion of water, gives a precipitate of PSn. Therefore the usually employed PSn solutions are on the verge of crystallization (or gelation). From other work[20] it is also known that PSn may crystallize in certain solvents. The same observation of precipitate formation on storage is found for solutions of poly (2,6-dimethyl-1,4-phenylene oxi-

de) (PPO) in mixtures of trichloroethylene and octanol, from which UF membranes can be prepared.[12] For this system we have done some DSC measurements which clearly show heat effects (crystallization and melting peaks) on cooling and reheating samples, even for the highest scanning rates. The results compare well to those reported for PPO/toluene.[35]

2.4.1 Phase separation and asymmetric membranes

We will investigate what can be said about the processes during membrane formation which lead to asymmetric membrane structures. In this discussion we will treat the formation of the skin and of the porous sublayer separately.

2.4.2 Skin formation

The ultimately determining factor for the skin formation is the local polymer concentration in the toplayer solution film. This is best illustrated by two completely different techniques of precipitation of membranes from cast films, coined by Strathmann[9] as

1. precipitation from the vapour phase
2. immersion precipitation

In the first method, developed long ago by Zsigmondy and Bachmann[21], the precipitation is accomplished at an effectively unchanged polymer concentration in the toplayer since the vapour phase is saturated with the solvent. Then, by diffusion of nonsolvent into the film, the only type of phase separation which can take place is L-L separation, giving an asymmetric membrane without a skin (see Figure 1d in Reference 9).

In the immersion technique the solvent depletion from the toplayer of the solution film is extremely fast (diffusion aided by stirring in the bath). An increase in polymer concentration in the toplayer is the result. This increase improves the conditions for the second type of phase separation to occur: gelation. Gelation will be favoured by the penetration of nonsolvent. The higher the polymer concentration has become before nucleation in the skin sets in, the

more numerous and the smaller will be the structural units, viz. the nuclei, because of higher supersaturation.

It will be clear now which factors favour the formation of a more finely structured, dense skin and therefore of a hyperfiltration membrane:

- a higher initial polymer concentration of the solution will favour the conditions for a larger supersaturation in the toplayer before nucleation sets in.

- a lower tendency of the nonsolvent to penetrate the toplayer will delay nucleation untill sufficient solvent depletion to high polymer concentration has been obtained. A proper choice of nonsolvent type and also certain additives to the coagulation bath (salt, glycerin, etc.) will serve this purpose.

- lowering the temperature of the coagulation bath will increase the supersaturation, while at the same time it will decrease the growth kinetics of formed nuclei; a denser skin will result.

A contrary effect, favouring the formation of UF membranes, can be found, apart from choosing a lower polymer concentration etc., in the addition of nonsolvent to the polymer casting solution. This effect can be explained as follows: one frequently observes that the precipitation concentration for L-L separation in a HF membrane forming system is relatively high, about 30% of nonsolvent at low polymer concentration being allowed before precipitation sets in, whereas the precipitation concentration for UF membrane forming systems is often very low, say 5% of nonsolvent content or lower; compare for instance CA/dioxane/water in Figure 3 with PSn/DMF/water in Figure 4 and see also reference 3 and 10. One can then calculate, using well established solutions for this diffusion problem[22] that for the increase in concentration to reach the precipitation value at a certain distance (say 1μ) below the solution surface a difference in time of a factor 5-10 is obtained for the two situations, with the HF system taking the longer time. This gives the HF system more time to lose solvent from the top-

layer. Addition of nonsolvent to the casting solution will diminish this effect, increasing the precipitation rate, and favouring the formation of a UF type skin.

2.4.3 Nodular structure of the skin

There is an increasing amount of experimental evidence that the skin of asymmetric membranes consists of spherical aggregates, called nodules, which in a densely packed or perhaps partially deformed arrangement form the selective skin of UF and HF membranes. Most of the data stem from transmission electron microscopy or from scanning electron microscopy[12,23-27] but also filtration (water flux) and gas adsorption data are used. [28,29] The size of the structural units reported are from 20 to 200 nm in diameter. Figure 5 obtained with SEM shows for the surface of a PPO membrane (UF) a typical example from our own work. In principle such a nodular structure could be in line with the picture given above for the built-up of ordered structural units (nuclei) in the skin layer.

2.4.4 The Porous Sublayer

The formation of the skin will increase the barrier for the diffusion of solvent out of and nonsolvent into the sublayer of the polymer solution. This means that in the film below the skin, phase separation will take place at a much lower polymer concentration as compared to that in the skin. For concentrations of the original casting composition (or a little higher by solvent loss) this phase separation will be of the L-L separation type as described above in Section 2.2.1 and as can be followed by optical microscopy during coagulation.

Two types of structures for the sublayer with clearly different morphologies can be distinguished:

1. sponge structured sublayer
2. conical voids or "fingerlike cavities" in the sublayer

2.4.5 Sponge structure

It will be clear from Section 2.2.1 that the pores in the sponge structure are the grown-out nuclei of the dilute phase in the matrix of the polymer solution, which has solidified after L-L separation by gelation at a certain stage. If the concentration of the polymer at the locus where L-L phase separation sets in does not increase too much over the depth of the solution layer, the nucleation density will not vary very much over the film thickness and a uniform pore structure will be the result. In order to obtain an "open pore" sponge structure, a certain amount of coalescence of the drops should occur before the walls of concentrated polymer solution between the pores solidify by gelation. This can be monitored by choosing the proper initial polymer concentration (not too high). A good example of coalescence of small pores with large voids is shown in Figure 6 for a Polysulfone membrane.

2.4.6 Conical voids (fingerlike cavities)

A very important feature in immersion-coagulated membranes (in UF membranes as well as in HF) is the presence of the large voids with a length of several microns to sometimes the total thickness of the membrane. These cavities were first observed in wet-spun fibres.[30-34] The absence of the voids in dry-spun fibres[33] and in dry-Ro membranes[25] indicates that their formation only occurs in the case of immersion precipitation.

At first it was assumed that the formation was associated with volume changes in the precipitated polymer phase.[31] Later Graig[30] proposed the mechanism of penetration of nonsolvent through defects (cracks) on the surface of the spinning filament. The same mechanism in the case of immersion-coagulated membranes was proposed by Strathmann.[8] In a systematic study of the kinetics of void formation in PAN fibre spinning, Gröbe[32] came to the conclusion that diffusion of both solvent and nonsolvent to certain areas was the basis for void formation. In our opinion the available

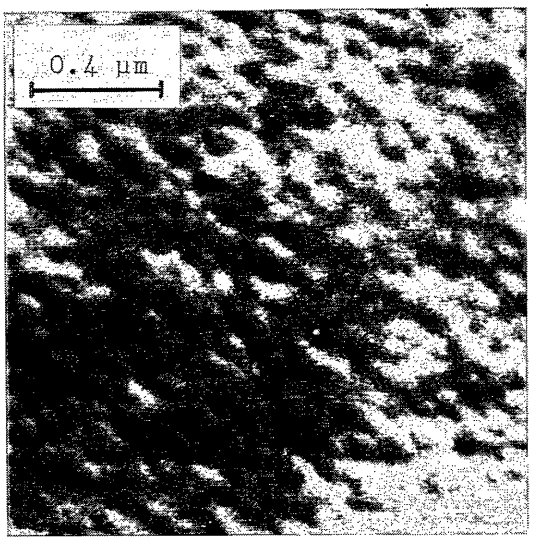


FIG.5. SEM-photograph of the nodular surface of a PPO/UF membrane (slight tilt of the surface under microscope)

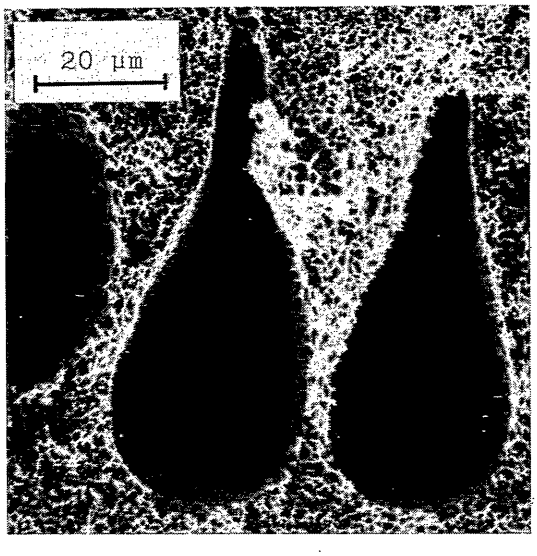


FIG.6. Cross section of a PSn membrane, showing voids with open walls.

experimental data are consistent with this mechanism. Some typical facts remain interesting for a further consideration:

- through optical microscopy one observes that the voids move inward faster than the, diffusion controlled, coagulation front.

- the boundary of the voids does not solidify by gelation during its growth, since coalescence with small pores remains possible (Figure 6).

- often the growth of the voids slows down and the coagulation front for L-L separation passes beyond the lower end of the cavity.

The main driving force for the growth of the void is the decrease in free enthalpy ($\Delta G_m$) upon mixing the solvent and nonsolvent in the void. This $\Delta G_m$ decrease should be so large that it can compensate for a possible increase in $\Delta G_m$ when solvent is depleted from the polymer solution surrounding the void. The situation is best illustrated by following the arrows in Figure 1 at point X (large decrease in $\Delta G_m$ if nonsolvent mixes with solvent) and at point Y (increase in $\Delta G_m$ when a polymer solutions becomes more concentrated). The general mechanism can be described as follows:

- when the skin is formed, nonsolvent penetrates into the underlying polymer solution faster at certain spots in the skin (e.g. a thinner part of the skin or a local loose arrangement of the structural units, giving a more favourable pathway for diffusion); this heterogeneous type of nucleus is formed only in systems with a large driving force for solvent/nonsolvent mixing.

- solvent diffuses from the surrounding polymer solution to these statistically spread loci and a gradient in concentration ranging from practically pure solvent (near the interface of this area with the polymer solution) to nonsolvent (near the skin surface) is set up; there is fluid interface between the polymer solution and the void.

- because mass transfer in the void is faster than through the polymer solution phase, the void may grow faster

initially than the moving coagulation front proceeds; at a certain point however, the driving force for solvent transport may vanish because of a decrease in the gradient. It is emphasized that the contents of the void during growth is not in equilibrium with the surrounding polymer solution, in the sense of L-L separated binodal phases. It is clear that after the void stops growing, normal L-L type phase separation takes place in the polymer solution surrounding the void and in front of it. A proof that the void/solution interface stays fluid during cavity growth is given by all those systems where we find in the membranes cavities with open walls (see Figure 6).

Our observations are in conceptual agreement with the earlier mechanism proposed by Gröbe[32] and with results on the effect of important monitoring variables to prevent void formation (see Frommer[3,4] and Strathmann[5-9] such as:

- lowering the tendency of nonsolvent to penetrate into the casting solution (T, salt addition to nonsolvent, solvent/nonsolvent pair with smaller affinity).
- increasing the skin thickness or the density of the skin (see above in this discussion).

In the Appendix (2.6) the above given formation mechanism of a conical or macro void is illustrated using available data of the system CA/dioxane/water.

## 2.5 REFERENCES


1. a. S.Sourirajan, Reverse Osmosis, Academic Press, New York, 1970
   b. R.E.Kesting, Synthetic Polymeric Membranes, McGraw-Hill, New York, 1971, Chap. 5
   c. H.K.Lonsdale and H.E.Podall, Eds., Reverse Osmosis Membrane Research, Plenum Press, New York, 1972
2. M.A.Frommer, I.Feiner, O.Kedem, R.Bloch, Desalination, 7,393(1970)

3. M.A.Frommer, D.Lancet, in Reverse Osmosis Membrane Research, H.K.Lonsdale and H.E.Podall, Edds., Plenum Press, New York, 1972, p.85
4. M.A.Frommer, R.M.Messalem, Ind.Eng.Chem.Prod.Res.Dev., 12,328(1973)
5. H.Strathmann, P.Scheible, Kolloid-Z.u.Z. Polymere, 246, 669(1971)
6. H.Strathmann, P.Scheible, R.W.Baker, J.Appl.Polym.Sci., 15,811(1971)
7. H.D.Saier, H.Strathmann, U.von Mylius, Angew.Makromol. Chem., 40,391(1974)
8. H.Strathmann, K.Koch, P.Amar, and R.W.Baker, Desalination, 16,179(1975)
9. H.Strathmann and K.Koch, Desalination, 21,241(1977)
10. M.Guillotin, C.Lemoyne, C.Noël, and L.Monnerie, Desalination, 21,165(1977)
11. D.M.Koenhen, M.H.V.Mulder, and C.A.Smolders, J.Appl. Polym.Sci., 21,199(1977)
12. L.Broens, D.M.Koenhen, and C.A.Smolders, Desalination, 22,205(1977)
13. J.W.Cahn, J.Chem.Phys., 42,93(1965)
14. C.A.Smolders, J.J. van Aartsen, and A.Steenbergen, Kolloid-Z.u.Z.Polym., 243,14(1971)
15. B.Wunderlich, Macromolecular Physics, Academic Press, New York, vol I, 1973, and vol II, 1976
16. J.H.Wendorff, E.W.Fischer, Kolloid-Z.u.Z.Polymere, 251, 884(1973)
17. P.T. van Emmerik and C.A.Smolders, Europ.Pol.J., 9,293 (1973)
18. M.E.Epstein, A.J.Rosenthal, Text.Res.J., 36,813(1966)
19. F.W.Altena and C.A.Smolders, J.Pol.Sci., Polym.Symp., 69,1(1981) (Chapter 3 of this thesis)
20. D.A.Blackadder, H.Ghavamikia, and A.H.Windle, Polymer, 20,781(1979)
21. R.Zsigmondy and W.Bachmann, Z.Anorg.Allg.Chem., 103,119 (1918)

22. J.Crank, The Mathematics of Diffusion, Clarendon Press, Oxford, 1975
23. R.D.Schulz and S.K.Asunmaa, Rec.Prog.Surface Sci., 3, 291(1970)
24. M.Panar, H.H.Hoehn, and R.R.Hebert, Macromolecules 6, 777(1973)
25. R.Kesting, J.Appl.Polym.Sci., 17,1771(1973)
26. C.W.Alegranti, D.G.Pye, H.H.Hoehn, and M.Panar, J.Appl. Polym.Sci., 19,1478(1975)
27. R.D.Sanderson and H.S.Pienaar, Desalination, 25,281(1978)
28. L.Broens, D.Bargeman, and C.A.Smolders, Proc. 6th Intern. Symp. Fresh Water from the Sea, 3,165(1978)
29. J. Le Moigne, and Ph.Gramain, Europ.Polym.J., 14,443, (1978)
30. J.P.Graig, J.P.Knudsen, and V.F.Holland, Textile Res.J., 32,435(1962)
31. V.Gröbe, and K.Meyer, Faserforsch.Textiltechn., 10,214 (1959)
32. V.Gröbe, G.Mann, and G.Duve, Faserforsch.Textiltechn., 17,142(1966)
33. A.Ziabicki, Fundamentals of fibre formation, John Wiley, London, 1976
34. J.P.Knudsen, Textile Res.J., 33,13(1963)
35. D.M.Koenhen, and C.A.Smolders, J.Polym.Sci.A-2, 15,167, (1977)

## 2.6 APPENDIX

In this Chapter we have stated that a large driving force for solvent/nonsolvent mixing is favourable for the growth of finger-like cavities.In this Appendix we modify this statement to the extent that also a solvent/nonsolvent combination with a rather low tendency of mixing, as expressed by the height of the minimum in the $\Delta G_m$-curve, for instance dioxane/water, gives macro voids in the resultant

membranes (for a photograph, see Chapter 3, Figure 7).

In Figure 1 we give $\Delta G_m$-curves for the dioxane (2)/water (1) combination and for the mixing of CA (3) and dioxane (2). These curves are calculated with the help of Chapters 4 and 5.

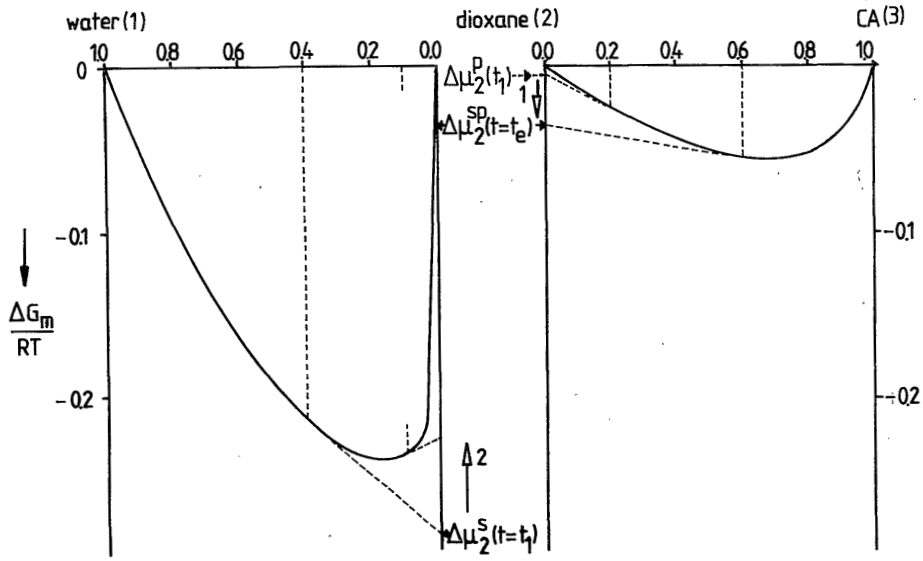


FIG.1. Illustration of the driving force for the growth of a void using available data for the system CA/dioxane/water.

At a certain spot under the skin an increased amount of nonsolvent is present at time $t=t_1$. Let us assume a volume fraction of water of 0.4. The chemical potential of the dioxane in this polymer free solvent/nonsolvent mixture is $\Delta\mu_2{}^s(t=t_1)$. The chemical potential of dioxane in the surrounding polymer solution is $\Delta\mu_2{}^p(t=t_1)$.*) Dioxane in the polymer solution can reduce its chemical potential to a large extent by diffusing into the region with the nonsolvent (direction of arrow 1 in Figure 1). The flow of dioxane causes the composition of the void to increase in solvent content; the chemical potential of dioxane increases(direc-

*) We assume that the nonsolvent has not yet diffused into the solution surrounding the nascent voids.

tion of arrow 2 in Figure 1). At some time, say $t=t_e$, the process stops. The chemical potential of dioxane in the solvent/nonsolvent mixture in the void and in the surrounding polymer solution (with e.g. $\phi_3=0.6$) are equal ($\Delta\mu_2^{s,p}(t=t_e)$). From the figure it appears that the composition of the liquid in the void is practically pure solvent.

The dioxane/water system is characterized by a rather small $\Delta G_m$ minimum compared with other solvent/water systems such as DMSO/water and DMF/water. In systems with a larger minimum value the driving force for solvent transport from the polymer solution into the void is expected to be larger.

Note:

Smolders suggested recently[1] that another driving force for the growth of a macro void is the decrease in $\Delta G_m$ of the system when the polymer molecules change to a less expanded conformation upon increasing the nonsolvent content. In a kind of syneresis process solvent is expelled by the polymer solution. Measurements of the intrinsic viscosity[2], however, indicate that for the system CA/dioxane/water the expansion factor first increases with increase of nonsolvent content. At a water percentage near the percentage required for phase separation the expansion factor for CA has the value of the pure solvent. The proposed conformational change needs to be experimentally verified in concentrated solution where interpenetration of polymer coils takes place to a large extent.

References

1. C.A.Smolders, in Ultrafiltration Membranes and Applications, Ed., A.R.Cooper, Plenum Press, New York, 1980, p.161
2. Chapter 6 of this thesis

# 3. PHASE SEPARATION PHENOMENA IN SOLUTIONS OF CELLULOSE ACETATE. I. DIFFERENTIAL SCANNING CALORIMETRY OF CELLULOSE ACETATE IN MIXTURES OF DIOXANE AND WATER.*)

F.W.ALTENA and C.A.SMOLDERS
Department of Chemical Technology, Twente University of Technology, Enschede, The Netherlands.

## 3.0 SYNOPSIS

The nature and kinetics of phase separation of solutions of cellulose acetate (degree of substitution, 2.5) in mixtures of dioxane and water are studied by differential scanning calorimetry. The thermograms on heating show small endothermic effects, detectable only after prolonged aging below the phase separation temperature.

Experiments in two regions of the ternary diagram are of interest for the description of the formation mechanism of asymmetric membranes, viz.: 1) at high polymer concentrations and low concentrations of nonsolvent (gelation); 2) at lower polymer concentrations and high concentrations of nonsolvent (liquid-liquid phase separation followed by gelation).

Endothermic effects after prolonged aging are found at high polymer concentrations (>40%). These results demonstrate that gelation is very slow in these systems. At lower polymer concentrations and high nonsolvent concentrations (up to 40%) a more rapid type of phase separation can be visually observed on cooling. The temperature where turbi-

*) Published in Journal of Polymer Science: Polymer Symposium, 69,1(1981)

dity sets in (cloud point) is independent of the rate of cooling. In DSC experiments no exothermic effect is present. The endothermic peak, which is situated below the cloud point, is probably a result of melting of the gelled concentrated phase.

## 3.1 INTRODUCTION

Several authors have tried to explain the formation of an asymmetric membrane. Most of the mechanisms are based on thermodynamic considerations of a polymer in a mixed solvent.[1-7] Detailed data, however, are missing on thermodynamics and kinetics of phase separation in concentrated polymer, solutions of e.g. cellulose acetate (CA) from which membranes are prepared.

In this Chapter we study a number of aspects of phase separation in solutions of CA to which nonsolvent has been added. We will keep circumstances during phase separation constant; hence, exchange processes with a coagulation bath, as in actual membrane formation, are not considered. Differential scanning calorimetry (DSC), as a technique, offers excellent possibilities for the study of phase separation phenomena.[8,9] With this technique we try to gain insight into the demixing process of CA (degree of substitution, 2.5) in mixtures of dioxane and water. The choice of this system is based on the frequent use of dioxane as a solvent in casting solutions.[10-14]

## 3.2 EXPERIMENTAL

### 3.2.1 Materials

The CA is from Eastman, catalogue number 4644, with acetyl content of 39.8%. Using gel permeation chromatography (GPC) its molecular weight has been characterized as: $\bar{M}_n$ = 24.000, $\bar{M}_w$ = 55.000, $\bar{M}_z$ = 118.000. Dioxane is 1,4-dioxane

of Baker Analyzed Reagent grade. The water used is distilled twice.

### 3.2.2 Cloud Point Measurements

Cloud points were determined in well-homogenized solutions. These mixtures were prepared in accordance with the method of Van Emmerik and Smolders.[8] The desired amounts were weighed in small Pyrex glass tubes. These were degassed and sealed under vacuum at liquid nitrogen temperature. The tubes were heated at 90°C for at least 2 days to obtain homogeneous solutions.

Phase separation (cloud) points were determined by heating or cooling the thermostat bath at a rate of 1°C/h, at 1°C/10 min or at 1°C/3 min.

### 3.2.3 Differential Scanning Calorimetry

The solutions were made by weighing the appropriate amounts in sample pans of aluminium or stainless steel. These pans were hermetically sealed. Only sample pans that showed no weight loss after 2 days at 100°C were used. The use of stainless steel pans is favourable because of the larger quantities that this type of pan can contain. The DSC apparatus used was Perkin-Elmer model DSC 2, equipped with provisions for working below room temperature and with an automatic baseline corrector.

## 3.3 RESULTS

### 3.3.1 Cloud Points

A series of homogeneous CA solutions (weight fractions 0-25%) was chosen, with constant but different ratios of solvent (dioxane) and nonsolvent (water). When this solution is cooled, a visual perceptible cloudiness appears at a certain temperature. The cloud point curves obtained in this manner are given in Figure 1.

The appearance of the cloudiness is not dependent on the ra-

te of cooling within the accuracy of the observations (about one degree C). When we heat the phase separated solutions from a temperature not far below the cloid point, say 5°C below it, the cloudiness disappears at the temperature where it appeared during the cooling stage. When a demixed solution is centrifuged we obtain a clear dilute phase on top of a cloudy gel-like concentrated phase. We note that this is also the result of aging of a solution at a temperature far below the cloud point temperature (syneresis).

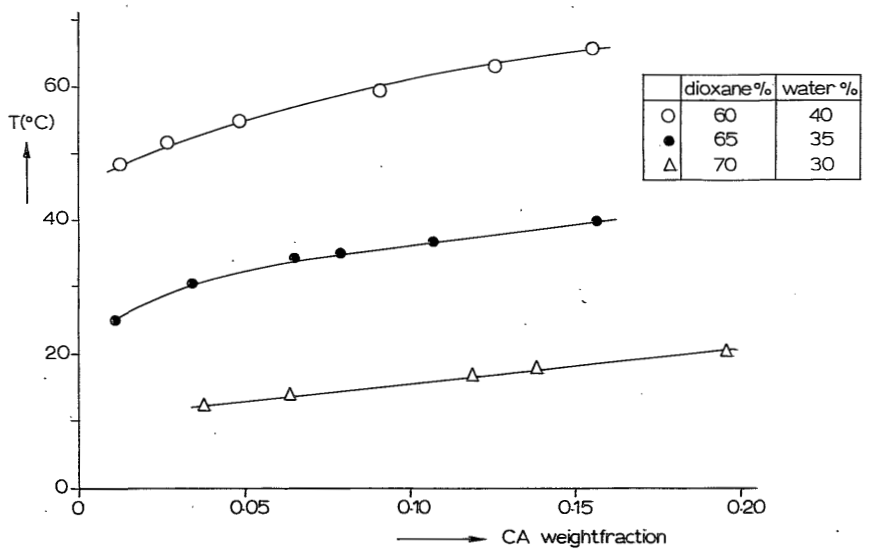


FIG.1. Cloud point curves in the system CA/dioxane/water

In Figure 2 cloud points have been plotted in a ternary diagram for three temperatures, viz., 20,30 and 60°C. We observe a dramatic influence of the watercontent on the cloud point temperature. The results above given indicate a process of liquid-liquid phase separation for the region of low polymer concentrations (up to 25%) and fairly high non-solvent concentrations (up to 40% in the solvent mixture).

In the Appendix additional information on cloud points and spinodal points is given.

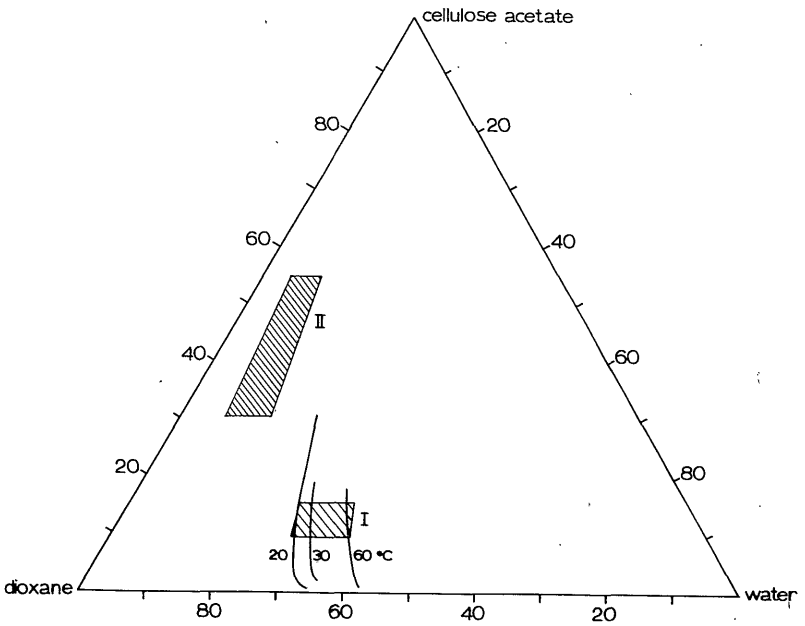


FIG.2. Ternary diagram for CA/dioxane/water at 20,30 and 60°C. In regions I and II special DSC experiments have been carried out.

3.3.2 Differential Scanning Calorimetry for solutions within the two-phase region

The area to the right of the curves in Figure 2 indicated by the region I, is the area with visual phase separation, i.e., we observe a cloudiness upon cooling solutions having compositions in this region of the diagram. We have done a few DSC experiments for solutions containing 9-15% polymer in a mixture of 60% dioxane and 40% water.

Upon cooling these solutions no exothermic heat effect could be observed. The temperature range is from 100 to 10°C. The cooling rate was varied between 0.3 and 40°C/min.

Endothermic effects upon reheating have been found only after prolonged aging at temperatures below the phase separation temperature. Some results are given in Figure 3. The samples were aged at 25°C and initially cooled to 10°C. Then the samples were heated at a rate of 10°C/min and the heat effect was recorded.

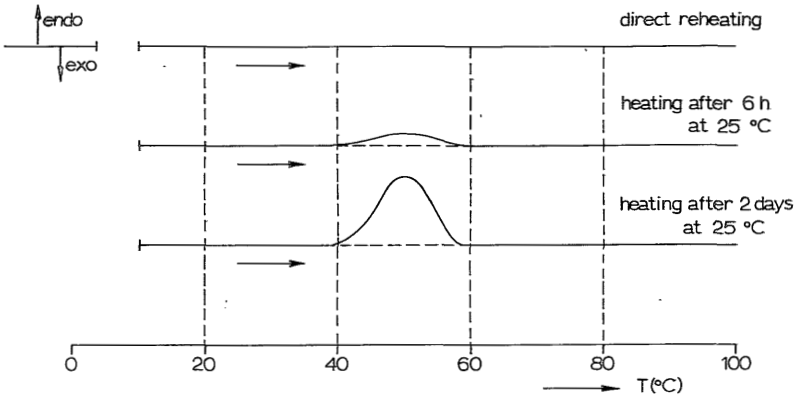


FIG.3. Endothermic heat effect for a 10% CA solution in a mixture of 60% dioxane and 40% water. Heating after aging at 25°C. The cloud point for this system is 61°C (see Figure 1)

3.3.3 Differential Scanning Calorimetry for solutions outside the two phase area.

A number of experiments have been performed in the area of high polymer concentrations and low water content; this is region II in Figure 2. Visually these solutions, which are 40-50% in polymer concentration, are clear at higher temperatures, say above 90°C, at water concentrations of up to 20%.

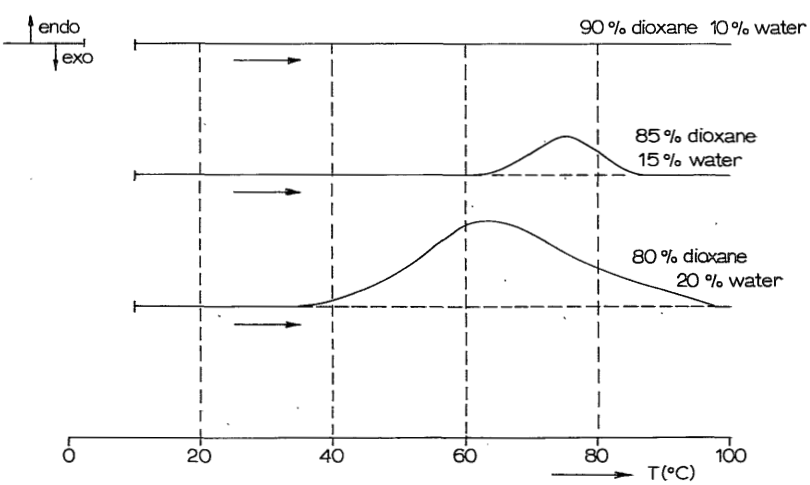


FIG.4. DSC traces for 40% CA in mixtures of different ratios dioxane/water. Aging for two days at room temperature.

Below 30% polymer concentration we could not detect endothermic effects in DSC heating curves in the range from -10 to 100°C, after 2 days of aging time at 25°C. At 40% polymer concentration an endothermic effect upon heating could be determined for mixtures containing 15% and 20% water, respectively, in the solvent mixture. No endothermic effects appears in the thermogram at the ratio of 90% dioxane/10% water after 2 days of aging at 25°C (Fig.4). The heating rate is 10°C/min from 10 to 100°C. In these experiments an exothermic effect could not be found during cooling with variable cooling rates (0.31-40°C/min).

The effect of aging at these high polymer concentrations is demonstrated in Figure 5. The sample with a solvent ratio of 80% dioxane and 20% water is cooled at a rate of 40°C/min from 100 to 10°C. After aging for different periods of time an endothermic effect is observed upon heating (heating rate 10°C/min). The appearance of this endothermic effect can be strongly influenced by the lowest cooling temperature. Cooling to -10°C and immediately reheating gives an endothermic heat effect comparable with 1 h aging at +10°C.

At still higher polymer concentrations (55%) endothermic effects on heating have also been found at 10% water content. Still no exothermic effect appears upon cooling. As in the case of Figure 5 the endothermic effect moves gradually to higher temperatures as a function of the aging time. No endothermic effect is found on immediate reheating after cooling from 100 to 10°C. Increasing the water content in the solvent mixture to 15% gives an endothermic effect on immediate reheating. There is also an exothermic effect on cooling, as opposed to all other experiments (Fig.6). Maybe some higher melting nuclei are still present at the highest temperature used for obtaining a homogeneous solution, 100°C.

In general we can state that the presence of exothermic and endothermic heat effects strongly depends on the water content and the polymer concentration of the sample. Furthermore, the rate of temperature change and the tempera-

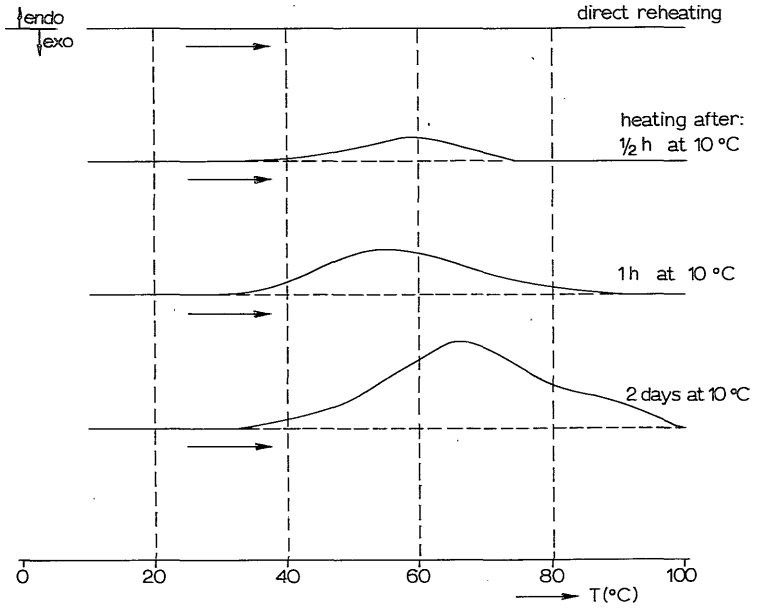


FIG.5. Endothermic effects for 40% CA in mixture 80% dioxane/20% water after aging at 10°C for different time periods.

ture to which the sample is cooled determine to a great extent the kinetics of the process under study. These kinetic effects appear in a shift in the position of the peaks and in a change in the area under the peaks in the DSC thermograms. More experiments are necessary to reveal these kinetic aspects in full detail.

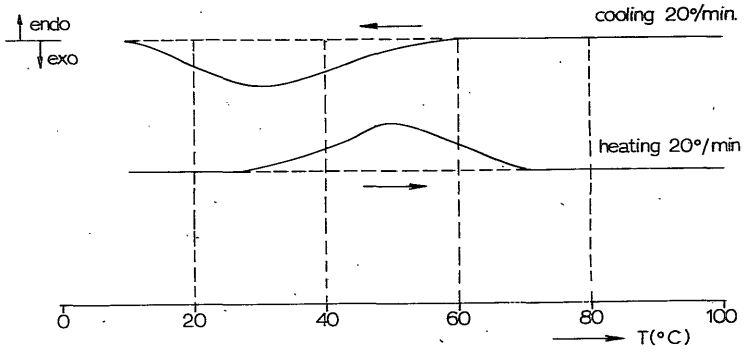


FIG.6. Endothermic and exothermic effects for 55% CA in a mixture 85% dioxane/15% water.

## 3.4 DISCUSSION

In discussing the results reported here we must distinguish between two types of systems for which thermograms have been obtained:

(I) Polymer solutions in region I (Fig.2) show a fast type of phase separation upon cooling, which takes place without caloric effect; after prolonged aging, however, these systems show measurable heat effects in DSC measurements upon heating.

(II) Polymer solutions in region II (Fig.2) which do not show visible signs of phase separation upon cooling, but which show peaks in the DSC thermograms after aging. We will discuss these systems separately.

Polymer solutions from region I

For solutions of up to 20% polymer concentration and with the appropriate amount of nonsolvent in the mixture, cloud points can be measured upon cooling. Turbidity appears on cooling and disappears at the same temperature on heating. The cloud points are independent of the rate of cooling. These observations indicate a liquid-liquid type of phase separation. With DSC experiments there are no detectable heat effects during this phase separation.

Upon aging the turbid solutions at room temperature for several hours, a clear dilute polymer phase appears on top of a cloudy, concentrated gel-like phase. This concentrated phase "melts" on heating. In the DSC experiments this shows up as an endothermic peak. It follows from the thermograms that the melting peak falls entirely below the cloud point temperature.

From the peak area in the thermogram it can be calculated that the endothermic effect for a 10% CA solution in a dioxane(60%)/water(40%) mixture, after aging for 2 days at room temperature, amounts to 9.6 J/g of solution, or 5 kJ/mole of monomer units of the polymer. This value agrees quite well with published values[15] found in gelling systems,

where crystallization plays a role.

In conclusion it can be stated that for solutions in region I upon cooling, liquid-liquid phase separation sets in, which is a kinetically fast process. In the system under study this is followed by a slow gelation process taking place in the concentrated polymer phase. These gelled structures melt on reheating; this process can be detected by DSC experiments.

Polymer solutions from region II

At polymer concentrations of 40-55% and fairly low nonsolvent content (10-20% water in the solvent mixture) we do not find any visible sign of phase separation upon cooling, but again we find endothermic DSC peaks upon aging the solutions at ambient temperature. The appearance and the area of the peaks in the thermograms can be influenced strongly by varying the polymer concentration or the nonsolvent content. Even exothermic effects may appear (Fig.6). These effects demonstrate that gelation/crystallization occurs in these systems. For most of the solutions studied the processes leading to endothermic heat effects are rather slow. This is similar to the effects for the two-phase region I.

The peak areas for region II are smaller than those found in region I. The peaks found in Figure 4 correspond to values for the heat effect of 1.2 kJ/mole of monomer units of CA for the solution in a mixture of dioxane(80%)/water (20%) and only 250 J/mole for the solution of CA in a mixture of dioxane(85%)/water(15%). For a CA solution in dioxane (90%)/water(19%) there is no endothermic peak for the normal aging period and temperature. Probably differences in nucleation of the microcrystalline phase at different water contents could explain these results, but further experimentation is necessary.

Relevance to membrane formation

A membrane forming system which shows liquid-liquid

phase separation for certain compositions and gelation at different,higher, polymer content, has been reported earlier by Koenhen et al.[5] Although the polyurethane/DMF/water system which was studied in Ref.5, is not a very practical membrane forming system, the same two types of phase separation were found to be important for the formation of the layered structure in membranes, viz. gelation being responsible for skin formation and liquid-liquid phase separation (followed by gelation of the concentrated phase) generating the open, porous sublayer of the membrane.

Cellulose acetate is a well known membrane material, but it appears that there are no thermodynamic or kinetic data to be found in the literature about its phase separation. The experimental results reported here show that both liquid-liquid phase separation and gelation (or crystallization) are possible for the system CA/dioxane/water. Analogous results have been found in our laboratory for other membrane forming systems.[16]

As an illustration of the membrane structures obtainable we give two scanning electron microscope photographs of the cross-section of membranes formed by casting a 10wt% solution of CA in dioxane as a 0.2-mm-thick film on a glass plate, and immersing the film in a nonsolvent (water) bath held at two different temperatures, 52°C (Fig.7(a)) and 3°C (fig.7(b)), respectively. We see the porous structure typical for liquid-liquid phase separation, in which the pores are the regions of the dilute polymer phase, which have nucleated and grown in the second,polymer-rich phase.

## 3.5 CONCLUSION

From cloud point measurements and DSC thermograms we conclude that in the system CA/dioxane/water both liquid-liquid phase separation and crystallization are possible. This is relevant to the description of the formation of the dense skin and the porous sublayer of a membrane.

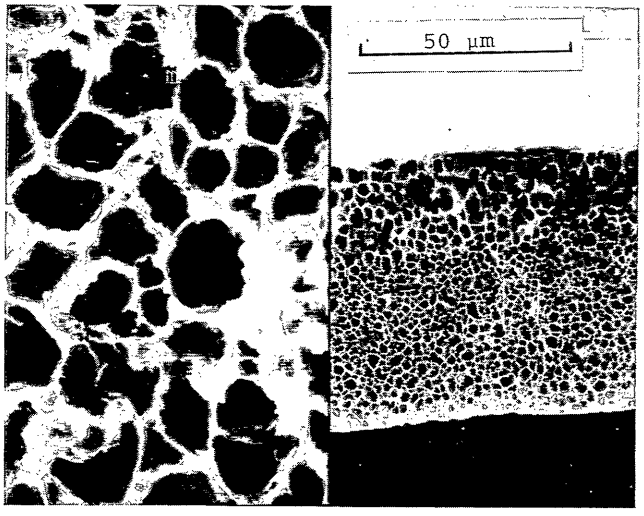


(a)

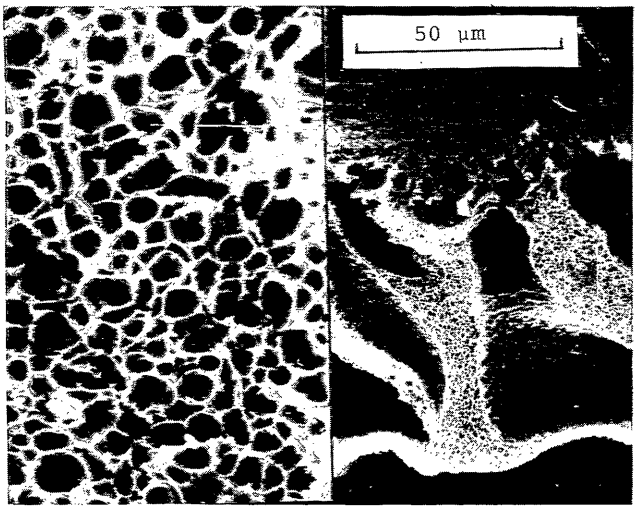


(b)

FIG.7. SEM photographs of porous substructure in membranes. The left parts give a 10x enlargement of the porous substructure. Coagulation at (a) 52°C and (b) 3°C.

Acknowledgement

The authors thank J. Smid for carrying out part of the experiments and Dr. D.M. Koenhen for the SEM photographs.

## 3.6 REFERENCES

1. M.A.Frommer, I.Feiner, O.Kedem, and R.Bloch, Desalination, 7,393(1970)
2. H.Strathmann, P.Scheible, and R.W.Baker, J.Appl.Polym. Sci., 15,811(1971)
3. H.Strathmann and K.Kock, Desalination, 21,241(1977)
4. M.Guillotin, C.Lemoyne, C.Noël, and L.Monnerie, Desalination, 21,165(1977)
5. D.M.Koenhen, M.H.V.Mulder, and C.A.Smolders, J.Appl.Polym.Sci., 21,199(1977)
6. L.Broens, D.M.Koenhen, and C.A.Smolders, Desalination, 22,205(1977)
7. C.Cohen, G.B.Tanny, and S.Prager, J.Polym.Sci.A-2, 17, 477(1979)
8. P.T. van Emmerik and C.A.Smolders, Eur.Polym.J., 9,293 (1973)
9. D.M.Koenhen and C.A.Smolders, J.Polym.Sci.A-2,15,167(1977)
10. R.Bloch and M.A.Frommer, Desalination, 7,259(1970)
11. U.Rosenthal, J.Nechushtan, A.Kedem, D.Lancet, and M.A. Frommer, Desalination, 9,193(1971)
12. G.J.Gittens, P.A.Hitchkock, D.C.Sammon, and G.E.Wakley, Desalination, 8,369(1970)
13. K.Sirkar, N.K.Agarwal, and G.P.Rangaiah, J.Appl.Polym. Sci., 22,1919(1978)
14. S.Sourirajan, Reverse Osmosis and Synthetic Membranes, National Research Council Canada Ottawa, 1977,pp.147-148
15. M.Pyrlik and G.Rehage, Colloid Polym.Sci., 254,329(1976)
16. Chapter 2 of this thesis.

## 3.7 APPENDIX

## SPINODAL AND CLOUD POINTS DETERMINED BY PICS

Pulse Induced Critical Scattering (PICS) is a technique for determining thermodynamic and kinetic parameters of polymer solutions. It is especially suitable for the determination of cloud points and spinodal points of liquid-liquid phase separation in a polymer solution. The intensities of scattered laser light are measured after a fast temperature step of the sample into the metastable region. For theoretical considerations regarding the relation between the intensity of the scattered light and the thermodynamics of the system the reader is referred to the original literature.[1-3]

With this instrument one can also obtain very useful information on crystallization processes in polymer solutions. Koenhen[4] studied crystallization of PPO in toluene with the PICS apparatus.

In this Appendix we report results of spinodal and cloud point determinations in the system CA/dioxane/water. This is a ternary system; we assume the same theoretical considerations to be applicable.

Measurements on gelation behaviour have recently been undertaken. Kinetic information on liquid-liquid phase separation and crystallization processes can contribute much to the description of the formation of asymmetric membranes.

### Experimental

We have built the PICS instrument following the design given by Derham et al.[1] A thin walled capillary cell with a diameter of 1 mm containing a few microlitres of solution is cooled stepwise from a temperature well above (say 20°C) the cloud point temperature to a temperature below the cloud point. The light source is a helium-neon laser and light

guides at two angles of 30° ($I_{30}$) and 90° ($I_{90}$) collect the scattered light. The light guides pass the light to solid-state detectors. The temperature is measured with a thermistor.

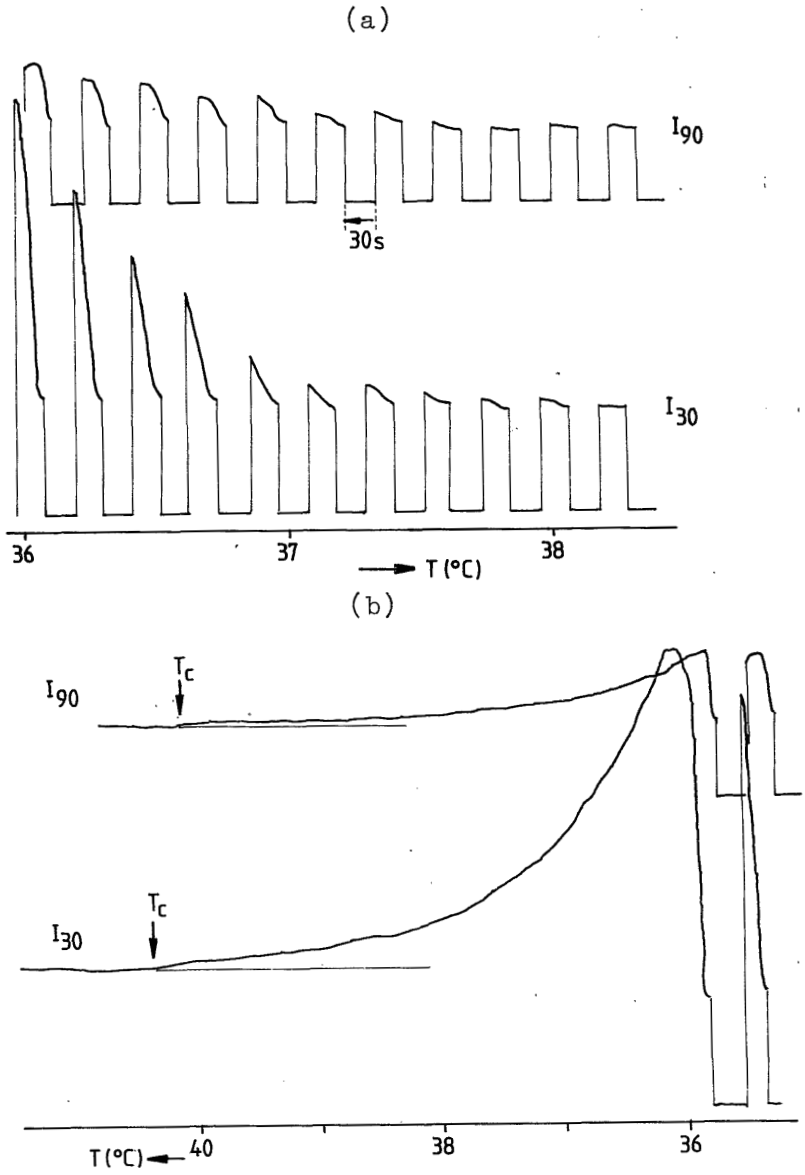


FIG.1. Pulse cooling run (a) and cloud point determination (b) of a 2.6 wt% CA solution in a 65/35 mixture of dioxane and water. Intensities at two angles of 30° and 90°. Arrows indicate cloud point ($T_c$).

In a spinodal point determination experiment the thermostate bath is cooled with a controlled rate of about $0.1^{\circ}C$/min. The temperature step is produced by rotating the sample from a place of high temperature (heated air stream) to the thermostat bath. The light scattering is followed for 10-30 s. An example is given in Figure 1a. After this step the sample is brought again to high temperature. The intensity of the scattered light is registered during every pulse and in the course of time as a function of temperature. The reciprocal intensity difference $I = I_f - I_o$, where $I_f$ is the intensity at the end of the pulse and $I_o$ is measured just above the cloud point, is plotted against the temperature, and the spinodal point is obtained from this curve-extrapolation to $I^{-1} \rightarrow 0$ (Figure 2).

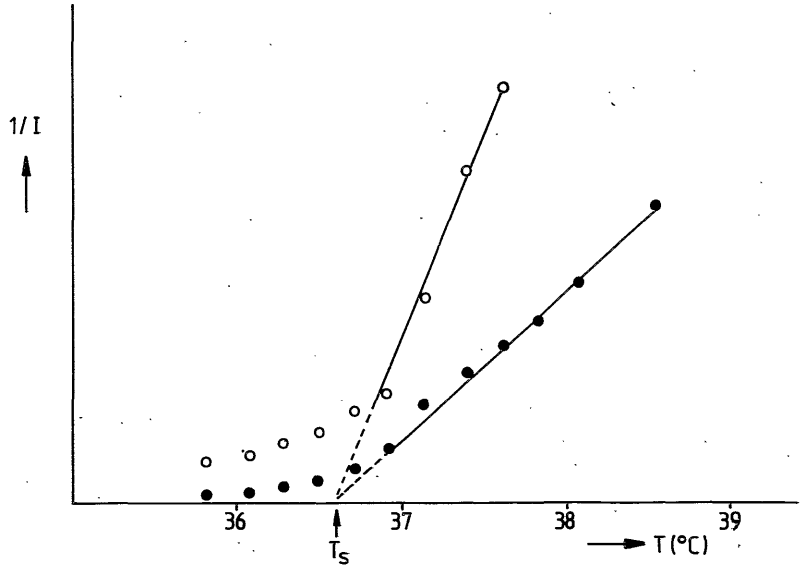


FIG.2. Reciprocal of intensity as a function of temperature. The sample has the same composition as in Figure 1. The arrow indicates the spinodal point ($T_s$).

A cloud point can be determined by approaching the equilibrium from the two-phase side, i.e. by heating the phase separated emulsion.[1] The emulsion is seeded by a sudden

step from above to below the cloud point. A sudden increase in $I_{30}$ is taken as evidence of emulsion formation. Then the linear heating of the thermostat bath at a rate of $0.2^{o}$/min is switched on. This leads to a rapid decline of $I_{30}$. The cloud point is the point where $I_{30}$ (or $I_{90}$) returns to the baseline (Figure 1b).

In Chapter 3 we have mentioned the occurrence of syneresis after entering the demixing region. After waiting for some time at a temperature of only a few degrees below the cloud point temperature, a clear dilute phase appears on top of a cloudy gel-like phase. This gel-like phase disappears only after heating to much higher temperature than the cloud point. This rather fast process of syneresis interferes with an accurate determination of cloud points and spinodal points. A reasonable reproducibility in repeated runs was obtained when centrifuging the solution at high temperatures before every run to obtain a high degree of homogeniety. Still the reproducibility is not better than $0.4^{o}$C.

Results and discussion

Spinodal and cloud points were determined (Figure 3) for samples with two different solvent/nonsolvent ratios as a function of polymer weight fraction. The values given are mean values of at least three spinodal/cloud points runs. Also given are cloud points obtained from visual observation (section 3.3.1). There is a large discrepancy in the location on the temperature axis. Apparently a PICS determination of the cloud point is more sensitive since we could not see any sign of turbidity with the naked eye at the (PICS) cloud point temperature.

The fact that we can determine a spinodal point is another proof of liquid-liquid phase separation in this system. (see section 3.4).

For a composition of 65/35 dioxane/water in the solvent mixture we see that at CA concentrations of 10-15% the mean spinodal point appears to be situated at the same or at high-

er temperature than the cloud point. The points lie within their respective range of reproducibility (or accuracy). At lower polymer concentration the difference between the spinodal and cloud point is much larger; this is also the case at higher polymer concentration. The reason for the fact that cloud points and spinodal points appear to coincide may be that the critical point is situated in this region,

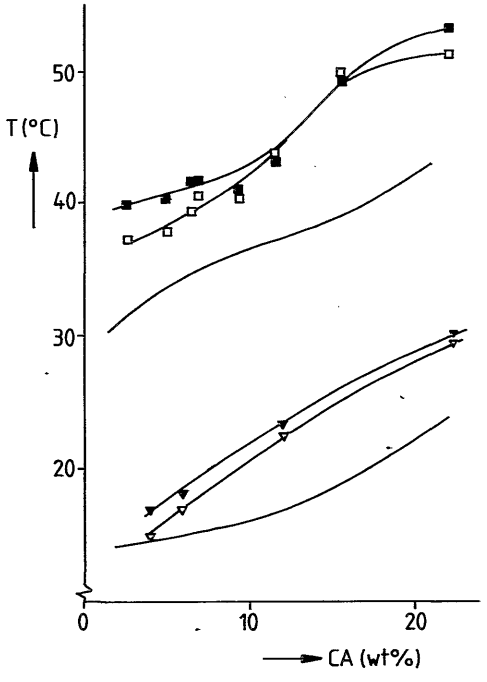


FIG.3. Spinodal and cloud points at two dioxane/water ratios as a function of CA percentage: upper three curves for a dioxane/water mixture 65/35 (■) cloud point, (□) spinodal and (—) visual observation; lower curves for a mixture 70/30 (▼) cloud point, (▽) spinodal point and (—) from visual observation.

and at about this dioxane to water ratio. At this point the metastable region vanishes and one may expect a much steeper increase in the intensity of the scattered light as a function of the temperature. Analyzing the pulsed runs

it appears that the rate of increase of $I_{30}$ (and $I_{90}$) is much larger at about 15% CA than at lower or higher polymer concentrations.

We have not performed a detailed analysis of the kinetic aspects of the liquid-liquid demixing process. Only at the lowest polymer concentration considered (2.6% CA, see Figure 1) we saw a decrease of $I_{90}$ during an increase of $I_{30}$. Following Derham [1] this can be interpreted as having reached the situation where the scattering particles have a size comparable to the wavelength of the light (± 600 nm). This occurs at about 36.1°C in the case given by Figure 1a, which is about 4 degrees below the cloud point and perhaps 1 degree below the spinodal point of the homogeneous solution. At higher polymer concentrations, coalescence and subsequently syneresis are likely to influence the intensity of the scattered light. Only maxima in $I_{30}$ are observed and not in $I_{90}$.

Acknowledgement

The author thanks Mr. H.G. Koetsier for his technical assistance and for performing the experiments.

References

1. K.Derham, J.Goldsbrough and M.Gordon, Pure Appl.Chem., 38,97(1974)
2. J.Goldsbrough, Sci.Progr. (Oxford), 60,281(1972)
3. M.Gordon, J.Goldsbrough, B.W.Ready and K.Derham, Characterization by molecular weight, in Industrial Polymers, J.H.S.Green and R.Dietz, Eds., Transcripta Books, London, 1973,p.45
4. D.M.Koenhen, C.A.Smolders and M.Gordon, J.Polym.Sci., Polym.Symp., 61,93(1977)

# 4. PHASE SEPARATION PHENOMENA IN SOLUTIONS OF CELLULOSE ACETATE. II. MELTING POINTS OF THERMOREVERSIBLE GELS OF CELLULOSE ACETATE IN MIXTURES OF DIOXANE AND WATER

F.W.ALTENA, J.S.SCHRÖDER, R.van de HULST and C.A.SMOLDERS
Department of Chemical Technology, Twente University of Technology, Enschede, The Netherlands.

## 4.0 SYNOPSIS

Thermoreversible gels of cellulose acetate can be obtained by cooling a concentrated solution of the polymer (40-60%) in a mixture of a solvent (dioxane) and a nonsolvent (water). This is a polymer/solvent/nonsolvent system which is frequently used in the preparation of reverse osmosis membranes of CA.

Upon heating these gels endothermic effects can be measured by differential scanning calorimetry. These heat effects are ascribed to the melting of a crystalline phase consisting of cellulose triacetate units.

The concentration dependence of the melting points is reasonably well described by the Flory expression for the melting point depression. In our case we assume equilibrium between a pure crystalline phase and a liquid phase of a polymer in a mixed solvent. The heat of fusion per mole of crystalline units increases from 6 to 12 kJ when the concentration of water in the mixture increases from 0 to 20%. With these values a maximum degree of crystallinity of 5% has been calculated.

Kinetic effects of increasing water content are discussed.

## 4.1 INTRODUCTION

Recently Koenhen et al.[1] suggested that two distinctly different demixing processes are responsible for the formation of an asymmetric membrane, viz. (i) gelation for the toplayer and (ii) liquid-liquid phase separation for the lower layer. Liquid-liquid phase separation takes place at low and medium polymer concentration and variable nonsolvent content, whereas gelation is operative at high polymer concentration and low nonsolvent content. We have shown[2] that these two types of phase separation can also be found in the system CA/dioxane/water.

Only few authors have studied systems in which both liquid-liquid phase separation and crystallization take place.[3,4]

In the present Chapter we try to explain gelation of CA as a result of a crystallization process, though other types of cross links are not excluded. Evidence for this explanation is based on thermodynamic grounds, viz. melting points and heats of melting as a function of composition. No structural information is available at present.

## 4.2 THERMODYNAMIC CONSIDERATIONS

Following Flory[5] we assume equilibrium between the crystalline phase and the liquid phase. The temperature at which this equilibrium exists is the melting point $T_m$. When we take the pure liquid (the melt) as the reference state, the equilibrium is expressed in the relation:

$$\mu_u^c - \mu_u^o = \mu_u - \mu_u^o \qquad (1)$$

where $\mu_u^o$ is the chemical potential per mole of repeating units in the standard state, $\mu_u^c$ is the chemical potential per mole of crystalline units and $\mu_u$ is the chemical potential per mole of units in the solution.

We assume that the left-hand part of equation (1) may be written as follows:

$$\mu_u^c - \mu_u^o = -\Delta Hu(1-T_m/T_m^o) \qquad (2)$$

where $\Delta Hu$ is the heat of fusion per mole of repeating units and $T_m^o$ is the melting temperature of the pure crystal.

An expression for the right-hand part of equation (1) is derived from the free enthalpy of mixing, usually expressed in the form of the Flory-Huggins equation.[5,6] In this Chapter we will use this equation expressed in volume fractions and with a free enthalpy correction parameter g according to Koningsveld[7]:

$$\frac{\Delta G_m}{RT} = \phi_1 \ln\phi_1 + s\phi_2 \ln\phi_2 + r\phi_3 \ln\phi_3 + g_{12}\phi_1\phi_2 + g_{13}\phi_1\phi_3 + sg_{23}\phi_2\phi_3 \qquad (3)$$

$\Delta G_m$ is expressed in Joules per mole of lattice sites. $\phi_1$, $\phi_2$ and $\phi_3$ are the respective volume fractions of the components used. The indices refer to the nonsolvent (1), the solvent (2) and the polymer (3) respectively. The ratios of the molar volumes of the components ($s = \nu_1/\nu_2$; $r = \nu_1/\nu_3$) are included in the relation to account for the number of lattice sites occupied by the components. At present we assume that the contribution of the polymer to the free enthalpy of mixing is suitably well described by one molecular weight $M_3$, set equal to the number averaged molecular weight $\bar{M}_n$. The g-parameters are binary interaction parameters, and if we assume no concentration dependence the g-parameters equal the Flory-Huggins interaction parameters $\chi_{12}$, $\chi_{13}$ and $\chi_{23}$.

When equation (3) is differentiated with respect to the number of moles of component 3, equation (4) is derived:

$$\frac{\mu_u - \mu_u^o}{RT} = r\ln\phi_3 + r(1-\phi_3) - \phi_1 - s\phi_2 + (g_{13}\phi_1 + sg_{23}\phi_2)(\phi_1+\phi_2) - g_{12}\phi_1\phi_2 \qquad (4)$$

where $\mu_u - \mu_u^o$ is expressed in Joules per mole of units of com-

ponent 1. Inserting (2) and (4) in equation (1), while multiplying (4) with $\nu_u/\nu_1$ in order to equalize the units and taking $T = T_m$, gives:

$$-\Delta Hu\left(1-\frac{T_m}{T_m^o}\right) = RT_m\frac{\nu_u}{\nu_1}\left[-\phi_1-s\phi_2+(g_{13}\phi_1+sg_{23}\phi_2)(\phi_1+\phi_2)-g_{12}\phi_1\phi_2\right] \qquad (5)$$

where $\nu_u$ is the molar volume of the repeating unit, and it is assumed that $r\to 0$.

Usually an equation such as (5) is used for a two component system ($\phi_1=0$), after rearranging:

$$\left(\frac{1}{T_m}-\frac{1}{T_m^o}\right)/\phi_2 = -\frac{R\nu_u}{\Delta Hu\nu_2}\left[-1+g_{23}\phi_2\right] \qquad (6)$$

$\Delta Hu$ and $g_{23}$ are derived from the plot of $(1/T_m - 1/T_m^o)/\phi_2$ against $\phi_2$.

The experiments for the three component system are performed with a constant volume ratio of components 1 and 2:

$$\phi_1 = p\phi_2 \qquad (7)$$

Inserting this in equation (5) we find after rearranging:

$$\left(\frac{1}{T_m}-\frac{1}{T_m^o}\right)/\phi_2 = \frac{R\nu_u}{\Delta Hu\nu_1}\left[-p-s+\phi_2(p^2g_{13}+p(g_{13}+sg_{23}-g_{12})+sg_{23})\right] \qquad (8)$$

In our experiments the proportion ratio p of solvent and nonsolvent is varied and the melting point dependence on the polymer weight fraction ($\phi_3$) and the solvent fraction ($\phi_2$) is determined. We will introduce literature values for the g-parameters.

## 4.3 EXPERIMENTAL

### 4.3.1 Materials

Details of the materials are given in Chapter 3.

### 4.3.2 Cloud points Measurements

Cloud points were determined by using the method described earlier.[8]

In this Chapter we concentrate on observations of demixing in the very concentrated region in the phase diagram. The composition of the samples lie preferably outside the (extrapolated) cloud point lines of the liquid-liquid phase separation region.

### 4.3.3 Differential Scanning Calorimetry

The solutions were prepared as described in Chapter 3. The low temperature handling of the samples in the instrument was considerably improved by using an improved cooling head and by careful introduction of liquid nitrogen.[9]

We have shown earlier[2] that measurable endothermic effects upon heating are only present after considerable aging periods at low temperatures. We now use the fact that this is a slow process to obtain a quantitative value for the heat effect.

This value is determined by substracting the thermogram after aging from the one obtained without aging before reheating. In this way a minimal value for the heat effect is determined. If the fast cooling and immediate reheating procedure would result in an endothermic effect upon heating, this effect is hidden in the baseline noise. The normal heating rate is $10^{o}$C per minute. The lowest heat value which we can determine with a certain degree of accuracy is about 0.2 J/g polymer units. In this region the accuracy of the instrument is very limited. The melting point is determined as the end of the endothermic peak, where the last traces of material "melt". The accuracy is not better than ± 3K.

## 4.4 RESULTS

### 4.4.1 Turbidity Measurements

Apart from the region where cloud point determinations have been made at lower polymer concentrations (see Figure 1) we have also studied a region at higher concentrations of polymer (dashed region in Figure 1). One can roughly distinguish three different zones in this region according to visual evaluation of these ternary systems:

I: systems homogeneous at 90°C and also homogeneous at 10°C,

II: systems homogeneous at 90°C, but turbid at 10°C,

III: systems turbid over the complete temperature range from 10-90°C.

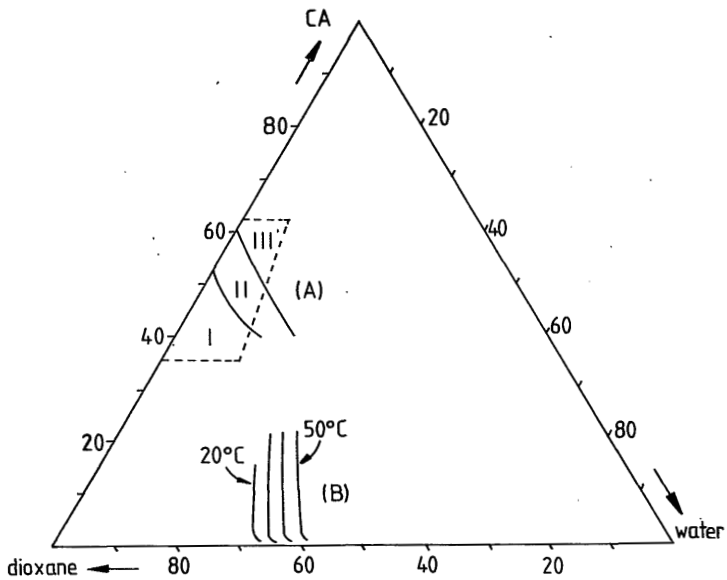


FIG.1. Gelation (A) and liquid-liquid phase separation (B) in the system CA/dioxane/water. Coexistence lines for the latter at different temperatures. For explanation of symbols I, II and III see text. Dashed line indicates the region where DSC measurements have been made.

Especially at high concentrations of polymer the mixing process is difficult. The general trend, however, seems clear: increasing the nonsolvent content gives turbidity at a lower overall polymer concentration. Two important points may be noted here. First, systems without nonsolvent, i.e. on the polymer/solvent axis, show phase separation. Secondly, many systems which give an endothermic heat effect in DSC upon heating, are visually clear at low temperature. The systems which do show turbidity at room temperature have a very elastic gel-like behaviour.

### 4.4.2 Differential Scanning Calorimetry

#### 4.4.2.1 Melting Points

The dependence of the melting point of the mixture on the weight fraction of polymer is determined as a function of the water content in the solvent/nonsolvent mixture. The results are given in Figure 2a. The values for the melting points at 40, 50 and 60 wt% CA are obtained by interpolation of the experimental results. In Figure 2b the values for the endothermic heat effects upon heating from 20 to 100°C are given. The systems have been aged at 20°C for a period of three days. The following observations may be noted:

- the melting points increase, as expected, with the weight fraction of the polymer,
- there is a tendency for the melting point to decrease with an increasing nonsolvent content,
- in general Q, the amount of heat per gram of CA, increases with increasing water content. We notice a peculiar maximum, not yet understood, in the curve for 60% polymer.
- even without adding water to the system CA/dioxane there is a small but measurable endothermic heat effect.

#### 4.4.2.2 Influence of aging time at 20°C

In Figure 2 results are presented for samples after aging for three days. If we compare the melting points and the values for the heat effect at shorter aging periods, we

can make the following remarks:

- the melting points do not differ within the accuracy of the experiments,
- at high water content (20%) the value for Q after one day aging does not differ from that after three days aging, whereas at lower water content (e.g. 10%) the one day value is much smaller than that after three days. Hence increasing the water percentage has a positive kinetic influence.

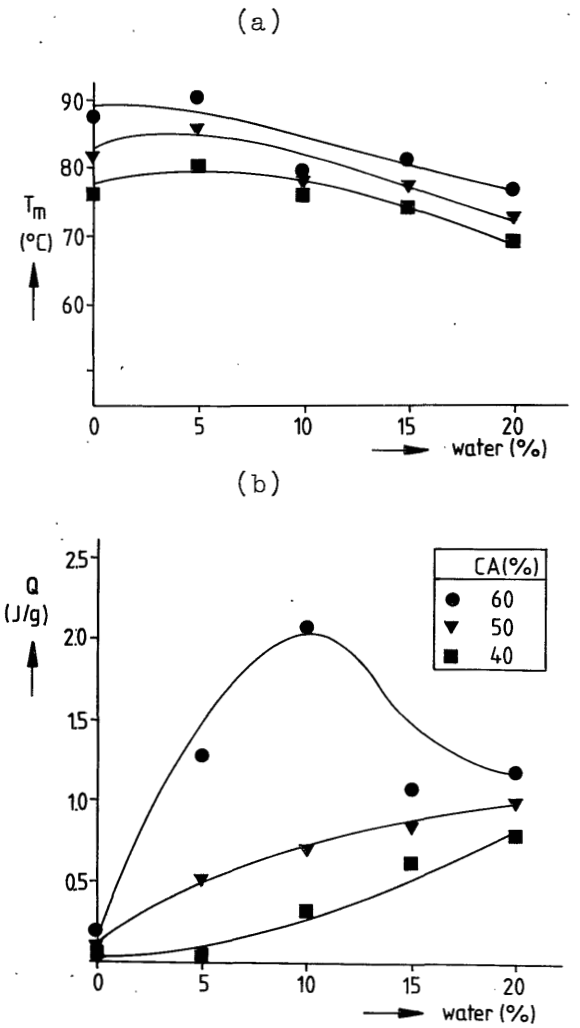


FIG.2. Melting points (a) and heat effects (b) from DSC experiments as a function of nonsolvent content in the dioxane/water mixture.

4.4.2.3 Influence of different cooling rates on the melting endotherm

We have mentioned before that direct reheating after cooling gives no appreciable heat effects. On the other hand we have found small heat effects during heating (10°C per minute) after cooling at sufficiently low cooling rates. The polymer concentration is high, about 60%. The water content in the solvent/nonsolvent mixture is 15-20%. These small heat effects could be made visible after subtracting the (reheating) curves for rapidly cooled samples (40°C/minute and higher) from the curves for slowly cooled samples (1.25°C/minute). The heat effect is in the same temperature range as those in Figure 2a. No effect could be observed at 10% water content in the mixture.

4.4.2.4 Influence of cooling to -10°C

When we performed the same experiment as under 4.4.2.3, but if we cooled down to -10°C, instead of 20°C, we noticed that:

- endothermic heat effects upon heating are situated below 30°C,
- only low cooling rates (below 2.5°C/minute) gave these heat effects upon heating,
- heat effects are also visible at water percentages of 10%.

From these observations it appears that cooling to a lower temperature results in "melting" peaks which are shifted to lower temperatures. It gives rise to heat effects occurring at lower water content and to a slow gelation process.

4.4.2.5 Gelation after liquid-liquid phase separation

In Figure 3 we present results obtained in a similar way as those in Figure 2, but now with a water content in the solvent/nonsolvent mixture of 40% and a lower polymer concentration. The systems lie in that region in the ternary phase diagram where liquid-liquid phase separation occurs immediately after cooling to a temperature below about 60°C. We notice that the melting point increases with polymer con-

centration (as in the highly concentrated systems of Figure 2) but the area under the endotherm decreases with increasing polymer concentration. Furthermore, even the lowest Q-value determined is a factor 2 or 3 higher than that determined in the region of high polymer weight fraction and low nonsolvent content (Figure 2). These results are not yet fully understood.

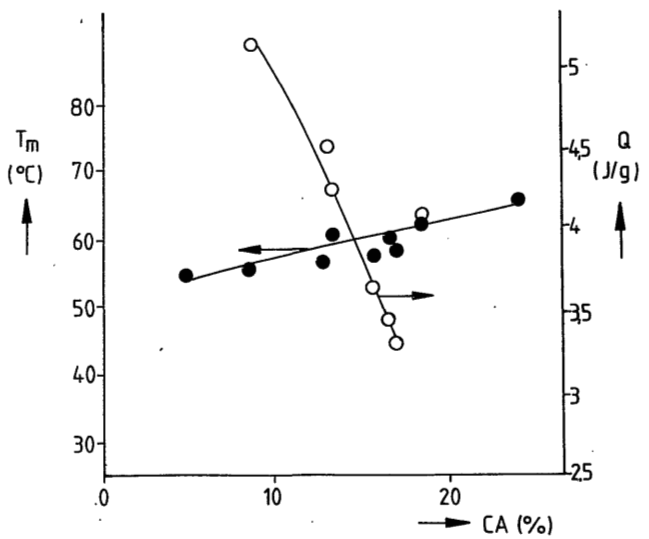


FIG.3. Melting points and heats of melting from DSC experiments as a function of polymer weight fraction. These systems have a water percentage of 40% in the dioxane/water mixture.

A complicated phase separation process takes place: first there is liquid-liquid phase separation resulting in a dilute and a concentrated phase , followed by gelation (crystallization) in the concentrated phase. In terms of membrane formation the latter phenomena of liquid-liquid phase separation and gelation combined take care of the formation and solidification of the porous sublayer.

### 4.4.2.6 Dependence of melting point on the solvent volume fraction in the system CA/dioxane/water

In the theoretical section we derived an equation for the dependence of $T_m$, the melting point, on $\phi_2$, the solvent volume fraction. We expect a linear relationship between $(1/T_m - 1/T_m^o)/\phi_2$ and $\phi_2$. From $T_m^o$, the melting point of the pure crystal, we have chosen the value of 579K[16] valid for cellulose triacetate. The experimental data are plotted in Figure 4 for five different ratios of dioxane/water. Reasonably straight lines are obtained. The quantities calculated from the slope and the intercept of this plot are discussed in the following section.

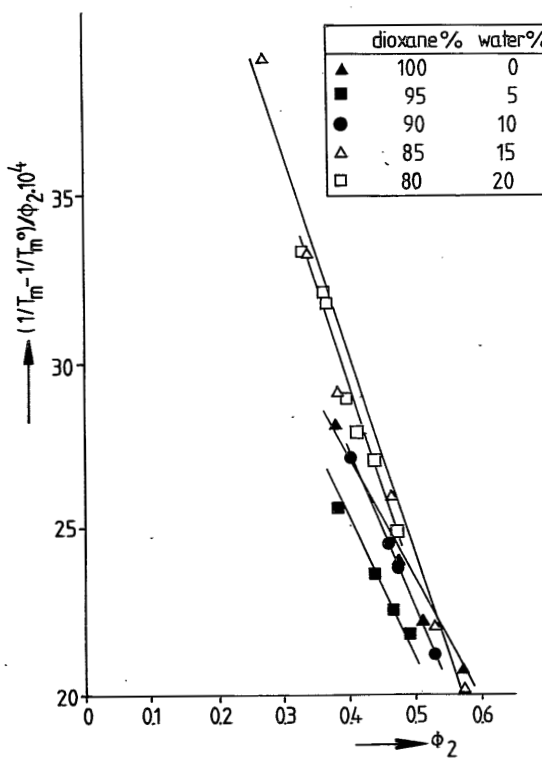


FIG.4. Dependence of $(1/T_m - 1/T_m^o)/\phi_2$ on $\phi_2$, calculated from experimental data on which Figure 2a is based.

## 4.5 DISCUSSION

In this discussion section we would like to focus our attention on the following three points:

1. Evidence for crystalline regions in the gels,
2. Thermodynamic description of the melting point of the crystalline regions as a function of polymer concentration and nonsolvent content,
3. Some further remarks: kinetics, degree of crystallinity and mixed crystals.

### 4.5.1 Evidence for crystallinity

Thermoreversible gels can be obtained from CA in mixtures of dioxane/water. A high polymer concentration is necessary for the formation of the gel (see Figure 1). We must first make certain that the phenomenon of gelation is due to a different type of demixing than the liquid-liquid phase separation found earlier[2]:

- The systems under study have a composition outside the (extrapolated) liquid-liquid phase separation coexistence lines. Even concentrated solutions of CA in dioxane alone (i.e. without any nonsolvent present) became turbid and gelatinous when cooled from 90°C to 20°C.
- It takes long aging periods (sometimes days) to obtain effects of demixing that can be detected by DSC measurements. As we know from earlier measurements liquid-liquid separation is a fast process.

We think that crystalline regions are responsible for the physical crosslinks in the demixing that leads to gelation. We do not exclude that crosslinks of a different type are also operative.

A thermodynamic description of the melting point of the gel as a function of polymer volume fraction and nonsolvent content in the system gives reasonable values for the heat of melting per mole of crystalline units (see below). So far we have no structural evidence for crystallinity in our systems. We could not observe a change in birefringence in the

gel in the same temperature interval in which we performed our DSC experiments.

4.5.2 Thermodynamic data from melting point curves

A thermodynamic description of gelation often concentrates on the melting point dependence as a function of the polymer weight fraction.[5,14,15] There is however a conceptual problem in defining the melting point: in general, melting does not occur at a sharply defined temperature, but over a certain temperature interval. This is also the case in our systems. The temperature interval is about 20°C. Several methods can be used to determine a "melting" point:

- disappearance of turbidity (very inaccurate),
- the onset of flow of the gel when the temperature is changed,[10-13]
- Calorimetric determination, as used in this Chapter, where the melting point is taken at the end of the melting endotherm.

Several authors have given a theoretical treatment of the melting point as a function of the polymer weight fraction. The descriptions of Flory[5] and Takahashi[15] are suitable for gels in which there are crosslinks of a crystalline nature. From the equation of Flory, one derives $\Delta Hu$, the heat of fusion per mole of crystalline units and interaction parameter $\chi$ between polymer and solvent in a binary system. Takahashi calculates $\xi$, the number of crystallized units entering into a crystallite, and $\sigma_e$, the interfacial free energy per crystalline sequence, using values for $\Delta Hu$ and the interaction parameter already known. Both descriptions use a value for the melting temperature of the pure crystal $T_m^o$. The equation of Takahashi for the melting point dependence on the polymer weight fraction is limited to low polymer concentrations.

The equation of Eldridge and Ferry[14] does not require specific knowledge of the nature of the crosslinks of the gel. The inverse of the melting point should depend linearly on the logarithm of the polymer weight fraction. The

slope of this plot gives ΔHm, the heat of melting per mole of crosslinks. Problems will arise if the dispersion at high temperature is not complete (because equilibrium is assumed between potential crosslinks and actual crosslinks), and if the sequences of the chains which take part in the crosslinks are of different lengths or if varying numbers of chains cooperate in a crosslink. In this situation a spectrum of ΔHm will result and ΔHm might vary with the logarithm of the polymer concentration. The relation of Eldridge and Ferry has been applied to gelation of CA in benzylalcohol by several authors, see ref. 13. They found a value of -60kJ/mole for CTA and -44 kJ/mole for CA.

Although one usually does not apply the relation of Eldridge and Ferry to polymer concentrations higher than 10%, we calculated ΔHm from our experimental data at 40-60% CA. The results are given in Table 1.

| percentage of water in dioxane/water mixture | ΔHm, heat of melting (kJ/mole crosslinks) |
|---|---|
| 0 | -31 |
| 10 | -60 |
| 15 | -50 |
| 20 | -38 |

Table 1: Heat of melting of the gel, calculated from $d(\ln c)/d(1/T_m) = \Delta Hm/R$ (Eldridge[14]).

The accuracy of the results given in Table 1 is not better than 10 kJ/mole.

For a further evaluation of the experimental data we refer to equation (8) and to Figure 4. Assuming a certain value for $T_m^o$ and for the values of the interaction parameters $g_{12}$ and $g_{13}$, we shall find values for ΔHu from the intercept and for $g_{23}$ from the slope of the curves in Figure 4. One could of course equally well choose a different g-para-

meter as an unknown variable. At this stage we assume that no solvent is present in the crystalline phase. For $T_m^o$ we have chosen the value for CTA as given by Malm[16], viz.579K.

The melting point depression equation has been modified by Hoffman[17], to account for a large difference between $T_m$ and $T_m^o$. Instead of plotting $(1/T_m-1/T_m^o)/\phi_2$ against $\phi_2$, we then have to plot $(1/T_m^o-T_m/(T_m^o)^2)/\phi_2$ against $\phi_2$. Different values of $\Delta Hu$ and $g_{23}$ will then result.

In the case of a binary system one generally plots on the abscissa the weight or volume fraction divided by the absolute temperature, to account for the usually inverse temperature dependence of the interaction parameter. Because of the limited accuracy and the relatively small temperature interval we used $\phi_2$ at the abscissa. The limited accuracy makes it difficult anyhow to determine a temperature or concentration dependence of the interaction parameters from these melting point data.

We used the following parameter values: $\nu_1 = 18.07$; $\nu_2 = 85.9$; $M_u = 288$; $\rho(CA) = 1.3$ g/cm$^3$, $g_{12} = 1.1$ and $g_{13} = 1.4$. The results are given in Table 2 and in Figure 5.

| water % | p | Flory | | Hoffman | | $g_{23}$=0.4 | $g_{23}$=0.5 |
|---|---|---|---|---|---|---|---|
| | | $\Delta Hu$ | $\chi$ exp | $\Delta Hu$ | $\chi$ exp | $\chi$ theor | $\chi$ theor |
| 0 | 0.0 | 6.3 | 0.18 | 9.8 | 0.19 | 0.08 | 0.10 |
| 5 | 0.052 | 8.3 | 0.22 | 12.6 | 0.23 | 0.10 | 0.12 |
| 10 | 0.111 | 8.8 | 0.26 | 14.1 | 0.27 | 0.14 | 0.16 |
| 15 | 0.176 | 9.7 | 0.33 | 13.9 | 0.32 | 0.19 | 0.21 |
| 20 | 0.25 | 11.4 | 0.38 | 18.0 | 0.39 | 0.26 | 0.29 |

Table 2: $\Delta Hu$ (kJ/mole) and experimental and theoretical values for $\chi$-parameter as a function of percentage of water. $\chi$ exp is given by $\chi$ exp = slope.$\Delta Hu\nu_1/R\nu_u$) and $\chi$ theor = $p^2 g_{13}+p(g_{13}+sg_{23}-g_{12})+sg_{23}$.

The value for the term $\chi$ determined from the experiments is given in the columns 4 and 6. We calculate the $\chi$-values given in columns 7 and 8 assuming values for $g_{12}$ = 1.1 and $g_{13}$ = 1.4 and taking for $g_{23}$ 0.4 or 0.5 respectively. It is obvious that a very high value of the interaction parameter $g_{23}$ (greater than 1) should be introduced to obtain a good agreement between $\chi$ exp and $\chi$ theor.

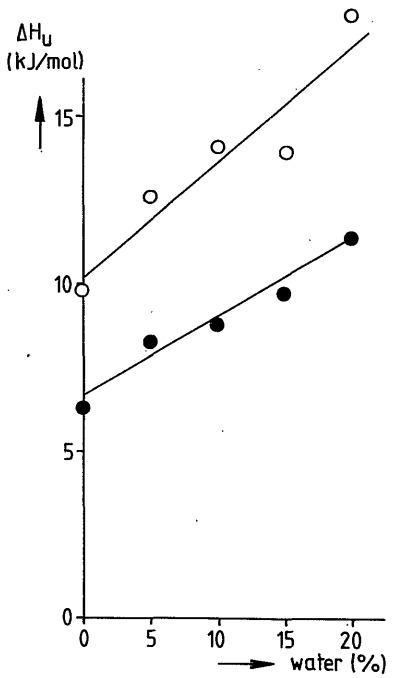


FIG.5. Heats of fusion as a function of percentage of water in the dioxane/water mixture, (•) Flory expression, (o) Hoffman modification.

A few remarks should be made here concerning the choice of the interaction parameters:

- we assumed a concentration independence of the polymer/solvent interaction parameter $g_{23}$. A partial justification of this assumption comes from a separate determination of this parameter by osmometry. We have found that below 25% polymer in the system and in the temperature range

from 20-40°C there is only a very small dependence on temperature and concentration.[18] The dependence on concentration is less than the one given by Moore.[24]

- the interaction parameter $g_{13}$ has been estimated from equilibrium swelling measurement data from several authors, for instance Toprak.[19]
- for the parameter $g_{12}$ we have taken an effective value of 1.1.
- The choice of these parameters ($g_{12}$ = 1.1 and $g_{13}$ = 1.4) also serves as a good basis for the calculation of ternary phase diagrams for liquid-liquid phase separation in the same polymer/solvent/nonsolvent, if we compare calculated diagrams with experimental liquid-liquid phase separation cloud point lines of Figure 1.[22] The g-parameters introduced are room temperature values.

In Figure 5 the ΔHu values of Table 2 are presented. The apparent heat of melting in our systems increases with increasing water content. Only one literature value for the heat of fusion seems to be available. Takahashi[12] determined a value of 9.9 kJ per mole of CTA in Dibutylphtalate, using the Flory equation for the melting point depression.

The experimentally found melting point dependence is qualitatively predicted by equation (8): $T_m$ decreases upon increasing the nonsolvent content at fixed polymer volume fraction. The theory predicts a much steeper dependence of $T_m$ on the nonsolvent content.*) To correct mathematically for this small dependence we have to introduce the dependence of ΔHu on the nonsolvent concentration.

Another important point to consider is the high $g_{23}$-parameter which follows when comparing the experimental and theoretical behaviour of $T_m$ as a function of polymer volume fraction at a fixed solvent/nonsolvent composition-ratio.

*) Paul[25] states that the melting point of a gel in a solvent/nonsolvent mixture is always higher than without a nonsolvent.

Again the experimentally found dependence is lower than predicted with our set of interaction parameters. The discrepancy is present at p = 0(in the absence of nonsolvent) and it is preserved at higher p values. Possibly a better agreement can be found when composition dependent interaction parameters are used.

The simple equation requires future improvement to understand the apparent dependence of ΔHu on the nonsolvent content of the solvent/nonsolvent mixture. One improvement will be suggested in 4.5.3.3.

From our results we conclude that water has an ordering effect on cellulose acetate giving rise to a larger apparent heat of fusion per mole of crystalline units upon increasing the water content in the solvent/nonsolvent mixture.

### 4.5.3 Some further remarks

#### 4.5.3.1 Kinetic effects of increasing water content

From our measurements we conclude that water increases the ordering of the cellulose acetate in the gel. We have also found indications that an increase in the water content has an influence on the kinetics of the process: The area under the endotherm approaches its final value faster.

In this way we can understand that it might sometimes be useful to add a certain amount of nonsolvent to the casting solution prior to coagulation of the cast film.

#### 4.5.3.2 Degree of crystallinity

Using the value of the heat of fusion, we determine the degree of crystallinity in the gels. A value of 10 kJ per mole of crystalline units (Mu = 288) equals 35 J/g polymer units. A value for Q of 1.2 J/g polymer gives a degree of crystallinity of about 4%. If we use the same value for the systems which undergo liquid-liquid phase separation prior to gelation the result is 14%, quite a high value for the degree of crystallinity. Analyzing the melting point dependence of this type of gels we find a value for ΔHu of 28 kJ/mole.Using this value the degree of crystallinity would

become about 5%.

4.5.3.3 Surface effects

In our simplified description we did not take into account the possibility of a mixed crystal, e.g. a crystalline phase containing (mixed) solvent. Further experiments are necessary to test whether this assumption is justified.

Equation (5) describes the melting of an ideal (infinite dimensions) crystal in equilibrium with the solution, without the introduction of surface phenomena. As has been noted in section 4.4.2.4 of the results, the melting temperature depends on the temperature of aging. This indicates that surface effects should be taken into consideration. The crystal size is expected to be small. Borchard et al.[23] have treated this problem recently for the case of gelatin gels. If, in further experiments with our system, the same results should be found as in his DSC experiments, then the melting point taken from DSC experiments would be lower than the true equilibrium values (surface effects gave an additional melting point depression). The melting point dependence would give an underestimate of the true $\Delta H_u$ value, and the slope dependence (or the interaction parameter $g_{23}$) would be overestimated by introducing our (nonequilibrium) melting points. In order to test the theory of Borchard one should perform the same experiments as given in Figure 2a at different crystallization or annealing temperatures.

In the Appendix the crystal-liquid phase diagram is calculated on the basis of the equations given in this Chapter.

## 4.6 CONCLUSIONS

In the membrane forming system cellulose acetate/dioxane/water crystallization is found to occur at high polymer weight fractions and at low nonsolvent content (water).

The melting point curves for the gel can be described

by the melting point depression equation of Flory, although high values of the polymer-solvent interaction parameter must be introduced. The apparent heat of fusion per mole of crystalline units increases with the nonsolvent content. Probably consideration of surface effects can lead to improvement of the description.

Water is a nonsolvent in the system and it has a positive effect on the ordering of the cellulose acetate; the rate of crystallization and the final degree of crystallinity are increased upon increasing the water content.

## 4.7 REFERENCES


1. D.M.Koenhen, M.H.V.Mulder and C.A.Smolders, J.Appl.Polym. Sci., 21,199(1977)
2. Chapter 3 of this thesis
3. R.B.Richards, Trans.Faraday Soc., 42,10(1946)
4. P.J.Flory, L.Mandelkern, and H.K.Hall, J.Am.Chem.Soc., 73,2532(1951)
5. P.J.Flory, Principles of Polymer Chemistry, Cornell University Press, New York, 1953, p.549 and 568
6. H.Tompa, Polymer Solutions, Butterworths, London 1956, p.183
7. R.Koningsveld, H.A.G.Chermin, and M.Gordon, Proc.Roy. Soc., A319,331(1970)
8. P.T. van Emmerik and C.A.Smolders, J.Polym.Sci., A2,9, 293(1973)
9. Dr.J.L.P.Pijpers, DSM, personal communication
10. M.A.Harrison, P.H.Morgan, and G.S.Park, Faraday Disc., 57,38(1974)
11. M.A.Harrison, P.H.Morgan, and G.S.Park, Europ.Polym.J., 8,1361(1972)
12. A.Takahashi, T.Kawaharada, and T.Kato, Polym.J., 11,571 (1979)
13. I.I.Ryskina and V.M.Averyanova, Polym.Sci.USSR, 13,2457 (1971)

14. J.E.Eldridge and J.D.Ferry, J.Phys.Chem., 58,992(1954)
15. A.Takahashi, T.Nakamura, and I.Kagawa, Polym.J., 3,207 (1972)
16. C.J.Malm, J.W.Mench, D.L.Kendall, and G.D.Hiatt, Ind.Eng. Chem., 43,688(1951)
17. J.D.Hoffman, J.Chem.Phys., 28,1192(1958)
18. Chapter 6 of this thesis
19. C.Toprak, J.N.Agar, and M.Falk, J.Chem.Soc.Faraday Trans. I., 75,803(1979)
20. G.N.Malcolm and J.S.Rowlinson, Trans.Far.Soc., 53,921 (1957)
21. J.R.Goates and R.J.Sullivan, J.Phys.Chem., 62,188(1958)
22. Chapter 5 of this thesis
23. W.Borchard, W.Bremer, and A.Keese, Colloid Polym.Sci., 258,516(1980)
24. W.R.Moore and R.Shuttleworth, J.Polym.Sci., A1,733(1963)
25. D.R.Paul, J.Appl.Polym.Sci., 11,439(1967)

## 4.8 APPENDIX

### CRYSTAL-LIQUID PHASE DIAGRAM

The crystal-liquid phase diagram can be predicted when we apply the Flory-Huggins theory for the melting point depression (equation (5)). As an example we consider the system CA/dioxane/water.

Suppose that the lowering of the chemical potential of the crystalline polymer can be represented by equation (2) $(1/T_m-1/T_m^o)\Delta Hu/R$, with a constant value $\Delta Hu=10kJ/mole$. $T_m$ and $T_m^o$ are the melting point of the gel and of the pure crystal (579K) respectively. The chemical potential of the polymer in the liquid phase is calculated at constant ratio of solvent and nonsolvent with $g_{12}=1.1$, $g_{13}=1.4$ and $g_{23}=0.4$. From

equation (5) the polymer volume fraction can be calculated at which the polymer is expected to crystallize. The result is given in a ternary diagram in Figure 1.

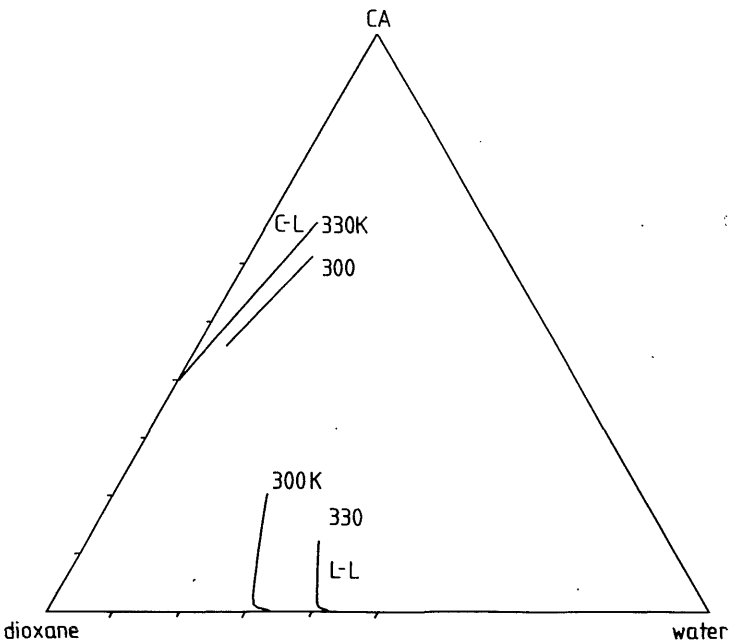


FIG.1. Crystal-liquid (C-L) transition at 300 and 330 K in CA/dioxane/water. Also shown is the L-L transition.

This presentation is in accordance with the trend of the melting point experiments: introduction of water gives a lower melting point at constant polymer concentration. CA is expected to crystallize at higher concentration when the waterpercentage in the solvent/nonsolvent increases.

# 5. CALCULATION OF LIQUID-LIQUID PHASE SEPARATION IN A TERNARY SYSTEM OF A POLYMER IN A MIXTURE OF A SOLVENT AND A NONSOLVENT.*)

F.W.ALTENA and C.A.SMOLDERS
Department of Chemical Technology, Twente University of Technology, P.O.Box 217, 7500 AE Enschede, The Netherlands.

## 5.0 ABSTRACT

A numerical method for the calculation of the binodal of liquid-liquid phase separation in a ternary system is described. The Flory-Huggins theory for three component systems is used. Binodals are calculated for polymer/solvent/nonsolvent systems which are used in the preparation of asymmetric ultrafiltration or reverse osmosis membranes: cellulose acetate/solvent/water and polysulfone/solvent/water. The values for the binary interaction parameters are taken from literature sources. The effect of a concentration dependent solvent/nonsolvent interaction parameter is discussed. Although knowlegde of the interaction parameters for all compositions in the ternary system is rather poor, a fairly good agreement has been found between calculated and experimentally found miscibility gaps, when the solvent/nonsolvent parameter is taken to be concentration dependent and the other parameters, the polymer/solvent and the polymer/nonsolvent interaction parameter are kept constant.

*) Submitted for publication to Macromolecules

## 5.1 INTRODUCTION

The equilibrium thermodynamic properties of the system polymer/solvent/nonsolvent play an important role in the description of the formation process of an asymmetric reverse osmosis or ultrafiltration membrane. Such membranes are usually prepared by casting a concentrated polymer solution in a thin film on a supporting surface and immersing this film in a nonsolvent bath. Depending on the choice of the system there are three possible results[1,2]: (i) a uniformly dense film having a porosity comparable to that of the bulk polymer obtained from evaporation procedures, (ii) a porous membrane containing an important void fraction, or (iii) a thin dense toplayer on a porous supporting layer. The latter is the desired asymmetric structure. Examples are membranes formed from solutions of cellulose acetate (CA) and polysulfone (PSn), coagulated in water. An example of the first category, a homogeneous, dense CA membrane, is obtained when using acetone as the solvent. A rather porous membrane is the result if triethylphosphate (TEP) is used as the solvent. Examples of the third category are membranes from casting solutions of CA with solvents dioxane, acetic acid or DMF, and solutions of PSn with DMF or DMAc as the solvent. Some of these membranes have reverse osmosis (salt rejection) properties whereas others have typical ultrafiltration properties.

An explanation of these observations should be based on two sets of factors: (I) the equilibrium thermodynamic properties of the three component system polymer/solvent/nonsolvent, such as liquid-liquid phase separation and gelation, and (II) the exchange of solvent and nonsolvent during membrane formation and the effect on the kinetics of the above-mentioned demixing phenomena. A proper model for the formation process of asymmetric membranes should of course include both sets of factors.

An interesting observation concerning the thermodynamic properties of the systems is that systems which require only small amounts of nonsolvent (i.e.<10% water) to obtain li-

quid-liquid phase separation, e.g.CA in TEP or DMF, and PSn in DMF or DMAc, give a membrane with ultrafiltration properties.[1,3-5] If a large amount of water is needed to achieve precipitation (≃ 30% water) the result is a membrane with reverse osmosis properties, e.g. CA in dioxane, acetic acid or acetone. These facts are illustrated in Figure 1.

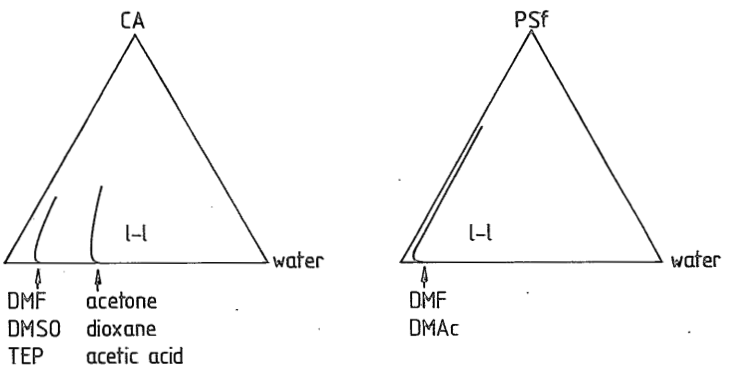


FIG.1. Approximate situation of the liquid-liquid (l-l) phase separation gap in important membrane forming systems.

We have suggested before[3,6] that the porosity of the sublayer can be ascribed to liquid-liquid phase separation, the pores being formed most probably by nucleation and growth of the dilute polymer phase. In this paper we will try to predict binodal liquid-liquid phase separation curves in a few polymer/solvent/nonsolvent systems on the basis of the thermodynamics of polymer solutions.

Recently Cohen et al.[2] proposed a different model for the formation of porous structures in the coagulation step during membrane formation. Their model is not based on the nucleation and growth mechanism but on diffusion-induced liquid-liquid phase separation at the spinodal in the ternary system. In their model, which also includes a solution of the diffusion problem, the location and the form of the spinodal and binodal are of decisive importance. These curves have

been calculated on the basis of the Flory-Huggins theory.[7] The binary interaction parameters which enter the equations have been estimated from literature data. In our opinion these parameters have not been taken from the best possible sources. As will be shown later the spinodal and binodal depend very strongly on the choice of these parameters. Moreover the authors do not give details of their calculation procedure. This calculation is not a trivial matter.[7,8]

Tompa[8] was the first to present calculated phase diagrams for liquid-liquid phase separation in a ternary polymer/solvent/nonsolvent system. Later Koningsveld et al.[9] extensively studied the influence of the molecular weight distribution on the location of the liquid-liquid phase separation gap and the fractionation of the polymer in this demixing process. In principle Koningsveld's calculation procedures can be used. The location of the miscibility gap however depends primarily on the values of the interaction parameters. For our studies on membrane formation we are at this stage not interested in the much less pronounced effect of the molecular weight distribution. Knowlegde of the values of the binary interaction parameters is still rather poor; at least a strong dependence of the binary parameter on the composition of the system and possibly also ternary interaction parameters must be taken into account. Our aim is to compare calculated miscibility gaps in widely different polymer/solvent/nonsolvent systems with experimentally determined phase transitions boundaries.

If equations for the chemical potentials of the components are available, the least-squares calculation procedure of Hsu and Prausnitz[10] seems in principle to be appropriate for the calculation of the binodal in a ternary system.

## 5.2 THERMODYNAMICS OF THREE COMPONENT SYSTEMS

We use the Flory-Huggins theory for polymer solutions[7] extended to systems with three components by Tompa.[8] In recent years equation-of-state theories have been formulated as improvements of the Flory-Huggins theory, but application to (polar) ternary systems is scarce and full of limitations, e.g. see Horta.[11]

The Gibbs free energy of mixing is given by the following relation:

$$\Delta G_m/RT = n_1 \ln\phi_1 + n_2 \ln\phi_2 + n_3 \ln\phi_3 + g_{12}(u_2) n_1 \phi_2 + \chi_{13} n_1 \phi_3 + \chi_{23} n_2 \phi_3 \qquad (1)$$

The subscripts refer to nonsolvent(1), solvent(2) and polymer(3). $n_i$ and $\phi_i$ are the number of moles and the volume fraction of component i respectively. R and T have their usual significance. $\chi_{13}$ is the nonsolvent-polymer interaction parameter and $\chi_{23}$ is the solvent-polymer interaction parameter. $g_{12}$ is the solvent-nonsolvent parameter and it is assumed to be a function of $u_2$, with $u_2 = \phi_2/(\phi_2+\phi_1)$ in the notation of Pouchly et al.[12]

The conditions for liquid-liquid equilibrium are:

$$\Delta\mu_i' = \Delta\mu_i'' \qquad i = 1,2,3 \qquad (2)$$

The superscripts ' and " denote the dilute and concentrated phases respectively.

From equation (1) we derive the following equations for the chemical potentials of the components in the mixture:

$$\Delta\mu_1/RT = \ln\phi_1 - \phi_1 - s\phi_2 - r\phi_3 + (g_{12}\phi_2 + \chi_{13}\phi_3)(\phi_2+\phi_3) - s\chi_{23}\phi_2\phi_3 \phi_2 u_1 u_2 (dg_{12}/du_2) \qquad (3)$$

$$\Delta\mu_2/RT = s\ln\phi_2 - \phi_1 - s\phi_2 - r\phi_3 + (g_{12}\phi_2 + \chi_{23} s\phi_3)(\phi_1+\phi_3) - \chi_{13}\phi_1\phi_3 + \phi_1 u_1 u_2 (dg_{12}/du_2) \qquad (4)$$

$$\Delta\mu_3/RT = r\ln\phi_3-\phi_1-s\phi_2-r\phi_3+(\chi_{13}\phi_1+\chi_{23}s\phi_2)(\phi_2+\phi_1) -g_{12}\phi_1\phi_2 \qquad (5)$$

The chemical potentials are expressed per mole of segments of component (1); s and r are the ratios of the molar volumina $v_1/v_2$ and $v_1/v_3$ respectively.

Only binary interaction parameters are considered. Their values have either been taken from the literature ($g_{12}=g_{12}(u_2)$) or they have been determined from separate experiments ($\chi_{13}$ and $\chi_{23}$; at this stage assumed to be constant with change in composition). In the calculations the effect of constant or composition dependent solvent/nonsolvent ($g_{12}$) interaction parameters on liquid-liquid phase separation has been investigated.

## 5.3 METHOD OF COMPUTATION

### 5.3.1 Calculation of the binodal

Tielines connect the coexisting phases (points on the binodal curve) which have compositions in the dilute phase ($\phi_1', \phi_2', \phi_3'$) and in the concentrated phase ($\phi_1'', \phi_2'', \phi_3''$). In order to determine the tieline we must determine these six unknowns. Three relations between the variables are given by equations (3) to (5). The material balance equations ($\Sigma\phi_i=1$ for the dilute and the concentrated phase) give another two equations. By choosing one variable (in our case $\phi_3'$) and substituting the material balance equations into (3) to (5) the problem reduces to computation of three unknowns from three non-linear transcedental equations. As independent variables we have chosen $\phi_2''$, $\phi_3''$ and $\phi_2'$.

The numerical procedure is essentially the same as that of Hsu and Prausnitz.[10] They used a least-squares procedure, which appears to be effective. The objective function which has to be minimized is:

$$F = \Sigma f_i^2 \qquad (6a)$$

$$\text{with } f_i = (\Delta\mu_i' - \Delta\mu_i''), \quad i=1,2,3 \tag{6b}$$

and the chemical potentials are given by the equations (3), (4) and (5). By expressing the chemical potentials per mole of segments of component 1 the contributions of the residuals $f_i$ are of comparable size.

The coexisting compositions are found by an iterative process. We have used the numerical procedure given by Gill and Murray.[13] This procedure uses first (and second) derivatives of the expressions for the chemical potentials. In this way considerable improvements were obtained as compared with the calculation procedure used by Hsu:

- no penalty functions are needed to avoid a trivial solution,
- scaling of the volume fractions is not necessary,
- the starting point of the iteration process is less sensitive than in the method used by Hsu.

Convergence was considered to be attained when $F<10^{-10}$. The CPU time required for the calculation of 20-50 tielines in the ternary diagram was about 1-3 seconds, depending on whether concentration dependent $g_{12}$ parameters were used or not. The complete miscibility gap is obtained by varying the chosen variable, the polymer concentration in the dilute phase $\phi_3$, by a factor ten.

5.3.2 Calculation of the spinodal

The equation for the spinodal is:[8]

$$G_{22}G_{33} = G_{23}^2 \tag{7}$$

$$\text{where } G_{ij} = \frac{\partial^2 \Delta G_m}{\partial\phi_i \partial\phi_j}$$

It follows, using equation (1):

$$G_{22} = \frac{1}{\phi_1} + \frac{1}{\nu_2\phi_2} - 2g_{12} + 2g_{12}'(u_1-u_2) + g_{12}''u_1u_2 \tag{8}$$

$$G_{33} = \frac{1}{\phi_1} + \frac{1}{\nu_3\phi_3} - 2\chi_{13}+2u_2^2(1+u_1)g'_{12}+u_2^3u_1g''_{12} \qquad (9)$$

$$G_{23} = \frac{1}{\phi_1} - \chi_{13} + \frac{\chi_{23}}{\nu_2} - g_{12}-u_1u_2g'_{12}-u_1u_2^2g''_{12} \qquad (10)$$

where $g'_{12} = \partial g_{12}/\partial u_2$ and $g''_{12} = \partial^2 g_{12}/\partial u_2^2$.

We assumed $\nu_1=1$.
For the case of constant interaction parameters, the equations reduce to the equation given by Tompa[8]:

$$\sum\nu_i\phi_i-2\sum\nu_i\nu_j(\chi_i+\chi_j)\phi_i\phi_j+4\nu_1\nu_2\nu_3(\chi_1\chi_2+\chi_1\chi_3+\chi_2\chi_3)\phi_1\phi_2\phi_3 = 0 \qquad (11)$$

where
$$\begin{aligned} 2\chi_1 &= \chi_{12}+\chi_{13}-\chi_{23}/\nu_2 \\ 2\chi_2 &= \chi_{12}+\chi_{23}/\nu_2-\chi_{13} \\ 2\chi_3 &= \chi_{13}+\chi_{23}/\nu_2-\chi_{12} \end{aligned} \qquad (12)$$

When the interaction parameters are known and one variable is chosen (e.g. $\phi_3$), substitution of the material balance equation $\sum\phi_i=1$ in equation (8) will give one equation with one variable to be solved. This is done by using the same numerical procedure as has been used for the calculation of the binodal.

## 5.4 EVALUATION OF THE BINARY FUNCTION $g_{12}$

The function $g_{12}$ is needed at the temperature at which cloud point curves have been obtained. The parameters are calculated from literature data on $G^E$, generally obtained from vapour pressure experiments. For a two component system $G^E$ is related to the Gibbs free energy of mixing by the equation:

$$G^E = \Delta G_{mix}-RT(x_1\ln x_1+x_2\ln x_2) \qquad (13)$$

where $x_1$ and $x_2$ are the mole fractions of the nonsolvent (1) and the solvent (2). For 1 mole of mixture:

$$\frac{\Delta G_{mix}}{RT} = x_1 \ln\phi_1 + x_2 \ln\phi_2 + g_{12} x_1 \phi_2 \qquad (14)$$

From equation (14) $g_{12}$ is calculated as a function of $\phi_2$.

Only for a few solvent/water systems experimental data on $G^E$ are available (see compilation of literature references by Wisniak and Tamir[14]). In Table 1 the sources are listed from which data on $G^E$ have been taken.

| solvent | nonsolvent: water |
|---|---|
| dioxane | Kortüm[15], Goates[16], Malcolm[17] |
| acetone | Orye[18], Othmer[19] |
| DMF | Saphon[20] |
| DMSO | Lam[21], Chan[22] |
| acetic acid*) | Gieskes[23], Haase[24] |
| TEP | no data available |
| DMAc | no data available |

*) Conflicting data

Table 1: Literature sources on $G^E$ of solvent/nonsolvent mixtures.

The binary parameter $g_{12}$ calculated from these data is given for the different solvents in Figure 2. For acetic acid we have used data of Haase[24]

The magnitude of $g_{12}$ and its variation with concentration influence the thermodynamic properties of a ternary system to a great extent, see e.g. Aminabhavi.[25]

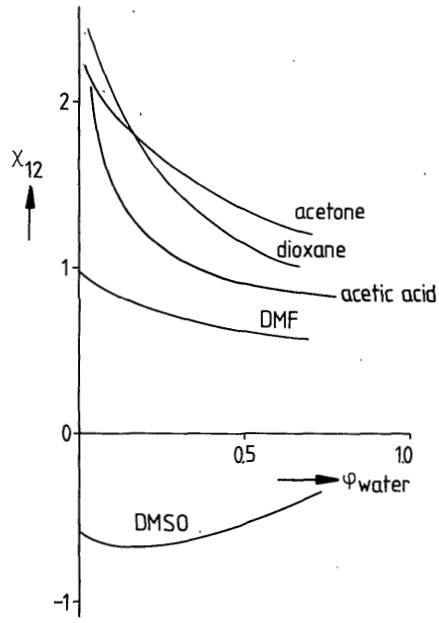


FIG.2. Concentration dependent interaction parameters in binary solvent/water systems.

## 5.5 EVALUATION OF BINARY PARAMETERS $\chi_{13}$ AND $\chi_{23}$

The interaction parameter $\chi_{13}$ is determined from equilibrium swelling measurements carried out by Mulder[26] for instance at different temperatures. We have used the value of 1.4 for the interaction parameter for CA/water and the value of 3.7 for PSn/water (25°C).

The solvent/polymer parameter $\chi_{23}$ is taken from work done in our laboratory.[27] We determined this parameter using osmometry. For CA/acetone and CA/dioxane we have found the values 0.45 and 0.40 respectively, at 10 wt% polymer and 25°C. In this Chapter we do not consider the concentration dependence of this parameter. For other polymer/solvent combinations there are no data available.

## 5.6 RESULTS AND DISCUSSION

### 5.6.1 General

The predicted polymer concentration in the dilute phase rapidly approaches a very small value. For each successive tieline given in the figures the polymer concentration in the dilute phase is a factor ten lower if one moves to the right. In some figures tielines have been calculated for a polymer concentration $\phi_3'$ of $10^{-30}$. Of course this value can have no physical meaning.

Tompa[8] calculated tielines for a simple case: $\nu_1=\nu_2$; $\chi_{12}=\chi_{13}=1.5$ and $\chi_{23}=0$. The results of our calculations with these values for the parameters agree completely with his phase diagram.

### 5.6.2 Constant interaction parameters

Our procedure allows for arbitrarily chosen values of the interaction parameters $\chi_{ij}$ and molar volume ratios $\nu_i/\nu_j$. All practical systems which we consider have a large ratio of solvent and nonsolvent molar volumes. i.e. $\nu_1/\nu_2 \simeq 0.2$. For the polymer volume ratio we have chosen $\nu_1/\nu_3 = 0.002$.

First we will consider the case of changing the solvent in the system (thus changing $\chi_{12}$) while keeping the polymer-solvent and polymer-nonsolvent parameters constant. At two fixed values of $\chi_{13}$, 1 and 1.5, the effect of changing the solvent-nonsolvent parameter can be seen from the Figures 3a and 3b. Increasing the $\chi_{12}$ parameter results in a quite drastic change in the location of the miscibility gap. It appears that a low tendency of mixing of solvent and nonsolvent, as expressed by a large value of $\chi_{12}$, favours the mixing of the ternary system: more nonsolvent is needed for liquid-liquid phase separation. Another interesting point to observe is the polymer concentration in the concentrated phase which is much higher at low $\chi_{12}$ than at high $\chi_{12}$ for the same degree of penetration of the liquid-liquid phase separation region (here measured as $\phi_3''$ at the same $\phi_3'$ at curves for different $\chi_{12}$). The tendency of the location of

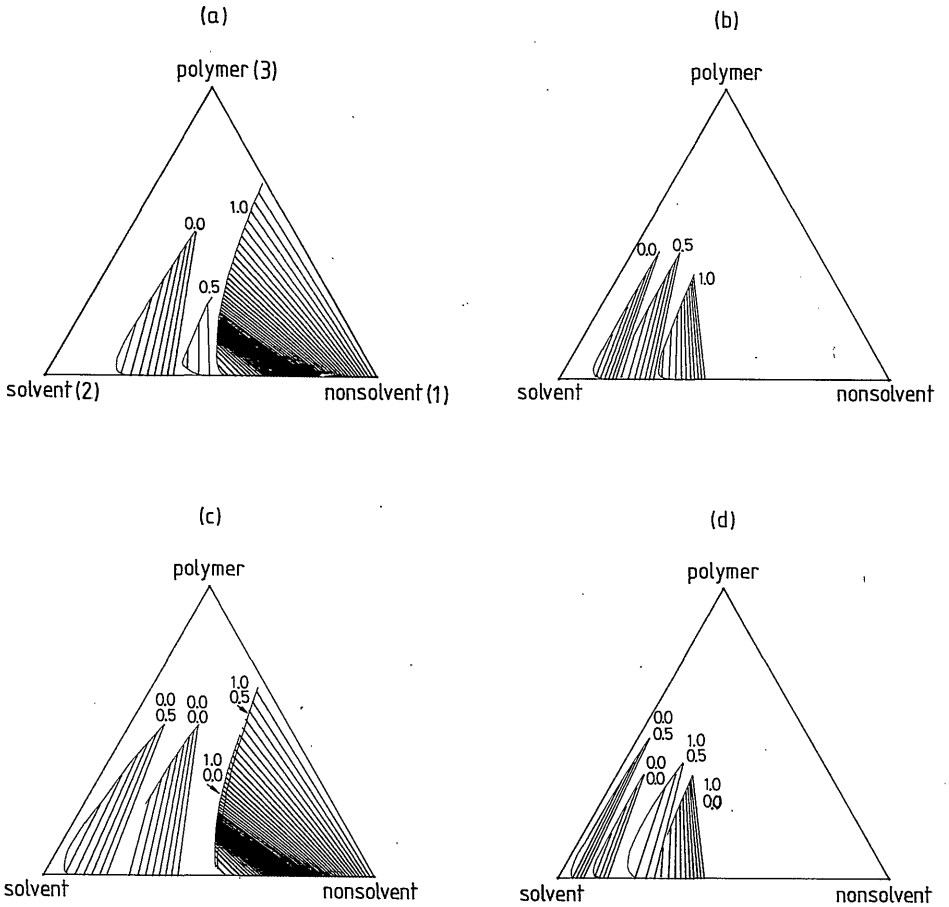


FIG.3. Tielines and binodals in polymer/solvent/nonsolvent systems for constant interaction parameters. Effect of varying $\chi_{12}$ (values given in the figure) at (a) $\chi_{13}=1.0$ and (b) $\chi_{13}=1.5$. Effect of varying $\chi_{23}$ (lower number at each curve) at certain values of $\chi_{12}$ (upper number for (c) $\chi_{13}=1.0$ and (d) $\chi_{13}=1.5$.

the miscibility gap to move to the right in the ternary diagrams is not yet understood on physical grounds.

Secondly, we consider the influence of a changing solvent quality for the polymer ($\chi_{23}$) on the location of the tielines. Results are presented in Figures 3c and 3d.
At low values of $\chi_{12}$ the effect of increasing $\chi_{23}$ is consi-

derable, but in opposite direction of increasing $\chi_{12}$, whereas at high values of $\chi_{12}$, especially at $\chi_{12}=1$, there is only a small effect on the location of the liquid-liquid phase separation region. A higher value of $\chi_{23}$ decreases the amount of nonsolvent necessary for phase separation. This is also the result of choosing a higher $\chi_{13}$ parameter. Qualitatively these effects are not difficult to understand. The effect of changing $\chi_{13}$ can be seen more clearly by comparing Figures 3a and 3b.

### 5.6.3 Comparison with phase diagram for CA/acetone/water from Cohen et al.

Cohen et al.[2] have calculated the binodal for the system CA/acetone/water and CA/acetic acid/water. For the acetone system they used the following interaction parameters: $\chi_{12}=-0.30$, $\chi_{13}=1$ and $\chi_{23}=0.2$ with $\nu_1:\nu_2:\nu_3=1:4:500$. We calculated tielines of the liquid-liquid phase separation with the same set of parameters. Our results and the diagram of Cohen are compared in Figure 4. There are small differences in the location of the binodals. Cohen gives no details of his calculation procedure, so that the exact origin of these differences cannot be traced.

In our opinion a much better choice of the interaction parameters is possible from literature data. Swelling measurements indicate a CA/water parameter of about 1.4. The CA/acetone parameter takes the value of about 0.45. More important, however, is the influence of the solvent/nonsolvent parameter. From Figure 2 we conclude that $\chi_{12}$ has at least a large positive value, and not a value of -0.3 as assumed by Cohen. Cohen et al. based their estimate of the $\chi_{12}$ parameter only on the enthalpy of mixing and not on the free energy of mixing as they should have done.

In Figure 5 the phase diagram is given for a positive value of $\chi_{12}$, i.e. 0.5. The other parameters are kept at the values which Cohen used. The spinodal has also been calculated for this case. The result could have a very serious effect on the conclusion of the study of Cohen et al., that

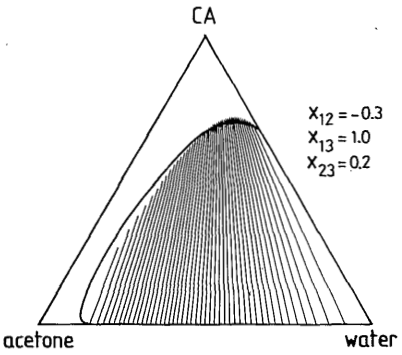


FIG.4. Comparison of calculated binodal with literature (Cohen et al.[2], solid curve) for the system CA/acetone/water. Values of interaction parameters are given.

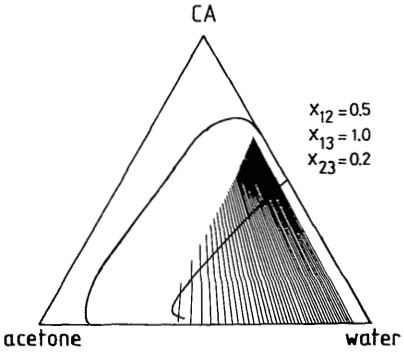


FIG.5. Effect of change in acetone/water interaction parameter from -0.3 to 0.5. The left full curve has been taken from Cohen et al. The right full curve is the spinodal.

phase separation at the spinodal produces the porous substructure of CA membranes. It appears to us that a curvature of the binodal and the spinodal at high polymer concentration as shown by the Cohen curve in Figures 4 and 5, is necessary to reach their conclusion. From Figure 5 we see that the curvature disappears if $\chi_{12}$ is given a more reasonable i.e. positive value. We suggest that their description could very well depend too critically on the choice of the interaction parameters. Another, more basic objection to their conclusion is that spinodal decomposition at not too high polymer concentrations (such as in the casting solution) has not yet been found experimentally.

5.6.4 Concentration dependent $g_{12}$ parameters

Keeping the other interaction parameters constant, we now consider a composition dependent $g_{12}$ parameter (cf. Fi-

gure 2); $g_{12}$ is calculated from literature data on $G^E$. In our calculations we use the data for each solvent from the first mentioned author in Table 1. There can be considerable differences between data of different authors, e.g. in $G^E$ for acetic acid/water.[23,24] These differences are reflected in the results of the calculation of the binodals.

For the $g_{12}(\phi_2)$-function a fourth grade polynomial relation has been chosen; the coefficients were found by using a least squares method. The function fits the $g_{12}$ values calculated from the experimental data within 3%. Using this $g_{12}$-function we calculated $\Delta G_{mix}$ (equation 14) over the full composition range to check if demixing in some range of the solvent/nonsolvent mixture without polymer is predicted. This would of course have a serious effect on the subsequent calculations. For instance the $g_{12}$-function calculated from the data of Goates[16] on dioxane/water predicts liquid-liquid phase separation at about a 50/50 mixture of dioxane/water. The coefficients of the interaction parameter function $g_{12}$ are given in Table 2.

| solvent | $\nu_1/\nu_2$ (25°C) | $g_{12}=a+b\phi_2+c\phi_2^2+d\phi_2^3+e\phi_2^4$ | | | | |
|---|---|---|---|---|---|---|
| | | a | b | c | d | e |
| dioxane | 0.2092 | 0.92 | -0.69 | 7.15 | -12.91 | 8.17 |
| acetone | 0.2442 | 1.10 | -0.42 | 4.09 | -6.70 | 4.28 |
| DMF | 0.2336 | 0.50 | 0.04 | 0.80 | -1.20 | 0.82 |
| DMSO | 0.2540 | -0.25 | -0.69 | 1.15 | -2.9 | 2.09 |
| acetic acid | 0.3151 | not considered further | | | | |

Table 2: Concentration dependent solvent/nonsolvent interaction parameters.

5.6.5 Comparison with experimental data

5.6.5.1 Cellulose acetate (CA)

There is not much information on the location of the liquid-liquid phase separation gap in CA systems. Frommer[1] and Guillotin[4] give values for the precipitation concentra-

tion for water at about 20% polymer. We have determined cloud points for CA/dioxane/water[3] and also for CA/DMF/water (Figure 8). Strathmann[28] and Lemoyne[5] give data on CA/acetone/water which deviate from the above mentioned sources.

CA/dioxane/water

Experimental points and curves are given in Figure 6. The full curve is calculated using the $g_{12}$ function from Table 2, and with $\chi_{13}=1.4$ and $\chi_{23}=0.4$.

We note a fairly good agreement in the position of experimental and calculated curves. The set of interaction parameters used appears to describe the demixing of the system reasonably well.

The only computed effect of introducing a smaller $\chi_{23}$ value is that the polymer concentration in the concentrated phase is higher at about the same solvent/nonsolvent ratio as compared to the situation drawn in the diagram.

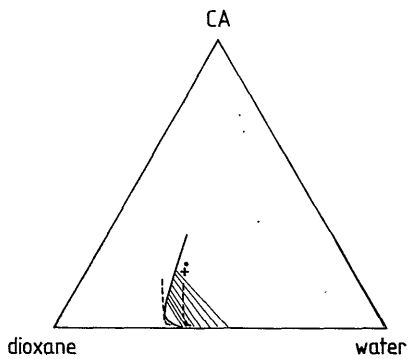


FIG.6. Calculated binodal for CA/dioxane/water (full curve). Dashed curves from cloud point measurements at 20°C (left) and 60°C (right).[31] Single point data from Frommer[1] (+) and Guillotin[4] (.) at 20°C.

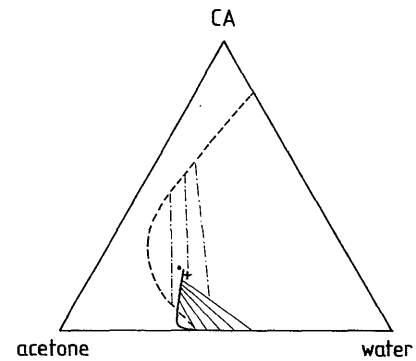


FIG.7. Calculated binodal and tielines for CA/acetone/water. Literature data from Frommer (+), Guillotin (.) ; Strathmann[28] and Lemoyne [5]: binodal (--------) and tielines (-.-.-.-.-).

When a smaller value of $\nu_1/\nu_3$ is used (a value of 0.002 means a molecular weight of 9000; whereas the CA often used has a molecular weight of about 20.000-30.000) no effect on the location of the miscibility gap is found. The distance between the tielines, differing a factor ten in the polymer concentration in the dilute phase, then becomes much smaller.

A similar agreement in location between experimental cloud point curves and theoretical binodals can be obtained by taking an effective, constant, $\chi_{12}$ value of 1.1 instead of $g_{12}(\phi_2)$.

The data from Frommer and Guillotin do not agree with our measurements. The reason for this deviation is not clear.

CA/acetone/water

The experimental information on liquid-liquid phase separation in CA/acetone/water is not very distinct. Strathmann[28] has given so-called tielines. These lines cannot be real tielines because he ignores the obscuring effect of gelation of the concentrated phase at some stage of the separation into two liquid phases in equilibrium. Lemoyne[5] gives a gelation line in the ternary diagram, but he also gives tielines which connect a dilute phase with a concentrated phase that lies within the gelation region of the system. Our calculated diagram ($g_{12}$ from Table 2, $\chi_{13}$=1.4 and $\chi_{23}$=0.45) agrees quite well with the data points from Frommer and Guilotin, see Figure 7.

CA/DMF/water

Results are presented in Figure 8. Our own experimental data confirm the results of Frommer and Guillotin. The calculated curves for polymer/solvent interaction parameters of 0.0 and 0.4 (the precise values are not known) do not agree well with the experimental data.

CA/DMSO/water

Again two calculated binodals are given, in Figure 9,

for $\chi_{23}$ is 0.0 and 0.4. The agreement in position between calculated curves and experimental points is much worse than with the other solvents considered. One reason might be the peculiar behaviour of the binary solvent/nonsolvent system itself. This is the only system with a strong negative value for $\chi_{12}$.

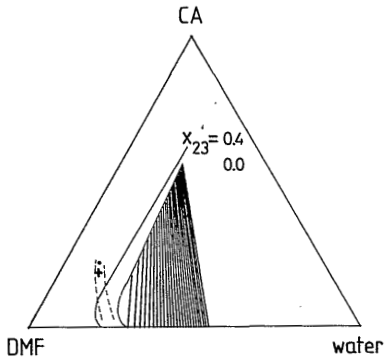


FIG.8. Calculated binodals for CA/DMF/water. Dashed lines from our cloud point experiments at 20°C (left) and 40°C (right). Literature data from Frommer (+) and Guillotine (.)(at 20°C).

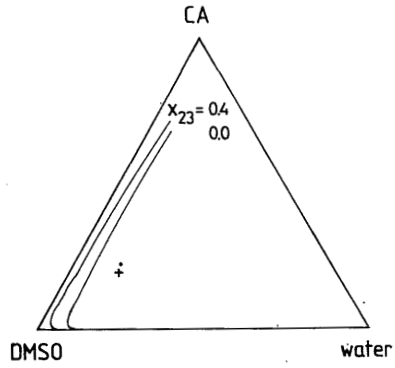


FIG.9. Calculated binodals for CA/DMSO/water for two values of $\chi_{23}$. Literature data from Frommer (+) and Guillotin (.).

5.6.5.2 Polysulfone (PSn)

Demixing data for PSn/DMF/water have been given by Broens[31], Wijmans[29] and Coplan.[30] Only a small amount of water, usually a few percent, is needed to achieve precipitation.

From Figure 10 it is clear that the demixing behaviour is mainly determined by $\chi_{13}$ (we used a value of 3.7). Large variations in $\chi_{12}$ and $\chi_{23}$ only have a small absolute effect on the precipitation concentration. Changing the solvent, for instance by taking DMAc instead of DMF, would have this small effect. A more precise comparison with experimental data can be carried out if $\chi_{23}$ and $\chi_{12}$ are known for both

solvents. The relative influence of a change of the solvent on the membrane forming properties is known to be large.[29]

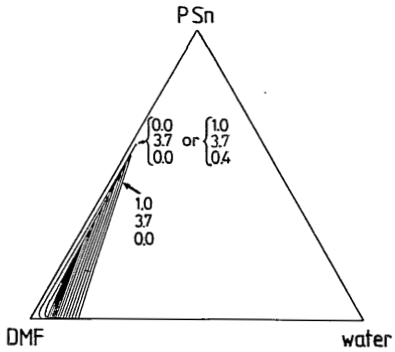


FIG.10. Binodals in PSn/DMF/water at different values of interaction parameters $\chi_{12}/\chi_{13}/\chi_{23}$ (given in figure)

Summarizing the results we can make the following remarks:

- A method of computation of phase diagrams has been developed, which works quite well.
- On the basis of literature information the solvent/nonsolvent interaction parameter $g_{12}$ is assumed to be composition dependent. From our study we conclude that $G^E$, the excess free energy of mixing has to be considered and not only the enthalpy of mixing.[1] Other binary parameters have been kept constant. At this stage a more precise study does not seem relevant without detailed information about the ternary interaction parameters in the system and the molecular weight distribution.
- A change in the solvent of the membrane forming system is reflected in a change in $g_{12}$. The qualitative and quantitative effects on the position of the liquid-liquid phase separation gap can be predicted reasonably well. This is shown for CA systems for which binary parameters are known.
- For PSn a large polymer/nonsolvent interaction parameter determines the demixing behaviour to a great extent. Changes in other binary parameters have only a small effect on the precipitation concentration.

## 5.7 CONCLUSIONS

For the calculation of the binodal in a system of polymer/solvent/nonsolvent we have developed a method of computations which works well.

Introduction of a concentration dependent solvent/nonsolvent interaction parameter gives a reasonable agreement between the experimentally found miscibility gap and the calculated binodal of the liquid-liquid phase separation.

## 5.8 REFERENCES


1. M.A.Frommer and D.Lancet, in Reverse Osmosis Membrane Research, H.K.Lonsdale and H.E.Podall, Eds., Plenum Press New York, 1972, p.85
2. C.Cohen, G.B.Tanny, and S.Prager, J.Polym.Sci.Polym.Phys. Ed., 17,477(1979)
3. Chapter 2 of this thesis
4. M.Guillotin, C.Lemoyne, C.Noël, and L.Monnerie, Desalination, 21,165(1977)
5. C.Lemoyne, J.L.Halary, C.Friedrich, C.Noël, and L.Monnerie, J.Appl.Polym.Sci., 25,1883(1980)
6. D.M.Koenhen, M.H.V.Mulder, and C.A.Smolders, J.Appl. Polym.Sci., 21,199(1977)
7. P.J.Flory, Principles of Polymer Chemistry, Cornell Univ.Press, Ithaca, 1953, p.541
8. H.Tompa, Polymer Solutions, Butterworths, London, 1956, p.182
9. R.Koningsveld, Chem.Zvesti, 26,263(1972) and Brit.Polym. J., 7,435(1975)
10. C.C.Hsu and J.M.Prausnitz, Macromolecules, 7,320(1974)
11. A.Horta, Macromolecules, 12,785(1979)
12. A.Zivný and J.Pouchlý, J.Polym.Sci., A-2,10,1467(1972)
13. P.E.Gill and W.Murray, SIAM J.Numer.Anal., 15,977(1978), available in the NAG library.
14. J.Wisniak and A.Tamir, Mixing and Excess Thermodynamic Properties, Elsevier, Amsterdam (1978)

15. G.Kortüm and V.Valent, Ber.Bunsen Ges.Phys.Chem., 81 752(1977)
16. J.R.Goates and J.R.Sullivan, J.Phys.Chem., 62,188(1958)
17. G.N.Malcolm and J.S.Rowlinson, Trans.Far.Soc., 53,921(1957)
18. R.V.Orye and J.M.Prausnitz, Ind.Eng.Chem., 57,18(1965)
19. D.F.Othmer,Ind.Eng.Chem., 44,1872(1952)
20. S.Sapnon and H.J.Bittrich, Z.Phys.Chem., Leipzig, 252, 113(1973)
21. S.Y.Lam and R.L.Benoit, Can.J.Chem., 52,718(1974)
22. T.C.Chan and W.A. Van Hook, J.Solut.Chem., 5,107(1976)
23. J.T.Th.Gieskes, Can,J,Chem., 43,2448(1965)
24. R.Haase, M.Pehlke, and K.H.Dücker, Zeitschr. für Naturforschung teil A, 28,1740(1973)
25. T.M.Aminabhavi and P.Munk, Macromolecules, 12,607(1979)
26. M.H.V.Mulder, to be published
27. Chapter 6 of this thesis
28. H.Strathmann, P.Scheible, and R.W.Baker, J.Appl.Polym. Sci., 15,811(1971)
29. J.G.Wijmans, private communication
30. M.J.Coplan, R.B.Davis, and J.K.Beale, NTIS PB 287990, Springfield (Va.), 1978
31. Chapter 3 of this thesis

# 6. THERMODYNAMIC PROPERTIES OF CELLULOSE ACETATE IN SOLVENT/NONSOLVENT MIXTURES STUDIED BY OSMOMETRY

F.W.ALTENA, R.J.MOSSEL, H.G.KOETSIER, J.W.A. van de BERG and C.A.SMOLDERS
Department of Chemical Technology, Twente University of Technology, Enschede, The Netherlands.

## 6.0 ABSTRACT

Using osmometry data,interaction parameters of a ternary system of a polymer in a mixed solvent/nonsolvent have been determined in order to predict the composition of the system where liquid-liquid phase separation occurs. The Flory-Huggins theory for a three component system is applied to cellulose acetate/dioxane/water. Both osmotic pressure and preferential sorption are determined at polymer concentrations of up to 10%. Comparison between predicted and experimental values of the osmotic pressure and the preferential sorption shows that reasonable agreement can only be found if, in addition to a concentration dependent solvent/nonsolvent interaction parameter, a ternary parameter is introduced and the polymer/nonsolvent interaction parameter is allowed to vary with the composition of the system. The interaction parameters are extrapolated outside the experimental composition range to predict liquid-liquid phase separation. This turned out to be unsuccessful. The binary CA/solvent parameters determined for acetone and dioxane do not agree with literature data.

## 6.1 INTRODUCTION

The thermodynamics of systems consisting of a polymer, a solvent and a nonsolvent play an important role in the description of asymmetric membrane formation.[1] The basic processes governing the structure formation are liquid-liquid phase separation and gelation.

In order to describe both processes we need a reliable expression for the Gibbs free energy function of the fluid polymer solution. In this Chapter we start from the Flory-Huggins theory[2] in an extended version valid for three components. For our purpose, which is the selection of a membrane forming solvent/nonsolvent combination for a given polymer material, we consider this semi-quantitative approach as being sufficient.

In this theory interaction parameters account for the non-ideality of the system. From earlier studies it is clear that these parameters generally depend on the composition of the system.[3]

Osmometry is a means for determining accurate values for the interaction parameters in a rather concentrated polymer solution. This is particularly the case for a binary polymer/solvent system. Both concentration and temperature dependence have been found in this way.[4] As far as we are aware, osmometry in a ternary system has never been applied for the determination of interaction parameters in concentrated ternary systems. In this Chapter we investigate the possibility of obtaining the interaction parameters from such an experiment. To this end not only the osmotic pressure (or the potential of total sorption[6]) but also the preferential sorption must be measured. Both quantities were measured in the same osmometry experiment for solutions of up to 10 wt% polymer.

The system to be studied here is cellulose acetate (CA)/dioxane/water. The nonsolvent content is such that liquid-liquid phase separation does not yet occur (below 30% by weight of nonsolvent (NS) in the solvent (S)/nonsolvent

(NS) mixture). Also values for the binary parameters CA/dioxane and CA/acetone are obtained from these experiments.

With the interaction parameter thus obtained the total sorption coefficient at infinite dilution is calculated and compared with the value determined from intrinsic viscosity measurements of CA in mixtures of dioxane and water.

The interaction parameters determined in a limited composition region have been extrapolated to higher polymer concentrations and higher nonsolvent content to predict the thermodynamic properties of the system at phase separation conditions.

## 6.2 THERMODYNAMIC RELATIONS

### 6.2.1 Concentration dependent interaction parameters: chemical potentials

We start from the Gibbs free energy function:[31]

$$\frac{\Delta G}{RT} = n_1 \ln\phi_1 + n_2 \ln\phi_2 + n_3 \ln\phi_3 + g_{12}(u_2) n_1\phi_2 + g_{13}(\phi_3) n_1\phi_3 + g_{23}(\phi_3) n_1\phi_3 + g_T(u_2,\phi_3) n_1\phi_2\phi_3 \quad (1)$$

The indices refer to (1) nonsolvent, (2) solvent and (3) polymer. In equation (1), $n_i$ and $\phi_i$ are the mole fraction and the volume fraction of component i. The binary interaction parameter $g_{12}$ (solvent/nonsolvent) is assumed to be a function of the composition of the solvent/nonsolvent mixture $u_2 = \phi_2/(\phi_1+\phi_2) = \phi_2/(1-\phi_3)$. The ternary parameter $g_T$ comprises all non-binary effects.

Differentiation with respect to the respective mole fractions, yields the following equations for the chemical potentials of components 1 and 2:

$$\frac{\Delta u_1}{RT} = \ln\phi_1 + (1-s)\phi_2 + (1-r)\phi_3 + g_{12}\phi_2(\phi_2+\phi_3) - u_1u_2\phi_2 g'_{12} + g_{13}\phi_3(\phi_2+\phi_3) - \phi_1\phi_3^2 g^*_{13} - s\phi_2\phi_3(g_{23}+\phi_3 g^*_{23}) + \phi_2\phi_3\{g_T(1-2\phi_1) - u_1u_2 g'_T - u_1\phi_3 g^*_T\} \quad (2)$$

$$\frac{s\Delta\mu_2}{RT} = s\ln\phi_2 - s\phi_2 - \phi_1 - r\phi_3 + g_{12}\phi_1(\phi_1+\phi_3) + u_1^2\phi_2 g'_{12} - \phi_1\phi_3(g_{13}+\phi_3 g^*_{13}) + sg_{23}\phi_3(\phi_1+\phi_3) - sg^*_{23}\phi_2\phi_3^2 + g_T\phi_1\phi_3(1-2\phi_2) + u_1^2\phi_2\phi_3 g'_T - u_1\phi_2\phi_3^2 g^*_T \qquad (3)$$

where the $g_{12}$ and the $g_T$-parameter are a function of $u_2$ and the superscripts' and * denote the partial derivatives with respect to $u_2$ and $\phi_3$ respectively. The symbols s and r refer to the ratios of the molar volumes $v_1/v_2$ and $v_1/v_3$, respectively.

The osmotic pressure and the equation for the preferential sorption are derived in the next section. Comparison with experimental values (in the Results section) shows that besides introduction of a ternary parameter, another parameter has to be chosen as composition dependent. When the polymer/nonsolvent parameter is taken to be a function of the composition of the solvent/nonsolvent ratio $u_2$, a fairly good agreement is obtained between experimental quantities and values derived from the theoretical equations. The interaction parameter $g_{13}$ then incorporates also ternary interactions. Equations (2) and (3) should contain extra terms, resp.: $-u_1u_2\phi_3 g'_{13}$ and $+u_1^2\phi_3 g'_{13}$. In the subsequent derivations these terms are included in the equations.

### 6.2.2 Osmotic pressure and preferential sorption

We assume osmotic equilibrium between two phases, one with a mixture of solvent and nonsolvent (composition $\phi_1^o$) and the other with polymer dissolved in this mixture. The quantities in the polymer free phase are denoted with the superscript $^o$. At equilibrium we have:

$$\Delta\mu_1^o = \Delta\mu_1 + \pi v_1/RT \qquad (4)$$

$$\Delta\mu_2^o = \Delta\mu_2 + \pi v_2/RT \qquad (5)$$

The equation for the osmotic pressure $\pi$ follows from substitution of (3) in (5):

$$-\frac{\pi v_1}{RT} = s\ln\left(\frac{\phi_2}{\phi_2^o}\right)+s(\phi_2^o-\phi_2)+\phi_1^o-\phi_1-r\phi_3+g_{12}\phi_1^2-g_{12}^o(\phi_1^o)^2$$
$$+g_{12}\phi_1\phi_3+u_1^2\phi_2 g_{12}'-(\phi_1^o)^2\phi_2^o g_{12}'^o-\phi_1\phi_3(g_{13}+\phi_3 g_{13}^*)$$
$$+u_1^2\phi_3 g_{13}'+sg_{23}\phi_3(\phi_1+\phi_3)-s\phi_2\phi_3^2 g_{23}^*+g_T\phi_1\phi_3(1-2\phi_2) \qquad (6)$$
$$+u_1^2\phi_2\phi_3 g_T'-u_1\phi_2\phi_3^2 g_T^*$$

The osmotic pressure $\pi$ can be calculated from equation (6) at constant $\phi_3$ if $\phi_1$(or $\phi_2$) and the values for the interaction parameters are known. The value of $\phi_1$ can be found from the equation defining the preferential sorption. This equation is derived from equations (4) and (5) by eliminating $\pi$ and substitution of equations (2) and (3):

$$\ln\left(\frac{\phi_1}{\phi_2}\right)-\ln\left(\frac{\phi_1^o}{\phi_2^o}\right)+(1-s)\ln\left(\frac{\phi_2}{\phi_2^o}\right)+g_{12}(\phi_2-\phi_1)+g_{12}^o(\phi_1^o-\phi_2^o)$$
$$-u_1\phi_2 g_{12}'+\phi_1^o\phi_2^o g_{12}'^o-u_1\phi_3 g_{13}' +(g_{13}-sg_{23})\phi_3 \qquad (7)$$
$$+g_T\phi_3(\phi_2-\phi_1)-\phi_2\phi_3 u_1 g_T' = 0$$

Above we have followed the derivation outlined by Scott[7], who derived expressions for the osmotic pressure in a ternary system with s=1 and constant (composition independent) parameters, and of Krigbaum and Carpenter[8], who have given equations for s≠1. Our equations reduce in the case of constant interaction parameters to their expressions. We can also compare our expressions with those obtained by Zivny and Pouchly.[6]

The preferential sorption is expressed by the factor:

$$\varepsilon = u_1-\phi_1^o = \phi_2^o-u_2 \qquad (8)$$

as the deviation of the composition $u_1$ of the liquid mixture in the polymer phase from the volume fraction of nonsolvent in the polymer free phase.

We are interested in the behaviour of the osmotic pressure and the preferential sorption upon increasing the nonsolvent content of the mixture. Except for the temperature

the ternary system possesses two degrees of freedom, the composition of the solvent phase $\phi_1^o$ and the volume fraction of the polymer $\phi_3$. These quantities determine the equilibrium values of $\pi$ and $\varepsilon$. The osmotic equilibrium can elegantly be represented for all compositions of the system by plotting osmotic isobars and coexistence lines.[9] An example relevant for our system is given in Figure 1. Coexistence lines represent the composition of the solvent mixture in the polymer phase, which, at an appropriate osmotic pressure difference, can be at equilibrium with a mixed solvent with fixed composition $\phi_1^o$. Osmotic isobars connect points having the same osmotic pressure.

In Figure 1 osmotic isobars and coexistence lines are given for the following set of interaction parameters: $g_{12}=1.1$, $g_{13}=1.4$, $g_{23}=0.4$ and $s=0.2$. The preferential sorption $\varepsilon$ can be read from the deviation of the coexistence curve from the vertical lines which represent (chosen) $\phi_1^o$ values. Four osmotic isobars at selected values of $\pi v_1/RT$ are given.

The chosen binary interaction parameters have previously[10] been used to calculate the liquid-liquid phase separation gap in the system CA/dioxane/water. With these parameters a fairly good agreement was obtained between the locations of the calculated binodal and the experimentally found demixing gap. Figure 1 contains the osmotic isobar $\pi=0$, which according to Pouchly[9] limits the region of restricted miscibility. Indeed this follows from equations (4) and (5) for the case of limiting high molecular weight ($r\to 0$). The phases that coexist at demixing are given in the figure (full dots). The dashed lines connect the two coexisting phases. The open dots indicate the points where inversion of the sign of the preferential sorption takes place.

We observe a predicted minimum in the osmotic isobar as a function of $u_1$. This indicates a maximum of the osmotic pressure as a function of the composition of the solvent/nonsolvent mixture. Furthermore, with this choice of the interaction parameters and at a certain polymer volume frac-

tion, say 10%, we expect a positive value of the preferential sorption at low $u_1$ values (preferential sorption of component 1, water) which increases, passes through a maximum and becomes negative at about $u_1=0.3$.

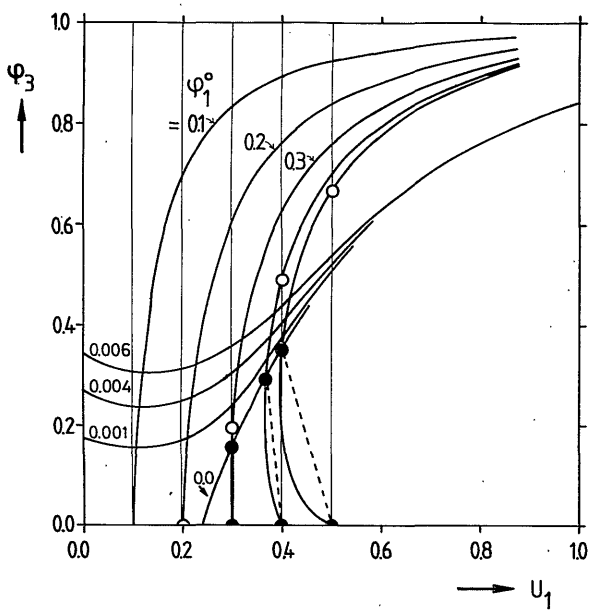


FIG.1. Coexistence lines and osmotic isobars in a ternary system. Values for $\pi v_1/RT$ are indicated for the isobars; values for $\phi_1^o$ are indicated for the coexistence lines. Parameter values: $g_{12}=1.1$, $g_{13}=1.4$, $g_{23}=0.4$ and $s=0.2$. Zero preferential sorption (o). Phases coexisting at demixing (•).

6.2.3 The dilute region

We are interested in the comparison of the behaviour of osmotic pressure and preferential sorption of both the concentrated and the dilute region. Experiments in the concentrated region require considerable experimental effort. The dilute region is much more accessible by osmometry at low polymer concentration or by intrinsic viscosity measurements. Hopefully, by measuring the thermodynamic properties both at limiting low and rather high polymer concentrations,

a sufficiently accurate description of the thermodynamic behaviour of the ternary system can be obtained.

In the dilute solution limit ($\phi_3 \to 0$) one finds[2,11]:

$$\frac{\pi \nu_1}{RT} = r\phi_3 + Y\phi_3^2 + \ldots \tag{9}$$

We follow the derivation of Pouchly et al.[11]:

$$Y(\phi_1^o) = \frac{\nu_1}{2RT}(M_{33} - A_1^2 M_{11}) \tag{10}$$

$$\text{with } A_1 = -M_{13}/M_{11} \tag{11}$$

$$M_{ij} = \partial^2 G_u / \partial u_i \partial u_j \tag{12}$$

$$G_u = \Delta G_m / V(1-\phi_3) \tag{13}$$

where $\Delta G_m$ is given by equation (1) and V is the volume of the total system.

After differentiation we find for the quantities $M_{ij}$:

$$\frac{M_{11}\nu_1}{RT} = \frac{1}{\phi_1^o} + \frac{s}{\phi_2^o} - 2g_{12}^o + 2(\phi_1^o - \phi_2^o)g_{12}'^o + \phi_1^o\phi_2^o g_{12}''^o \tag{14}$$

$$\frac{M_{13}\nu_1}{RT} = s - 1 + g_{13} - sg_{23} + (\phi_1^o - \phi_2^o)(g_{12}^o - g_T) - \phi_1^o(g_{13}')_{\phi_3 \to 0} + \phi_1^o\phi_2^o\{g_{12}'^o - (g_T')_{\phi_3 \to 0}\} \tag{15}$$

$$\frac{M_{33}\nu_1}{2RT} = \tfrac{1}{2}(\phi_1^o + s\phi_2^o) + (g_{12}^o - g_T)\phi_1^o\phi_2^o - (g_{12}^o\phi_1^o + sg_{23}\phi_2^o) + \phi_1^o(g_{13}^*)_{u_2} + \phi_1^o\phi_2^o(g_T^*)_{u_2} + s\phi_2^o(g_{23}^*)_{u_2} \tag{16}$$

The g-parameters and the derivatives with respect to $u_2$ in the above equations are the limiting values $(g_{ij})_{\phi_3 \to 0}$. The derivative with respect to $\phi_3$ is calculated at constant $u_2$.

The total sorption coefficient Y can be determined from low pressure osmometry or from intrinsic viscosity measurements as a function of the composition of the sol-

vent/nonsolvent mixture.

According to Shultz and Flory[12] the linear expansion factor $\alpha$ is a measure for the overall sorption:

$$Y(\phi_1^o) = (\alpha^5-\alpha^3)/2C_M M^{\frac{1}{2}} \qquad (17)$$

$$\text{where } C_M = (27/2^{5/2}\pi^{3/2}N_A)(\bar{v}_3^2/v_1)(M/(\bar{r}_o^2))^{3/2} \qquad (18)$$

M is the molecular weight of the polymer, $N_A$ Avogrado's number, $\bar{v}_3$ designates the partial specific volume of the polymer and $(\bar{r}_o^2)^{\frac{1}{2}}$ is the mean-quare end-to-end distance in the unperturbed state. We follow Flory by taking:

$$\alpha = \alpha_\eta; \quad \alpha_\eta^3 = [\eta]/[\eta_\theta] \qquad (19)$$

This gives us an opportunity to compare osmotic data at medium polymer concentration and interaction parameters derived from them with intrinsic viscosity data.

## 6.3 EXPERIMENTAL

### 6.3.1 Osmometry

A membrane osmometer was constructed with a design as given in Figure 2. This osmometer is very similar to the one used by Koenhen.[4] The device meets most of the requirements for proper functioning (see e.g. Schäfer[13]):

- a convenient and frequent change of solvent and solution is possible;
- the time required for osmotic equilibrium is short and concentration variations during measurement are negligible (volume transport through the membrane is minimal);
- a sufficient support for the membrane is available;
- the pressure difference across the membrane can externally be changed; equilibrium is attained starting from lower pressures[14];
- the temperature control is adequate: the osmometer is im-

mersed in a thermostat bath.
The pressure (compressed air) is exerted on the polymer solution via the mercury filled U-tube. The mercury prevents evaporation of the solvent.

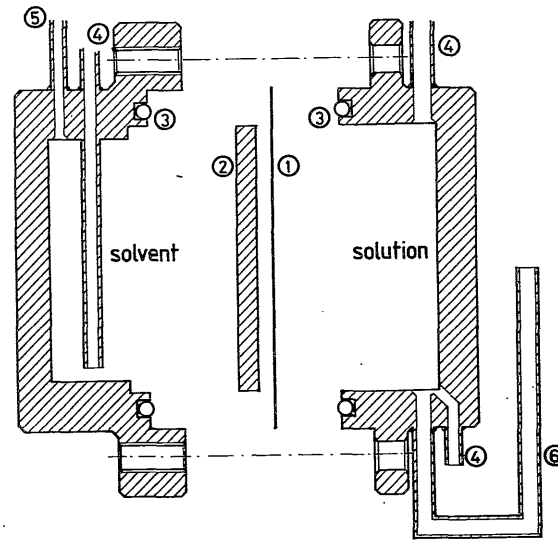


FIG.2. High pressure membrane osmometer: ① membrane, ② porous steel plate, ③ teflon gasket, ④ filling ports connected to valves, ⑤ glass capillary, ⑥ mercury filled capillary U-tube.

6.3.2 Membranes

The membranes used were Sartorius allerfeinst, catalogue number 11539, with a diameter of 47 mm. The membranes are made of regenerated cellulose. They are conditioned to the desired solvent within the cell in 8 steps of ½h duration. After the experiments no CA could be detected at the solvent side of the cell. Before an experiment with a mixed solvent the membrane is carefully conditioned and the solution and solvent compartments are flushed several times.

6.3.3 Experimental procedure

6.3.3.1 Osmotic pressure measurement

At the solution side the initially present solvent is replaced by the solution. The bottom filling port is closed,

and temperature equilibrium is reached in about 15 min. Then the upper valve is closed and this marks the start of the experiment. Through permeation of the (mixed) solvent the level of the meniscus in the mercury column changes. This change is used to correct the pressure until equilibrium is attained. The pressure is increased step-wise for about 3h. Equilibrium follows after another 3h during which the pressure is not changed. The osmotic pressure reproduces to within 3% in duplicate measurements.

After the experiment the weight fraction of the polymer in the solution is determined by evaporation of the (mixed) solvent and subsequent weighing of the polymer. The hydrophylicity of CA limits the accuracy of the determination of the weight fraction to a value of about 2%. During the measurement CA takes up a small amount of water.

The volume fraction of the polymer (before mixing) is calculated from addition of volumes of polymer and solvent.

6.3.3.2 Preferential sorption measurement

The value of $\varepsilon$ is determined by analyzing the composition of the solvent mixture in the solvent compartment side of the cell after equilibrium is attained. The solvent side of the cell is sealed from the environment during the osmotic experiment.

The refractive index increment (the reference is taken from the original mixed solvent composition $\phi_1^o$) is measured with a Brice Phoenix refractometer. The accuracy in the refractive index measurement is about $2.10^{-5}$. The estimated accuracy of the determination of the composition in the solvent compartment is about $2.10^{-4}$. The value of $\varepsilon$ follows from a mass balance of the total cell. The two cell halves have volumes of 12 $cm^3$ (solvent) and 20 $cm^3$ (solution).

The reproducibility, however, in the determination of $\varepsilon$ is worse than $2.10^{-4}$. For instance the values given in Figure 5 are mean values of duplicate measurements. The error in $\varepsilon$ is about $3.10^{-4}$.

Another way to determine $\varepsilon$ is via the determination of the

refractive index of the polymer in the solvent/nonsolvent mixture in the solution compartment. Our apparatus, however, does not allow us to take a sample of the polymer solution at osmotic equilibrium.

6.3.3.3 Viscometry

A capillary viscometer of the Ubbelohde suspended meniscus type, with efflux time of 90 s for dioxane 25°C, was used.

6.3.4 Materials

Details of the materials are given in Chapter 3.

## 6.4 RESULTS AND DISCUSSION

### 6.4.1 Binary CA/solvent interaction parameters

a. Concentration dependence

For a binary system ($\phi_1=0$) equation (6) reduces to:

$$-\frac{\pi v_2}{RT} = \ln\phi_2 - \phi_2 - \frac{r}{s}\phi_3 + \{g_{23} - (1-\phi_3)g_{23}^{*}\}\phi_3^2 \qquad (20)$$

From this equation the Flory-Huggins interaction parameter $\chi_{23}$ can be calculated:

$$\chi_{23} = g_{23} - (1-\phi_3)\frac{\partial g_{23}}{\partial \phi_3} \qquad (21)$$

A concentration dependence of $g_{23}$ of the following form is assumed[41]:

$$g_{23} = g_{23}^{0} + g_{23}^{1}\phi_3 \qquad (22)$$

Substitution of (22) in (21) gives:

$$\chi_{23} = (g_{23}^{0} - g_{23}^{1}) + 2g_{23}\phi_3 \qquad (23)$$

The value of $\chi_{23}$ and so of the $g_{23}$-function can be found from the osmotic pressure measurement in the binary system.

The concentration dependence of the polymer/solvent interaction parameter of the binary systems CA/dioxane and CA/acetone are given in Figure 3. Beyond a polymer weight fraction of 0.15 filling of the cell became very difficult. Figure 3 shows that dioxane is a better solvent for CA than acetone. The concentration dependence is not very large. On the $\chi_{23}$-axis we have given the value for dioxane at low polymer concentration, determined with the help of a low pressure osmometer (Hallikainen model 1361 automatic osmometer, with the same type of membrane as used in the high pressure osmometer). From Figure 3 and equation (23) it follows for dioxane:

$$g_{23} = 0.52+0.12\phi_3 \qquad (24)$$

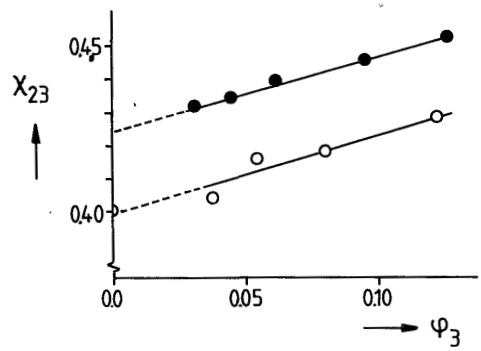


FIG.3. Binary polymer/solvent interaction parameter $\chi_{23}$ as a function of $\phi_3$: dioxane (o) and acetone (•).

The only literature source with which we can compare our $\chi_{23}$-results is Moore et al.[15,16] In Figure 4 the data are compared.

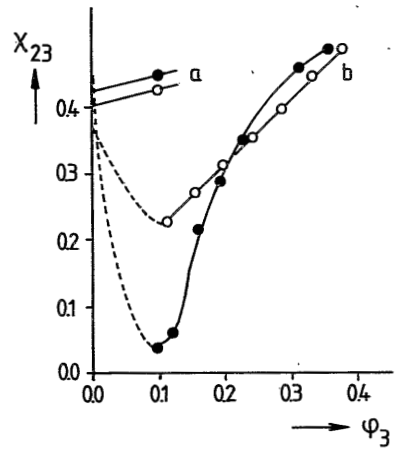


FIG.4. Comparison of $\chi_{23}$ determined in this Chapter (a) with literature data from Moore[15] (b): dioxane (o) and acetone (•).

b. Temperature dependence

The temperature dependence of the interaction parameter is another point of interest. This T-dependence can be used to determine the two contributions to $\chi$, the enthalpic ($\chi_H$) and the entropic contribution ($\chi_S$) to the interaction parameter:

$$\chi_S = \frac{\partial(\chi.T)}{\partial T} \tag{25}$$

$$\chi_H = - T \frac{\partial \chi}{\partial T} \tag{26}$$

A rather precise value of $\chi_H$ is desired. For example a relative error of 0.1 in $\chi_H$ means that $\chi$ has to be determined with an accuracy better than 0.01 (temperature interval 20K). Our experiments reproduce to within about this value.

Although a precise measurement is not possible, osmotic pressure measurements carried out at different temperatures indicate a value of $\chi_H$=0.1-0.3 for dioxane. This value is found when osmotic pressures are measured at 25°C and 40°C (for $\phi_3$ =0.05 and 0.1) using the same solution at the

two temperatures. In practice this means that after an experiment at 25°C, the upper valve is opened, and the whole cell is brought to 40°C. At this temperature the valve is closed and again the osmotic pressure is determined. This type of relative measurement gives the most reliable information on $\chi_H$ with our apparatus.

Again comparison with Moore learns that the results of this study and those of Moore disagree. Moore finds negative values for $\chi_H$ in the system CA/dioxane. A comment which can be made here concerns the accuracy of the determination of the chemical potential difference of the solvent in Moore's experiments. An accuracy of about 10% in RTlna, where a is the activity of the solvent, is given by Moore. Assuming this value to be correct, no reliable information on the temperature dependence of $\chi$ (and so of $\chi_H$) can be extracted from the experiments. We seriously doubt the sign and the magnitude of $\chi_H$ found by Moore.

### 6.4.2 Ternary system: osmotic pressure and preferential sorption

The values found for the osmotic pressure and the preferential sorption in the ternary system CA/dioxane/water are given in Figure 5. Measurements at two polymer weight fractions in the solution, 5 and 10%, have been performed. The osmotic pressure passes through a maximum upon increasing the water content ($\phi_1^o$) of the solvent/nonsolvent mixture. If $\pi$ is extrapolated to zero (dashed lines in Figure 5) we find the nonsolvent concentration where the system demixes into two liquid phases. This value is about 0.33. This is in good agreement with the value found from cloud point data[17], about 0.31 at 10 wt% CA.

As already has been mentioned in the experimental section, there is a large error in the determination of $\varepsilon$. The points given in Figure 5 are mean values of duplicate measurements. It appears that in general the preferential sorption for 10% CA solutions is smaller than the value at 5%. This is not expected on the basis of Figure 1. Even more im-

portant is the sign of ε: experimentally we find negative values. This means that dioxane is preferentially adsorbed, whereas from Figure 1 it follows that water adsorbs preferentially.

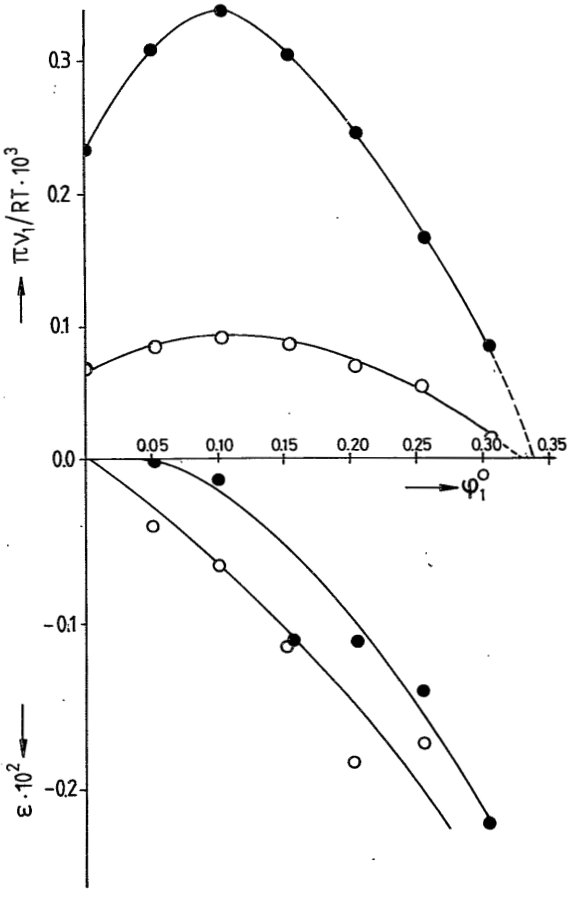


FIG.5. Osmotic pressure π and preferential sorption ε of CA/dioxane/water as a function of water content $\phi_1^o$ at 10 wt% (•) and 5 wt% (o).

6.4.3 Ternary system: intrinsic viscosity measurements

The intrinsic viscosity of CA in the dioxane/water mixture is given in Table 1 and in Figure 6.

| $\phi_1^o$ | [η] | α | $(\alpha^5-\alpha^3)/2C_M M^{\frac{1}{2}}$ | Y(eqn.(10)) |
|---|---|---|---|---|
| 0.0 | 0.854 | 1.02 | 0.0168 | 0.0203 |
| 0.05 | 0.902 | 1.039 | 0.0350 | 0.0200 |
| 0.10 | 0.914 | 1.044 | 0.0398 | 0.0342 |
| 0.15 | 0.889 | 1.034 | 0.0300 | 0.0455 |
| 0.20 | 0.881 | 1.031 | 0.0270 | 0.0490 |
| 0.25 | 0.865 | 1.024 | 0.0233 | 0.0354 |

Table 1: Total sorption coefficient from intrinsic viscosity measurements.

The calculation of Y proceeds as follows:
- we assume the linear expansion factor in pure dioxane to have the same value as for acetone, α=1.02 (Kamide[18]).
- according to Kamide: $(M/(\bar{r}_o^2))^{3/2}=1.344.10^{23}$ for a molecular weight of $M=6.10^4$.
- the partial specific volume of CA: $\bar{v}_3=0.70$.[19]

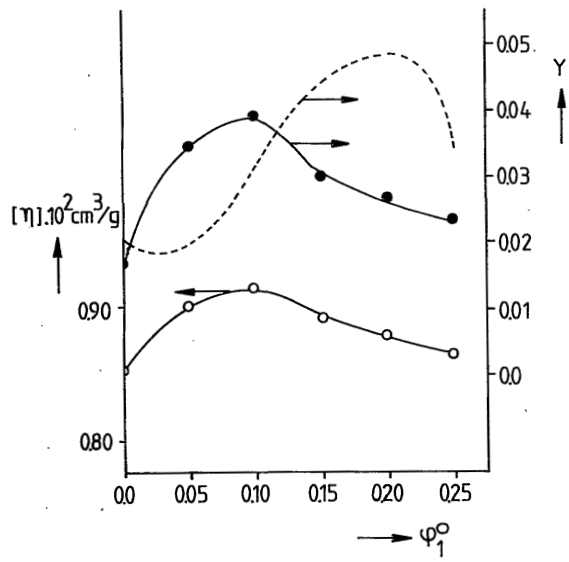


FIG.6. Intrinsic viscosity [η] (o) and total sorption coefficient Y (•) as a function of water content in the dioxane/water mixture. Y calculated from eqns. (10)-(16) with interaction parameters of Fig.10(dashed curve).

Both $Y(\phi_1^o)$ and the intrinsic viscosity show a maximum in the curve as a function of composition. This maximum is situated at the same nonsolvent concentrations as the maximum in the osmotic pressure at higer polymer concentrations (see Figure 5).
Also shown in Figure 6 is the Y-function calculated with the interaction parameters determined from the osmometry and preferential sorption data at a higher polymer concentration (see the next section).

6.4.4 The interaction parameters

We would like to discuss here the merits of determining interaction parameters in a ternary system using osmometric and intrinsic viscosity measurements.

We know that the osmotic pressure and the preferential sorption coefficient are very sensitive to changes in the interaction parameter values. An example is given in Figure 7. Here we changed the value of the polymer/nonsolvent interaction parameter $g_{13}$ and we observe the influence on $\pi$ and $\varepsilon$ at a polymer volume fraction of 0.1. One of the curves, with $g_{13}=1.4$ is directly related to Figure 1.

One of the interaction parameters is definitely composition dependent, viz. $\chi_{12}$, or $g_{12}(u_2)$. The functional dependence can be calculated from literature data on the excess free enthalpy of mixing the two molecular weight components. Precise knowledge of this parameter is desired since first and second derivatives contribute to the equations for the osmotic pressure and the preferential sorption (cp. equations (6)-(7) and (10)-(16)). In the following we take $g_{12}$ as a known parameter at all compositions. The function that represents the literature data on $G_E$ for dioxane/water taken from Kortüm[20] is (represented in Figure 10):

$$g_{12}(\phi_2) = 0.208+3.96\phi_2-5.43\phi_2^2+2.53\phi_2^3+1.23\phi_2^4 \qquad (27)$$

With this $g_{12}$-function and constant interaction parameters of $g_{13}=1.4$ (from swelling measurements at $\phi_3\to 1$) and $g_{23}=0.4$

we have been able to calculate the location of the liquid-liquid phase separation gap.[10] Now we calculate $\pi$ and $\varepsilon$ with this set of interaction parameters from equations (6) and (7) (procedure I in Table 2). The result is given in Figure 8. We note an oscillating behaviour of $\pi$ and a very high value of $\varepsilon$. If we take $g_{23}$ from equations (24) the result is practically the same.

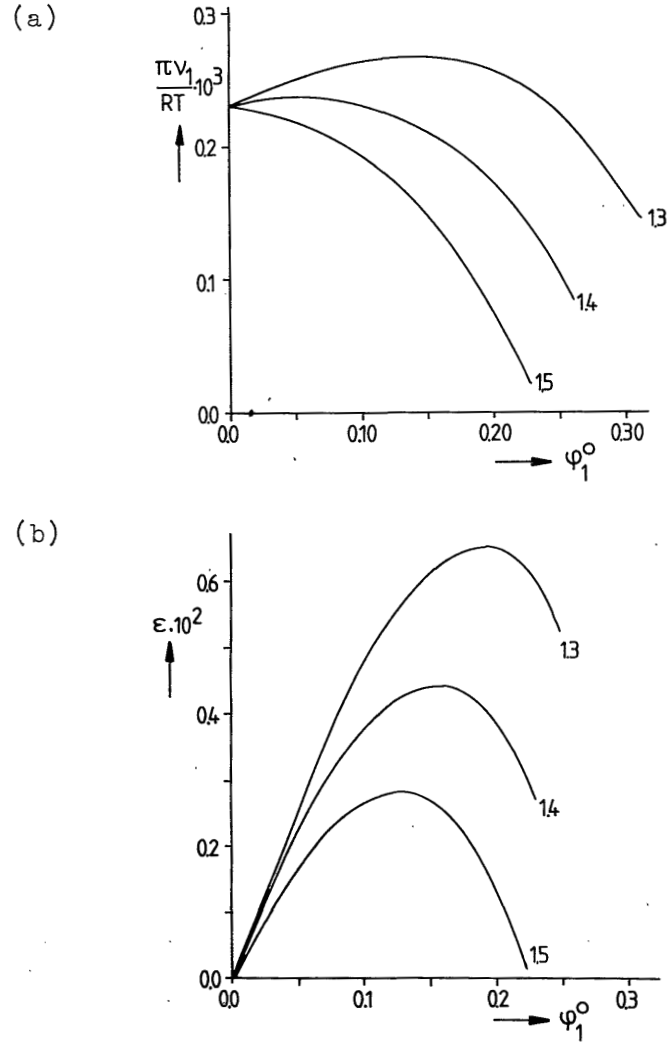


FIG.7. Effect of varying $g_{13}$ (values indicated in the figure) on osmotic pressure (a) and preferential sorption (b); $g_{12}=1.1$; $g_{23}=0.4$ and $s=0.2$.

To improve agreement between the experimental and calculated values a ternary parameter is introduced. A simple form was chosen for $g_T$:

$$g_T = a+bu_2+cu_2^2+d\phi_3 \qquad (28)$$

At the polymer concentrations used ($\phi_3<0.1$) we neglect the influence of the partial derivatives of $g_{13}$ with respect to $\phi_3$. This term contributes less than 5% of the main term with $g_{13}$ in equation (6).

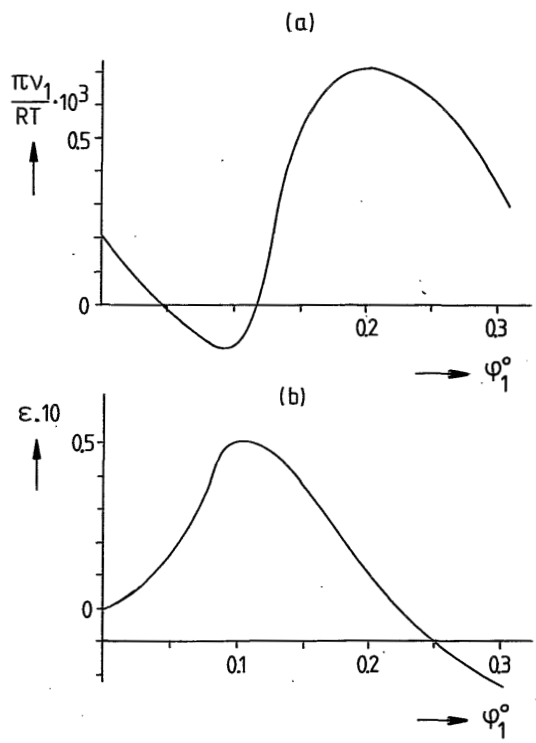


FIG.8. Predicted osmotic pressure $\pi$ (a) and preferential sorption $\varepsilon$ (b) with $g_{12}=g_{12}(u_2)$. Other parameters: $g_{13}=1.4$, $g_{23}=0.4$ and $s=0.2$

Several ways of choosing the unknown parameters $g_{13}$ and $g_T$ have been investigated. These are summarized in Table 2.

| procedure | $g_{12}$ | $g_{23}$ | $g_{13}$ | $g_T$ | result | number of variables |
|---|---|---|---|---|---|---|
| I | eqn.(27) | eqn.(24) | 1.4 | - | Fig.8 | none |
| II | ibid. | ibid. | 1.4 | eqn.(28) | - | 4 |
| III | ibid. | ibid. | e*) | ibid. | - | 5 |
| IV | ibid. | ibid. | e+f$u_2$*) | ibid. | Fig.9 and 10 | 6 |

*) a,b,c,d (eqn.(28)) and e and f are variables to be determined.

Table 2: Selected variables for optimization procedure.

We determined the variables in $g_T$ and $g_{13}$ from a non-linear least-squares optimization procedure for the osmotic pressure equations (6) for n(=6) data points. The number of variables is given in Table 2. Neither procedure II nor procedure III did yield an acceptable result. No good fit can be obtained between calculated and experimental values if $g_T$ is varied at a constant value of $g_{13}$. A reasonable agreement was found when $g_{13}$ also is assumed to be a function of the composition of the solvent/nonsolvent mixture (procedure IV). This means that the interaction between polymer and nonsolvent depends on the amount of solvent present. The results of procedure IV are given in the Figures 9 and 10. Figure 9 gives the best fit between experimental and calculated values for the osmotic pressure and the preferential sorption for the two polymer weight fractions at which we performed our experiments. The values for the interaction parameters found in the optimization procedure are given in Figure 10.

Some remarks concerning these results have to be made:

- The disagreement in the predicted and experimental ε values is not serious: the absolute size of ε has only a minor effect on the calculated g-parameters and the agreement between experimental and predicted osmotic pressure.
- The osmotic pressure equation involves the subtraction of

large numbers to obtain a small value for $\pi v_1/RT$. This makes it difficult to optimize.

- The experimental maximum in the osmotic pressure curve is situated at 10% nonsolvent. From the calculations we find a maximum at 15-20% water.
- The ternary parameter corrects mathematically the interaction of nonsolvent and solvent in the presence of polymer. Horta[21] gives a physical interpretation of $g_T$ in terms of the surface-to-volume ratios and free-volume dissimilarity. In order to do this, he has to introduce some simplifying assumptions in his derivation of Y and $\varepsilon$ from the Flory-Prigogine/Patterson theory. In our case, because of another "ternary" interaction parameter $g_{13}(u_2)$, the situation is even more complex. The molecular interpretation of the size and the form of the functions for the interaction parameters is left for future study.
- Usually $|g_T| < |g_{12}|$ and sign $(g_T)$ = sign $(g_{12})$. The ternary parameter modifies $g_{12}$ and the result is that the preferential sorption of component 1 is lowered. This weakening effect is expected to decrease with increasing polymer concentration.[6] We find a negative sign for $g_T$. The dependence of $g_T$ on $\phi_3$ is negligibly small in our case. Because of the other introduced ternary interaction parameter $g_{13}$ we do not attach much significance to the sign of $g_T$.
- Both a small value of s-1 and a high value for $g_{12}$ influence the preferential sorption in the sense that upon decreasing s-1 and increasing $g_{12}$ the preferential sorption of component 1 increases. In our case this would mean a positive value for $\varepsilon$. The experimentally found negative $\varepsilon$-values indicate that the effect of $g_{12}$ must be compensated by $g_{13}$.

Another way to obtain interaction parameter values is from intrinsic viscosity measurements as a function of the solvent/nonsolvent ratio. In Figure 6 experimental and calculated values of the total sorption coefficient Y are given. The calculated Y (dashed curve) is obtained by substituting the interaction parameters from Figure 10 in the equations (10)-(16).

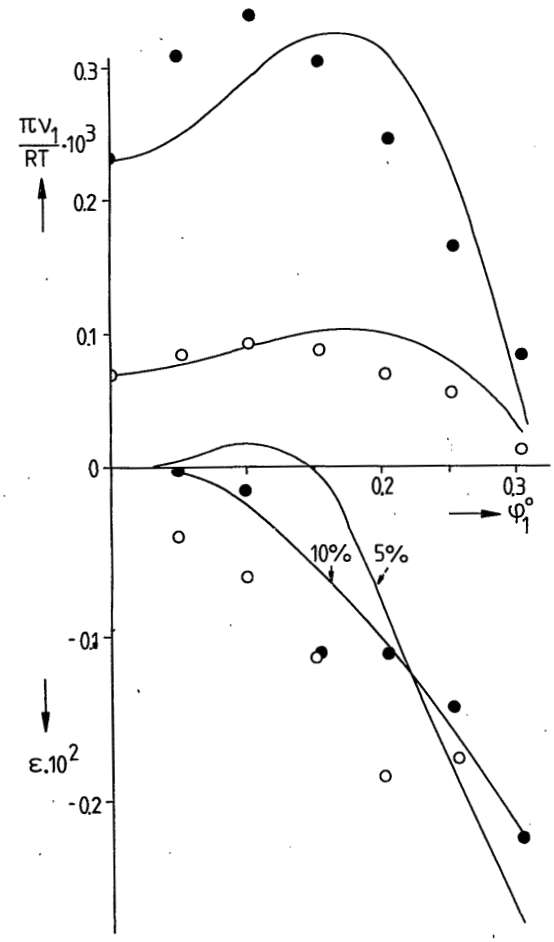


FIG.9. Comparison between experimental and calculated osmotic pressure $\pi$ and preferential sorption $\varepsilon$ : 10 wt% CA (•); 5 wt% CA (o). Full curve calculated with interaction parameters as given in Figure 10.

The experimental and calculated Y differ qualitatively in the same manner as the osmotic pressures at higher $\phi_3$. Again an experimental maximum is found at 10% water content, whereas the theoretical curve has a maximum at about 20% water. Quantative agreement depends on a) the validity of the assumptions underlying equations (17) to (19) and the precise

values of the constants which appear in these equations and b) on the same factors which cause the discrepancy between calculated and experimental values for preferential sorption and osmotic pressure at higher $\phi_3$.

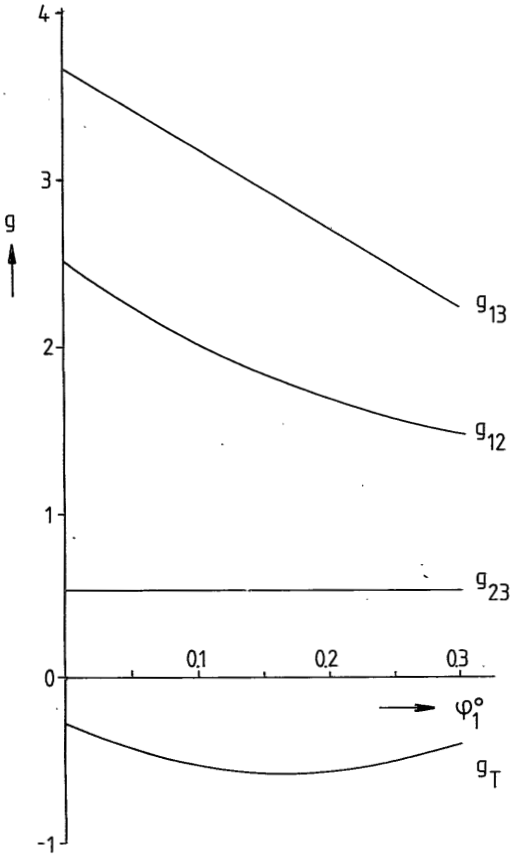


FIG.10. Interaction parameters $g_{13}$ and $g_T$ calculated from optimization procedure; $g_{12}$ and $g_{23}$ are known parameters.

The main purpose of this study is to obtain information on the interaction parameters and to use this information to predict liquid-liquid phase separation. To obtain a quick insight in the location of the miscibility gap and the coexisting phases a plot such as Figure 1 is useful. With the interaction parameters of Figure 10 we calculated the coexistence lines and the osmotic isobars of Figure 11. Only the

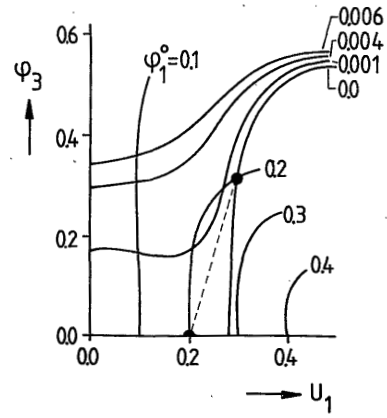


FIG.11. Osmotic isobars and coexistence lines calculated with interaction parameters from Figure 10. Values for $\pi v_1/RT$ and $\phi_1^o$ are given. Phases coexisting at phase separation are indicated by full dots.

relevant part of the diagram is shown. At infinite molecular weight the following phases are in equilibrium: a polymer-free phase with composition $\phi_1^o$=0.2 and a concentrated polymer solution phase with $u_1$=0.3 and $\phi_3$=0.3. This latter finding compares favourably with experimental information on demixing.[10] The polymer free phase, however, is expected to have much larger nonsolvent content, $u_1$>0.3.

## 6.5 CONCLUSIONS

Osmometry can in principle be used to determine interaction parameter values at high polymer concentrations from both osmotic pressure and preferential sorption.

The complexity of the thermodynamic behaviour of CA/dioxane/water manifests itself by the necessary introduction of composition dependent binary and ternary interaction parameters. The Flory-Huggins theory then gives a fairly good phenomenological description of the osmotic experiment.

The derived interaction parameters cannot yet be used successfully in predicting the liquid-liquid phase separation gap.

## 6.6 REFERENCES


1. Chapter 2 of this thesis
2. P.J.Flory, Principles of Polymer Chemistry, Cornell UP, Ithaca, 1953, p.548; H.Tompa, Polymer Solutions, Butterworths, London, 1956, p.182
3. S.G.Chu and P.Munk, Macromolecules, 11,879(1978)
4. D.M.Koenhen, Ph.D.Thesis Twenty University of Technology, Enschede, 1977
5. e.g. A.Zivny, J.Pouchly, and K.Solc.Coll.Czech.Chem. Commun., 32,2753(1967)
6. J.Pouchly and A.Zivny, J.Polym.Sci.A2, 10,1467,1481(1972)
7. R.L.Scott, J.Chem.Phys., 17,268(1949)
8. W.R.Krigbaum and D.K.Carpenter, J.Polym.Sci., 14,241(1954)
9. J.Pouchly, A.Zivny, and K.Solc, Coll.Czech.Chem.Commun., 37,988(1972)
10. Chapter 5 of this thesis
11. J.Pouchly, A.Zivny, and K.Solc, J.Polym.Sci., C23,245, (1968)
12. A.R.Schultz and P.J.Flory, J.Polym.Sci., 15,231(1955)
13. O.F.Schäfer, Colloid Polym.Sci., 257,1007(1979)
14. B.Philipp, K.Wulf and R.Kapelle, J.Polym.,Sci., C16,2681 (1967)
15. W.R.Moore and R.Shuttleworth, J.Polym.Sci.A1, 733(1963)
16. R.A.Orwoll, Rubber Chem.Techn., 50,471(1977)
17. Chapter 3 of this thesis
18. K.Kamide, T.Terakawa, and Y.Miyazaki, Polym.J., 11,285 (1979)
19. Polymer Handbook, J.Brandrup and E.H.Immergut, Eds., Wiley, New York, 1975
20. G.Kortüm and V.Valent, Ber.Bunsen.Ges.Phys.Chem., 81,752, (1977)
21. A.Horta, Macromolecules, 12,785(1979)

# 7. DIFFUSION DURING MEMBRANE FORMATION

## 7.0 ABSTRACT

A variety of CA membranes can be prepared by varying the solvent in the membrane forming system. Thermodynamics and kinetics of demixing processes and diffusional exchange of solvent and nonsolvent determine together the resulting membrane structure.

Measurements of diffusion during membrane formation are reviewed. The nascent skin is not found to be a big barrier for solvent diffusion. This follows from a simulation of the effect of a skin on binary diffusion and from a separate determination of diffusion coefficients in binary CA/solvent and ternary CA/solvent/water systems.

Solvent and nonsolvent flow can be related to the thermodynamic properties of the system. A composition path can be calculated which represents the local composition change in the solution up to phase separation. This composition path depends on the solvent/nonsolvent interaction parameter.

Indiffusion of water depends very much on the solvent chosen for the casting solution. Comparison of properties of CA membranes from solutions in dioxane and acetone leads to the conclusion that a nascent skin discriminates in some way between solvent and nonsolvent flow. Apparently a skin is a stronger barrier for nonsolvent than for solvent diffusion. No explanation can be given at present. More research to understand this discriminating effect is needed. More quantitative information is required on the kinetics of gelation and on the diffusion at high polymer concentration in ternary systems.

## 7.1 INTRODUCTION

Membranes of cellulose acetate (CA) can easily be prepared by casting a concentrated polymer solution (10-30wt%) on a supporting surface, and by subsequent immersion in a nonsolvent (water) bath. Depending on the solvent a variety of membrane properties can be obtained, ranging from hyperfiltration (reverse osmosis) to ultrafiltration membranes.

Important morphological properties are the overall degree of porosity and the presence of a skin, a dense toplayer with permselective properties very different from the porous sublayer.

First we will consider the dependence of the membrane porosity on the choice of the solvent. Values for the degree of porosity (wt% water per gram of dry polymer, present in sponge substructure and fingerlike cavities) have been given by Frommer[1] and So.[2] A quite interesting correlation has been proposed by these authors. The degree of porosity the membrane can be related to the tendency of mixing of solvent and nonsolvent. This relation has been put down by So et al. as the correlation of the porosity with the solubility parameter of the solvent (reproduced in Figure 1). The higher the solvent solubility parameter the higher the tendency of mixing of the solvent with water ($\delta \simeq 23$).

Instead of taking the difference in the solubility parameters as a measure for the tendency of mixing, we choose the much more exact excess free energy of mixing of the solvent and the nonsolvent.*)

The minimum values of $G^E$ for the solvent/nonsolvent pair for some of the solvents in Figure 1 are given in Table 1. (as far as this quantity is available from the literature). The $G^E$ value for TEP is somewhere in between acetic acid and DMF, judging from the excess enthalpy available.[9]

*) Another quantity that can be used and is related to $G^E$ is the magnitude of the solvent/nonsolvent interaction parameter (cf. section 5.4, Figure 2)

When we compare the rather scattered $G^E$ values of Table 1 with Figure 1 the proposed correlation does not appear to be so strong anymore. From dioxane to DMSO with large changes in $G^E/RT$ the porosity does not increase very much. We conclude that the membrane porosity cannot simply be related to the tendency of mixing.

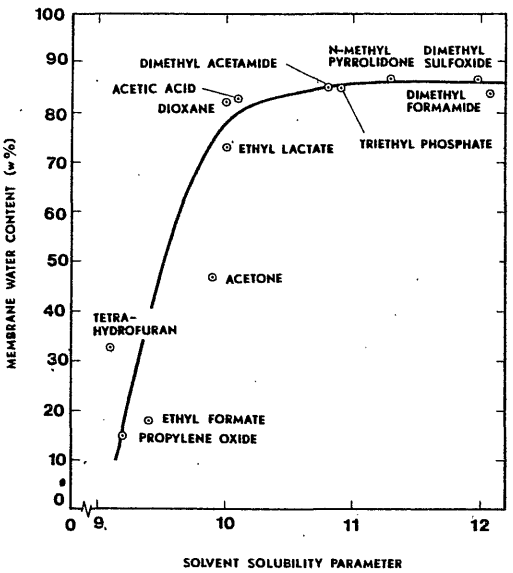


FIG.1. Correlation between membrane porosity and solubility parameter of the solvent. Reproduced from So et al.[2] Membranes cast from 20% CA solutions in the solvents mentioned.

The tendency of mixing is one important factor contributing to the rate of diffusive exchange. We agree with Frommer and So that in general the membrane porosity is largely governed by the rate of diffusive exchange of solvent and nonsolvent during the precipitation of the polymer. The formation of a skin, however, is expected to behave as a rate limiting barrier for solvent and nonsolvent transport. To have some quantitative idea of the overall ratio of solvent and nonsolvent flow one can calculate from porosity values of 40 to 80% that the ratio of indiffusing nonsolvent and outdiffusing solvent volumes is about 0.1 to 0.2. An e-

quilibrium swelling value of 15% found for the solvent propyleneoxide (Figure 1) indicates that the final membrane has a porosity or swelling value comparable to a dense film of CA obtained by evaporation of the solvent.

Some information on the permeability of the skin in the final membrane and possibly in the nascent state may follow from the study of the filtration properties. Going from acetone to DMSO (see Figure 1 or Table 1) the skin has a rapidly decreasing ability to reject dissolved salts. Simultaneously the water flux increases from 0.02 cm/h for acetone to 100 cm/h for DMSO (at 40 bar).[10] Membranes from a DMSO solution have a much more open and probably much thinner skin. These latter membranes are of the UF type. Therefore, although the porosity does not increase very much from dioxane to DMSO in Figure 1, the permeabilities of the membranes do increase, and again this can be roughly correlated with the tendency of mixing.

| solvent | $G^E/RT$(min) | porosity(%) |
|---|---|---|
| THF [3] | 0.20 | 32 |
| acetone [4] | 0.46 | 47 |
| dioxane [5] | 0.48 | 81 |
| acetic acid [6] | 0.34 | 82 |
| DMF [7] | 0.07 | 83 |
| DMSO [8] | -0.50 | 86 |

Table 1: Correlation between minimum of excess free energy of mixing and membrane porosity.

Some of the membranes from Figure 1 have such a low void fraction that they may be considered as consisting entirely of skin structure. Others have a very thin open skin layer with no salt rejection properties.

The skin selectively depends on the solvent used in the casting solution. This can to some extent be simulated by measuring the intrinsic reverse osmosis properties of films obtained by evaporation of the solvent. Such films show con-

siderable differences in permselectivity depending on the solvent that is evaporated.[11-12]

How can we explain these large differences in membrane properties if the solvent is varied, on the basis of the hypothesis on membrane formation outlined in Chapters 1 and 2? This question is the subject of this Chapter. We will first review results of diffusion experiments during membrane formation. Secondly we will try to combine these data with the concept given in previous Chapters regarding the demixing processes involved in the membrane formation: liquid-liquid phase separation and gelation. It will become apparent that more experiments are necessary to obtain a better understanding of asymmetric membrane formation.

## 7.2 EXCHANGE OF SOLVENT AND NONSOLVENT

The formation of an asymmetric membrane is a complex process involving both thermodynamics and kinetics of demixing processes and the exchange of solvent and nonsolvent during the precipitation of the solution. Several authors presume[13-14] that the formation of the skin occurs in a very short time interval after immersion in the coagulation bath (say in the order of microseconds). No experimental technique is available to study in-and outdiffusion in this short period of time. However, in our opinion study of the exchange process over longer periods of time (say minutes) may be useful for the following two reasons:

- The formation of a dense skin with diffusion properties much different from the sublayer of the still fluid polymer solution is bound to have some influence on the following exchange of solvent and nonsolvent. Measurement of the in- and outdiffusion can thus provide a means to study the barrier properties of the already formed skin.
- Although a rapidly initiated skin is present, exchange of solvent and nonsolvent over a longer period of time may induce significant changes in the morphology of the skin. An

example of a relatively slow change can be found in the preparation of a membrane in a two-bath procedure. Coagulation in a bath of low temperature for a short time (say 1 min) is followed by immersion in another bath at a higher temperature. The immersion time in the first bath (in the order of minutes) determines to a great extent the permselectivity of the final membrane.

7.2.1 Outdiffusion of solvent

As far as we know only Frommer[1] has given experimental information on the diffusional exchange in CA membrane forming systems. The outdiffusion can be easily monitored by determining the solvent in the coagulation bath as a function of time. Frommer has found that the concentration varies with the aquare root of time. The slope of the plot of $c_t/c_\infty$, where $c_t$ is the concentration at time t and $c_\infty$ at $t\to\infty$, against the square root of time, is found to have the same value for acetone, acetic acid, DMSO and DMF, about 0.12 and for TEP about 0.07.[1] One might infer from these measurements that the initial solvent outflow is the same in most cases.

We have done similar experiments[15], with the solvent dioxane. The concentration in the bath is determined as a function of time, and as a function of the polymer weight fraction of the casting solution. The outdiffusion is treated with a binary*) model[16] of outdiffusion from a sheet with constant diffusion coefficient in a well-stirred bath of a limited volume.[17] The mathematical equations are given in Appendix 1. An apparent diffusion coefficient can be calculated from the concentration profile in the bath as a function of time. The results are given in Table 2.

How can these results be interpreted? One possibility might be that we measure outdiffusion through an already formed dense skin with a very low diffusion coefficient. According to Anderson et al.[14], who studied the binary sys-

*) Treated as if there were only two components diffusing.

| $c_{pol}$ (wt% CA) | $D_s$ *$10^6$ ($cm^2/s$) |
|---|---|
| 13 | 2.9 ± 0.1 |
| 15 | 2.1 |
| 17 | 1.9 |
| 20 | 1.8 ± 0.2 |

Table 2: Apparent diffusion coefficient of dioxane calcuted from experimental data using a binary model.

tem CA/acetone, one should expect a very strong dependence of the diffusion coefficient on the polymer concentration. The diffusion coefficient is expected to vary over 4 decades ($5.10^{-5}$-$10^{-8}$cm/s) from pure acetone to 90% polymer. From our experiments (see below), however, it appears that the concentration dependence is smaller.

We now simulate the influence of a skin with a certain thickness and a constant diffusion coefficient which is smaller than that in the sublayer. The following situation is considered:

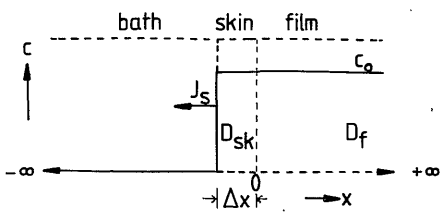


FIG.2. Binary outdiffusion from a film consisting of a skin ($D=D_{sk}$, thickness $\Delta x$) and a sublayer ($D=D_f$, semi-infinite)

Both the solvent bath and the polymer solution layer are considered to be semi-infinite. The diffusion coefficient in the skin is $D_{sk}$ and in the film $D_f$. The skin thickness is $\Delta x$. In Appendix 2 the solution for this problem (initial concen-

tration in the film $c=c_o$, in the bath $c=0$) is given.[17] If we assume certain values for $D_f$, $D_{sk}$ and $\Delta x$ the total outdiffusing mass $M_t$ can be calculated. The influence of the properties on the apparent D can be found by calculation of $D_s$ from the binary problem without a skin (Appendix 1). The ratio of $D_s$ and $D_f$ is given in Table 3 for several values of skin thickness and the ratio of $D_f/D_{sk}$.

| | | $D_f/D_{sk}$ | | | |
|---|---|---|---|---|---|
| $\Delta x$ (μm) | | 1 | 10 | $10^2$ | $10^3$ |
| 0.1 | $D_s/D_f$= | 1 | 1 | 0.92 | 0.44 |
| 0.2 | | 1 | 0.99 | 0.84 | 0.24 |
| 0.5 | | 1 | 0.96 | 0.65 | 0.07 |
| 1.0 | | 1 | 0.92 | 0.44 | 0.02 |

Table 3: Apparent binary diffusion coefficient expressed as the ratio of $D_s/D_f$ for a skinned membrane with skin with thickness $\Delta x$ and diffusion coefficient $D_{sk}$.

One will always find an apparent value for the diffusion coefficient $D_s$ smaller than $D_f$. From Table 3 it can be seen that the skin only forms a considerable barrier when the skin thickness is large and the diffusion coefficient of the skin is much smaller (orders of magnitude lower) than the diffusion coefficient of the sublayer. In asymmetric membranes the skin thickness is about 0.1-0.2 μm. This means that if $D_f/D_{sk}$=100 there is hardly any retarding influence of the skin.

Next we will critically evaluate the magnitude of the apparent diffusion coefficient given in Table 2. From measurements of diffusion coefficients under well defined conditions in both binary and ternary systems more can be said about the barrier properties of the skin layer.

### 7.2.2 Determination of diffusion coefficients in binary and ternary systems

Measurements of the diffusion coefficients were carried out in a Spinco Model E analytical ultracentrifuge.[15] A free diffusion experiment was set up in a double sector synthetic boundary cell. A Rayleigh interferometer was used to measure the refractive index as a function of composition in the cell. The creation of a boundary is difficult at high polymer concentrations (>10%). Accurate determination of high diffusion coefficients ($>10^{-5}$ cm$^2$/s) is also difficult. The concentration difference was 1% in polymer for the binary experiment or 1% in the solvent/nonsolvent composition (e.g. composition 95/5 versus 94/6) for three components present.

The application of this method to study diffusion in ternary systems requires some explanation. Consider a free diffusion experiment in the cell. Two semi-infinite media with a different composition touch at x=0, t=0. We assume a general form of Fick's law to be valid:[18]

$$\frac{\partial c_i}{\partial t} = \sum_{\substack{j=1 \\ j\neq 2}}^{3} D_{ij} \frac{\partial^2 c_i}{\partial x^2} \qquad i=1,3 \qquad (1)$$

The system consists of 2 solutes, these being the components nonsolvent (1) and polymer (3), in one common solvent (2). The boundary conditions for each solute are:

$$\begin{array}{lll} t=0 & x<0 & c_i = c_i(-\infty) \\ & x>0 & c_i = c_i(\infty) \end{array} \qquad \Delta c_i^o = c_i(\infty) - c_i(-\infty) \qquad (2a)$$

$$\begin{array}{lll} t>0 & x=-\infty & c_i = c_i(-\infty) \\ & x=\infty & c_i = c_i(\infty) \end{array} \qquad (2b)$$

$D_{11}$ and $D_{33}$ are the main diffusion coefficients; $D_{13}$ and $D_{31}$ are the crossterms. They are taken as independent of concentration in the narrow concentration interval of the experiment. The two coupled differential equations have been solved by Toor [19]:

$$\Delta c_1 = \phi_1 + \frac{D_{11}-D_3}{D_{31}}\,\phi_3 \qquad (3a)$$

$$\Delta c_3 = \phi_3 + \frac{D_{33}-D_3}{D_{13}}\,\phi_1 \qquad (3b)$$

$$\phi_i = \frac{|D_{ii}-D_j|\Delta c_i^o + D_{ij}\Delta c_j^o}{D_i-D_j} f_i \qquad i,j=1,3 \quad i\neq j \qquad (3c)$$

with $$D_1 = \tfrac{1}{2}(D_{11}+D_{33}+\sqrt{(D_{11}-D_{33})^2+4D_{13}D_{31}}) \qquad (3d)$$

$$D_3 = \tfrac{1}{2}(D_{11}+D_{33}-\sqrt{(D_{11}-D_{33})^2+4D_{13}D_{31}}) \qquad (3e)$$

$$f_i = \operatorname{erf}\left(\frac{x}{\sqrt{4D_i t}}\right) \qquad (3f)$$

In principle both main and cross terms can be determined from a ternary free diffusion experiment. A Rayleigh interferometer is, however, not accurate enough.[18]
We assume that $D_{11} \gg D_{33}$ and that $D_{13}D_{31} \ll (D_{11})^2$. In this case it follows from equation (3d) and (3e) that $D_1 = D_{11}$ and $D_3 = 0$. In the experiment no initial polymer concentration gradient is applied.

$$\Delta c_3^o = 0 \qquad (4)$$

From equation (3a)-(3c):

$$\phi_1 = \Delta c_1^o \operatorname{erf}\left(\frac{x}{\sqrt{4D_{11}t}}\right) \qquad (5a)$$

$$\phi_3 = -\frac{D_{31}}{D_{11}}\Delta c_1^o \qquad (5b)$$

and $$\Delta c_1 = \Delta c_1^o \operatorname{erf}\left(\frac{x}{\sqrt{4D_{11}t}}\right) \qquad (6a)$$

$$\Delta c_3 = \left[\frac{D_{33}}{D_{13}} \operatorname{erf}\left(\frac{x}{\sqrt{4D_{11}t}}\right) - \frac{D_{31}}{D_{11}}\right]\Delta c_1^o \qquad (6b)$$

And if $D_{33} << D_{13}$ and $D_{31} << D_{11}$, $\Delta c_3$ is small in comparison to $\Delta c_1$. This latter approximation may be a rather crude one.

This quasi-binary approach gives us $D_{11}$, the diffusion coefficient of nonsolvent (or the solvent) where the polymer present in the polymer solutions may have a retarding influence.

The results are summarized in Tables 4 and 5 for the two ternary systems studied: CA/acetone/water and CA/dioxane/water. There is not yet a complete set of measurements for all compositions.

| | $D_{11}.10^7$ cm²/s | | | | | |
|---|---|---|---|---|---|---|
| wt%CA | 0 | 1 | 2 | 4 | 5 | 10 |
| wt% $H_2O$ | | | | | | |
| 0 | | | 9.2 | 11 | 12 | |
| 5 | | 260 | | | 210 | |
| 10 | | 200 | | 170 | | 140 |
| 15 | 135 | | | 88 | | 50 |

Table 4: CA/acetone/water. Diffusion coefficient $D_{11}$ as a function of polymer concentration and water percentage in the solvent/nonsolvent mixture.

| | $D_{11}.10^7$ cm²/s | | | | | | | |
|---|---|---|---|---|---|---|---|---|
| wt%CA | 0 | 1 | 2 | 3 | 4 | 5 | 7 | 10 |
| wt% $H_2O$ | | | | | | | | |
| 0 | | 2.1 | 2.4 | 2.6 | 2.7 | 2.9 | | 3.6 |
| 5 | 100 | 100 | | | | 74 | 69 | |

Table 5: CA/dioxane/water. Diffusion coefficient $D_{11}$ as a function of polymer concentration and waterpercentage in the solvent/nonsolvent mixture.

Binary diffusion: CA in a solvent

The binary diffusion coefficients are much larger for acetone than for dioxane. The results are represented in Figure 3. The increase with concentration in both cases indicates the importance of the thermodynamic factor for the diffusion coefficient.

We can compare our data with literature values for CA/acetone of Singer[20], also given in Figure 3. For a molecular weight of $5.3.10^4$ (the CA used here has about the same $\bar{M}_w$) he found a diffusion coefficient ($\phi_3 \to 0$) of $7.7.10^{-7} cm^2/s$ in acetone. Park[21] determined diffusion coefficients for much higher CA concentrations in acetone. From Figure 3 it can be seen that the interdiffusion coefficient for CA/acetone varies probably over 2 decades from 0-90% polymer instead of 4 decades as assumed by Anderson.[14]

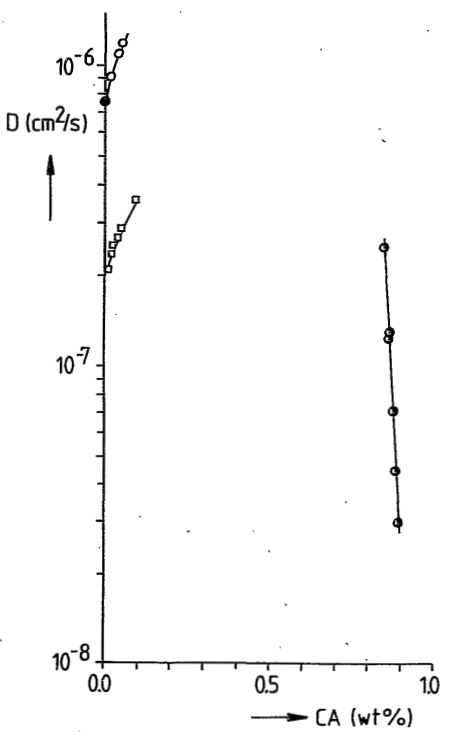


FIG.3. Binary interdiffusion coefficient as a function of weight fraction CA in acetone (O) and dioxane (□); literature data of Park (◑)[21] and Singer (●)[20] (acetone).

Ternary diffusion: CA/solvent/water

The apparent diffusion coefficients $D_{11}$ derived from the ternary experiment have the same order of magnitude as the binary solvent/nonsolvent diffusion coefficient. The value of $1.35.10^5 cm^2/s$ for 15% water in acetone agrees with literature data.[22]

Introduction of water has the effect of decreasing the diffusion coefficient. This is interpreted as a retarding effect of the polymer on diffusion of the low molecular weight substances. When the amount of water, at constant polymer concentration, is increased, $D_{11}$ decreases. This is in agreement with the behaviour of the binary system acetone/water.[22]

If only binary diffusion coefficients are considered a diffusion coefficient for dioxane of about $10^{-6} cm^2/s$ obtained from the film experiment (see 7.2.1) cannot be explained. We would expect a much smaller apparent value because of the influence of a (dense) skin. The magnitude of the determined diffusion coefficient is of order of the ternary diffusion coefficient in Table 5.

We conclude from these measurements that the apparent diffusion coefficient measured in the film experiment is not a binary coefficient but the diffusion coefficient of dioxane in water in the presence of polymer. The barrier effect of the skin on solvent diffusion is apparently not very strong.

Although the obstructive effect of a skin on the solvent outdiffusion is not spectacular, variations in the diffusion coefficients of a factor 10 can have a considerable influence on the change in local composition in the toplayer of the film (see 7.3). It is necessary in our opinion to extend the measurement of ternary diffusion coefficients to much higher polymer concentrations.

7.2.3 Indiffusion of nonsolvent

At the end of the membrane formation process a considerable amount of nonsolvent is present in the coagulated film. The indiffusion of water during coagulation can be

followed by optical microscopy (see Chapter 2).

Frommer[1] followed the coagulation front in the CA solution. A simple model (Appendix 3) may be used: a semi-infinite polymer solution in which the nonsolvent penetrates from the bath. At the coagulation front the local water percentage is the precipitation value, known from the liquid-liquid phase separation diagram, and is fairly independent of polymer concentration.[2,3] We used the data of Frommer (Figure 4 of ref. 1) to calculate the apparent diffusion coefficient and to give an estimate of the nonsolvent inflow in the precipitating film. The results are given in Table 6.

| solvent | c* | $D_{NS}$*10$^{6}$ cm$^2$/s | $J_{NS}$(0→2min) *10$^{4}$ g/cm$^2$s | $J_{NS}$(2→4min) *10$^{4}$ g/cm$^2$s |
|---|---|---|---|---|
| DMSO | 0.15 | 5.1 | 2.3 | 1.0 |
| DMF | 0.12 | 2.2 | 1.5 | 0.6 |
| dioxane | 0.30 | 1.9 | 1.4 | 0.6 |
| acetic acid | 0.31 | 0.6 | 0.8 | 0.3 |
| TEP | 0.10 | 0.1 | 0.4 | 0.2 |
| acetone | 0.28 | 0.1 | 0.4 | 0.1 |

Table 6: Nonsolvent diffusion coefficient and nonsolvent flow calculated with a binary model (Appendix 3) using data of Frommer.[1] c* is the water content at liquid-liquid phase separation.

The nonsolvent flow has been estimated over two penetration periods: averaged over the first two minutes and averaged over the second two minutes.

If we apply another simplified model for nonsolvent diffusion, that of Strathmann, also given in Appendix 3, we find values of $D_{NS}$ about 3 times as large as given in Table 6.

Going from DMSO to acetone, both apparent diffusion coefficient and nonsolvent flow decrease very much. The coefficient for dioxane has about the same value as found for

solvent outdiffusion (cf. 7.2.1). Going down in the table the decreasing value of the nonsolvent flow may reflect the retarding effect on nonsolvent diffusion of a thicker and/or a denser skin formed at the interface solution/coagulation bath.

The estimated nonsolvent flow has to be compared with the solvent flow. The average solvent outflow in the first 2 seconds is about $8.10^{-4}$g/cm$^2$s, in the first 30 s about $2.10^{-4}$g/cm$^2$s (20 wt% CA solution). For 30,60 and 120 s we calculate a nonsolvent flow of 2.8; 2.0 and $1.4.10^{-4}$g/cm$^2$s, respectively. The ratio $J_{NS}/J_S$ in the first 2 seconds is at least 0.2 and at t=30 s about 1. The absolute value should be treated with some reserve as both descriptions are essentially binary. Especially in the case of nonsolvent diffusion we did not take into account the simultaneous outdiffusion of dioxane. A smaller value of the nonsolvent flow rate would also suffice to have the same penetration distance of the coagulation front.

## 7.3 COUPLING OF DIFFUSION AND CHANGE IN LOCAL COMPOSITION

An interesting approach has been followed by Cohen[24] to relate the solvent and nonsolvent diffusion to the thermodynamic properties of the system. Although some, maybe crude, approximations have to be made, it is worthwhile considering the consequences of the model.

In Figure 4 a schematic representation of the diffusion problem is given. The fluxes of solvent ($J_2$) and nonsolvent ($J_1$) are considered. The volume fraction of polymer (or the weight fraction, if desired) is $\phi_3=1-\phi_1-\phi_2$.

Upon immersion the cast film equilibrates with the nonsolvent bath. After a time t, nonsolvent(1) and solvent(2) will have diffused in or out of the layer with thickness z=l(t). In the interior (z>l) the original casting solution composition is maintained: $\phi_1^c, \phi_2^c$ (usually $\phi_1^c=0$). At the surface the composition is $\phi_1^s, \phi_2^s$ (normally $\phi_2^s=0$). The flow

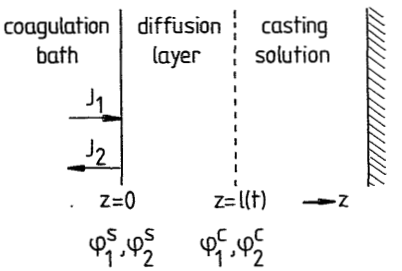


FIG.4. The diffusion problem: at time t=0 the whole layer is homogeneous. At time t a diffusion layer has propagated to z=l(t). The composition in the casting-solution is $\phi_1^c, \phi_2^c$; the composition in the bath is $\phi_1^s, \phi_2^s$.

of the solvent and nonsolvent is treated, as usual, as a one dimensional process. The model describes the local composition change in the film up to the point of reaching the composition required for liquid-liquid phase separation.

The complication arising from the motion of the membrane/bath interface can be avoided by introducing a new position coordinate m [25], which measures the volume of polymer per unit area of the membrane between the interface and the point of observation. The independent fluxes $J_1$ and $J_2$ are measured through a surface at fixed m. The fluxes are assumed to be linearly related to the driving forces, the gradients in the chemical potentials. Strictly speaking this is only possible in a system not far from equilibrium, which is a condition which may not be fulfilled upon immersion in the nonsolvent bath. Crossterms are neglected. Then by definition:

$$J_1 = - \frac{D_1(\phi_1, \phi_2)}{RT} \phi_1 \frac{\partial \mu_1}{\partial m} \qquad (7a)$$

$$J_2 = - \frac{D_2(\phi_1, \phi_1)}{RT} \phi_2 \frac{\partial \mu_2}{\partial m} \qquad (7b)$$

where $D_1$ and $D_2$ are the diffusion coefficients for solvent and nonsolvent in the polymer-fixed reference frame.

Cohen assumes that the coefficients are probably composition dependent, but that the ratio $\alpha = D_1/D_2$ is not, and takes the value of about 1.

Furthermore a steady state distribution is assumed to be present if $l(t)$ is smaller than the film thickness. That implies that at any instant $J_1$ and $J_2$ are independent of m throughout the layer. Their ratio can be written as:

$$\frac{J_1}{J_2} = \sigma = \alpha \frac{\phi_1 d\mu_1}{\phi_2 d\mu_2} \quad (\sigma < 0) \tag{8}$$

If the chemical potentials are expressed as functions of the volume fractions, one finds ($\alpha$=1):

$$\frac{d\phi_2}{d\phi_1} = \frac{\sigma\phi_2(\partial\mu_2/\partial\phi_1)-\phi_1(\partial\mu_1/\partial\phi_1)}{\phi_1(\partial\mu_1/\partial\phi_2)-\sigma\phi_2(\partial\mu_2/\partial\phi_2)} \tag{9}$$

Equation (9) is a first order differential equation for $\phi_1$ and $\phi_2$ in the diffusion layer. If the casting solution and the surface composition are specified, a curve in the $(\phi_1,\phi_2)$-plane for which $\sigma$ is constant can be calculated. This curve can only be calculated if the surface composition is situated outside the binodal, in the homogeneous one-phase region. When a composition near the spinodal of the liquid-liquid phase separation region is reached, the partial derivatives in the right-hand part of equation (9) vanish and the casting solution composition cannot be connected with a surface composition by a constant $\sigma$-path.

The chemical potentials $\mu_1$ and $\mu_2$ can be found from the Flory-Huggins theory[26] (see also Chapter 5):

$$\Delta\mu_1 = \ln\phi_1-\phi_1-s\phi_2-r\phi_3+(\chi_{12}\phi_2+\chi_{13}\phi_3)(\phi_2+\phi_3)-s\chi_{23}\phi_2\phi_3 \tag{10a}$$

$$\Delta\mu_2 = \ln\phi_2-\phi_1-s\phi_2-r\phi_3+(\chi_{12}\phi_2+s\chi_{23}\phi_3)(\phi_1+\phi_3)-\chi_{13}\phi_1\phi_3 \tag{10b}$$

where s and r are $\nu_1/\nu_2$ and $\nu_1/\nu_3$, the ratios of the molar volumes $\nu_i$ and $\chi_{ij}$ are the interaction parameters of components i and j.

So far we have followed the derivation of Cohen et al.

For some practical systems we will now consider the consequences. Several paths in the ternary diagram are plotted for an initial composition of 10% CA in the casting solution. The results are given in Figures 5 and 6. The values of $\sigma$ are also given. We only consider the numerical (absolute) value of $\sigma$. A small $\sigma$ means that more solvent flows out of than nonsolvent into the cast polymer solution film. When solvent and nonsolvent fluxes are of comparable size, $\sigma \simeq 1$.

Of course one cannot freely choose the ratio of the nonsolvent and solvent flux. The fluxes are determined by the concentration profiles of the respective components in the film in the course of time. These profiles can in principle be calculated from the solution of the diffusion equation. What factors determine the expected initial small value of $\sigma$ and the necessary change to a larger value ($\sigma \to 1$ for the sublayer) is a crucial point and will be the subject of future research.

A crude measure, following from the model, for the initial ratio of nonsolvent and solvent fluxes may be $[\phi_1 \Delta\mu_1 / \phi_2 \Delta\mu_2]_{initial}$ where the chemical potential steps are calculated at the interface from equation (10)*) and the volume fractions of solvent and nonsolvent at the interface in the film at small nonsolvent content. This ratio is small($<<0.1$) and stays small when the solvent is varied. On condition that the coagulation bath consists of pure nonsolvent (initially), the composition of the upper layer of the cast solution film always follows a path with a low $\sigma$-value.

In our description of asymmetric membrane formation (Chapter 2) skin formation is the result of a path with a low $\sigma$-value, whereas in the lower layer of the film a high $\sigma$ is involved.

In Figures 5 and 6 composition paths are given for poly-

*) We have to assume that a small amount of solvent has diffused into the bath and vice versa that some nonsolvent has penetrated into the film; otherwise the chemical potentials diverge (equation (10)).

mer/solvent/nonsolvent systems which represent to some extent CA/dioxane/water (Figure 5) and CA/DMSO/water (Figure 6). The binodal of the liquid-liquid phase separation (L-L) is drawn for reference. Only the solvent/nonsolvent interaction parameter $\chi_{12}$ differs in Figure 5 and 6. We observe that at a low absolute value of $\sigma$ (0.1) the $\chi_{12}$ parameter has only a small influence on the location of the composition path. At higher values of $\sigma$ (0.9) the change in polymer concentration is much steeper at high $\chi_{12}$ than at low $\chi_{12}$. Consequently, the model predicts that at same value of $\sigma$ the composition path at high $\chi_{12}$ intersects the binodal at a much higher polymer concentration than at low $\chi_{12}$. This could be relevant to the growth possibilities of the dilute phase nuclei in the nascent porous sublayer. In the case of a low $\chi_{12}$ nucleation and growth occur at an average lower polymer concentration and the volume fraction of the dilute phase (determined by the lever rule) will be much higher.

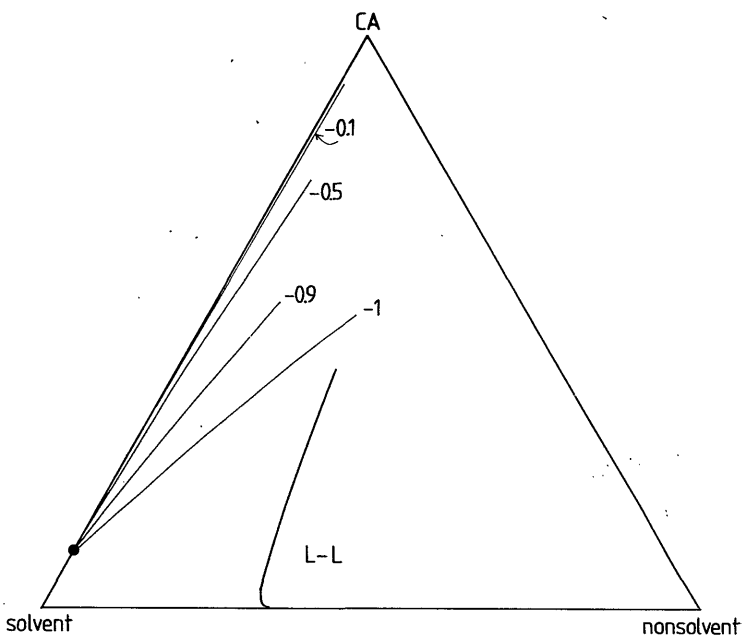


FIG.5. Composition paths for various values of $\sigma$ in the system P/S/NS with parameter values: $\chi_{12}=1, \chi_{13}=1.5$, $\chi_{23}=0, s=0.2$ and $r=0.002$. Binodal for liquid-liquid phase separation calculated with the method described in Chapter 5.

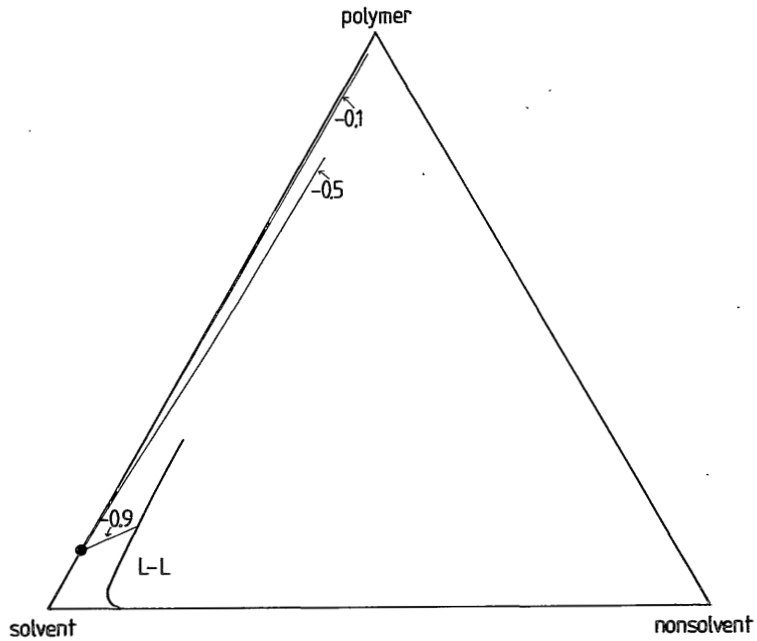


FIG.6. Composition paths for various of σ in the system P/S/NS with parameter values: $\chi_{12}=0, \chi_{13}=1.5$, $\chi_{23}=0$, s=0.2 and r=0.002. Binodal for liquid-liquid phase separation calculated with the method described in Chapter 5.

Time does not play an explicit role in the model. Kinetic factors are of course important. But in order to calculate actual concentration profiles and the penetration of the coagulation front as a function of time, specific knowledge of the diffusion coefficients is required.

The assumption that the ratio of diffusion coefficients is one, must be tested for all systems considered. α may depend on the location in the ternary phase diagram.*) In this case the local composition path cannot be represented by one σ but by a path consisting of small elements each with their own σ.

The skin is probably formed in the following way: a large amount of solvent exchanges with a relatively small amount

*) An absolute value for α larger than 1 could, for instance, explain the much higher apparent diffusion coefficient for water in some systems.

of nonsolvent. Measurements in the first few seconds support this assumption (section 7.2.3: $\sigma \simeq 0.2$). The densification of the skin and the resulting obstruction for in-and outdiffusion depends on the gelation behaviour of CA in the respective solvent. This gelation probably occurs at low nonsolvent content (Figures 5 and 6). Again kinetic factors are expected to be of utmost importance. Unfortunately, little information is available on the kinetics of the phase transitions involved.

## 7.4 DIFFUSION AND PHASE SEPARATION COMBINED

Now we come back to the questions put forward in the introduction. We observe that:

- the porosity of the membrane depends on the choice of the solvent;
- an increase in the tendency of mixing of solvent and nonsolvent gives a more UF type of membrane (a high permeate flux and a vanishing rejection for NaCl).

### 7.4.1 Liquid-liquid phase separation

In Chapter 5 we have shown that the location of the miscibility gap is primarily determined by the value of the solvent/nonsolvent interaction parameter $\chi_{12}$. This is true for the solvents considered: DMSO, DMF, acetone and dioxane.

### 7.4.2 Gelation and crystallization

Gelation is discussed here in terms of local crystallization of the polymer. From our own work only for the CA/dioxane/water system experimental information on the crystallization has been obtained. Crystallization occurs at rather high polymer concentrations, but appears to be a slow process under the circumstances studied (Chapter 4). Introduction of water improves the conditions for crystallization.

For CA/acetone, information on the gelation behaviour has been given by Fahey[27] and Lemoyne.[28] Together with

visual observations on the appearance of cloudiness (Chapter 4) these data are given in Figure 7. We have not yet performed DSC experiments on CA/acetone/water systems to see if the transition is accompanied by heat effects.

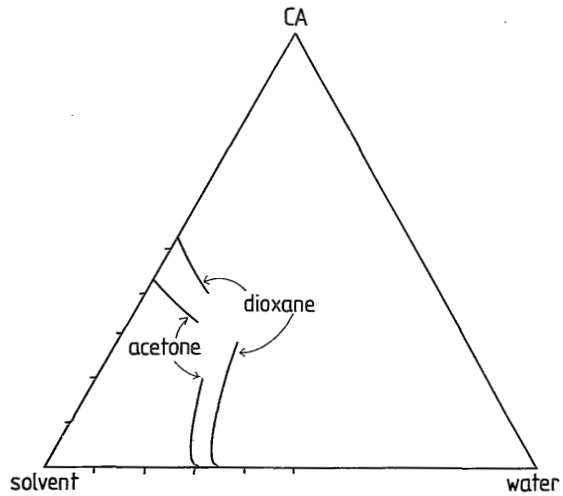


FIG.7. Gelation and liquid-liquid phase separation transitions in CA/acetone/water and CA/dioxane/water. Binodal curves (curves on the right) are taken from Chapter 5.

Preliminary experiments in our laboratory[29] on the appearance of turbidity as a function of composition with the PICS technique (see Appendix Chapter 3) do indeed indicate that systems with acetone as the solvent show gelation behaviour at a lower polymer concentration than the dioxane based systems.

Application of the Flory melting point depression equation (see Chapter 4) shows that one might expect crystallization of CA in acetone at a lower polymer concentration than in dioxane because of the higher polymer/solvent interaction parameter. This parameter affects one term in the melting point equation, the chemical potential of the polymer in the liquid phase.

Another important factor to be considered is the ability of CA to crystallize. This affects the lowering of the

chemical potential in the (solvent free?) solid state. Recently Kamide et al.[30] demonstrated that the equilibrium chain stiffness of CA depends very much on the solvent. The chain becomes stiffer when one goes from THF via acetone to DMAc as the solvent. The general view[31] is that the chain inflexibility of cellulose derivatives is an important factor causing the CA molecules to crystallize. Recently Navard et al.[32] found that CA also crystallizes in trifluoroacetic acid.

### 7.4.3 Diffusion

Toplayer

The thickness of the skin is determined by the thickness of the gellayer during precipitation. This layer will become thicker[33]: (i) when the concentration for gelation is lower and/or (ii) when the liquid-liquid phase separation curve is shifted to higher water concentrations. It then takes more time before the liquid-liquid phase separation process can compete against gelation.

For solvents such as DMSO and DMF the amount of water required for liquid-liquid phase separation is relatively small (see Table 6) compared with the amount needed for CA in dioxane or acetone. We expect that in the systems first mentioned liquid-liquid phase separation will take over rapidly. A thin gelled layer results. The structure of this layer, the retarding influence on solvent and nonsolvent diffusion, and the degree of porosity of the (UF type of) resulting membrane depends on yet unknown factors such as the location of the sol/gel transitions in DMSO and DMF systems, on the amount of nonsolvent present during gelation and the kinetics of the gelation process. A thin gelled layer is expected to be a small barrier for transport of nonsolvent into the precipitating film (see Table 3, which can also be used for nonsolvent indiffusion, and Table 6).

Sublayer

From the diffusion model (section 7.3) we have seen that a low degree of porosity in the resulting membrane is possibly due to the fact that at all locations in the film the binodal composition is reached at high polymer concentration. This latter fact means that a) there is a limited possibility for growth of nuclei and b) conditions for gelation of the concentrated phase around the droplets of the dilute phase are favoured. Obviously no interconnected pore structure in the sublayer is formed with solvents such as acetone of THF.

A high degree of porosity is found if the local composition path reaches the binodal at low polymer concentration. Apparently this happens for solvents such as DMSO, DMF, acetic acid, dioxane and TEP.

Dense or porous sublayer

The amount of water needed for liquid-liquid phase separation is large in solutions with dioxane or acetone as the solvent. A rather thick skin is expected for membranes cast from casting solutions with dioxane or acetone as basic solvent. The phase separation behaviour of CA in acetone and dioxane is considered to be very similar: (i) the interaction parameters are about the same, (ii) consequently the location of the liquid-liquid phase separation gap is about the same in the ternary diagram, and (iii) the composition path predicted is similar. But how can we explain the low degree of porosity of the sublayer in the membrane formed from the acetone solution? In our opinion in sufficient information is available at this moment.

The diffusion of nonsolvent is smaller for CA/acetone/water. This means that the upper precipitated layer of the polymer solution discriminates to some extent between the solvent and nonsolvent transport. From the experiments of Frommer[1] it seems that the solvent flow is not hindered (more precise measurements are needed to establish this latter observation more firmly).

A dense polymeric structure may be necessary to perform this test on selective solvent/nonsolvent transport. The local polymer concentration and the distribution of polymer in amorphous and crystalline regions are important with respect to diffusion. A dense layer in the acetone system can be formed in several ways different from the densification in the dioxane based system:

a) Evaporation may rapidly produce a dense toplayer. This toplayer is supposed to be much permeable for acetone than for water. The sublayer subsequently loses much solvent and relatively little nonsolvent enters the precipitating film. Crystallization occurs at high polymer concentration without much nonsolvent present;

b) The local polymer concentration necessary for gelation is low (in accordance with observations). An initially not very dense skin is formed in the presence of water. In a syneresis process the remaining solvent is expelled and a dense layer results which may or may not be more permeable to acetone.

Evaporation, case (a) is obviously an important factor if we use acetone (or THF, propylene oxide) as the solvent. In that case a densification occurs without presence of water. Possibly this layer has a better permeability for acetone or a lower permeability for water than a dense toplayer formed in the presence of water (case (b)). This proposed difference in permeability should be tested with experiments.

## 7.5 CONCLUSIONS

The nascent skin during membrane formation is not found to be a substantial barrier for solvent diffusion out of the precipitating polymer film.

The local composition change in the precipitating film can, in part, be regulated by the choice of the solvent. The location of the path in the ternary diagram for the upper layer of the solution is not affected by the solvent/nonsol-

vent interaction parameter; the ratio of nonsolvent and solvent fluxes is expected to have the same small value in the initial stage of membrane formation. The magnitudes of the fluxes, however, may be affected by the solvent chosen, and are likely to influence the kinetics of the gelation process. At a later stage when by the retarding influence of the skin the nonsolvent and the solvent flow are of comparable size, the composition change depends very much on the solvent/nonsolvent interaction parameter. A high tendency of mixing (a low $\chi_{12}$ parameter) gives a predicted path which reaches the binodal at a much smaller polymer concentration than at high $\chi_{12}$. The growth possibilities of the nuclei for the porous substructure are consequently favoured.

During the process of membrane formation a more or less dense skin is formed. Comparison between membranes formed from a CA solution in acetone or dioxane shows that the initially formed skin in the acetone based system discriminates between solvent and nonsolvent flow: the nonsolvent flow is much smaller than in the dioxane based system. At present it is not clear whether differences in gelation behaviour between the two systems are responsible for this phenomenon.

## 7.6 REFERENCES


1. M.A.Frommer and D.Lancet, in Reverse Osmosis Membrane Research, H.K.Lonsdale and H.E.Podall, Eds.,Plenum,New York, 1972, p.85
2. M.T.So, F.R.Eirich, H.Strathmann, and R.W.Baker, J.Polym. Sci.Polym.Lett., 11,201(1973)
3. J.Matous, A.Zivny, and J.Biros, Coll.Czech.Chem.Commun., 37,3960(1972)
4. R.V.Orye and J.M.Prausnitz, Ind.Eng.Chem., 57,18(1965)
5. G.Kortüm and V.Valent, Ber.Bunsen Ges.Phys.Chem., 81, 752,(1977)
6. J.T.Th.Gieskes, Can.J.Chem., 43,2448(1965)

7. H.Michalski, Polytechnika Lodezka Zest.Nauk., 12,73(1962)
8. S.Y.Lam and R.L.Benoit, Can.J.Chem., 52,718(1974)
9. A.S.Kertes and L.Tsimering, J.Phys.Chem., 81,120(1977)
10. R.Bloch and M.A.Frommer, Desalination, 7,259(1970)
11. H.K.Lonsdale, U.Merten, and R.L.Riley, J.Appl.Polym. Sci., 9,1341(1965)
12. G.Arneri, G.C.Richardson, and J.A.Sauer, Thermochim.Acta, 38,139(1980)
13. H.Strathmann, K.Kock, P.Amar and R.W.Baker, Desalination, 16,179(1975)
14. J.E.Anderson and R.Ullman, J.Appl.Phys., 44,2149(1974)
15. J.Smid, M.Sc.Thesis, Twente University of Technology,1981
16. A.Ziabicki, Fundamentals of Fibre Formation, Wiley, London, 1976, p.301
17. J.Crank, The Mathematics of Diffusion, Clarendon, Oxford, 1975, p.41,56
18. E.L.Cussler, Multicomponent Diffusion, Elsevier, Amsterdam, 1976, p.41,63
19. H.L.Toor, AIChE J., 10,448,460(1964)
20. S.J.Singer, J.Chem.Phys., 15,341(1947)
21. G.S.Park, Trans.Far.Soc., 57,2314(1961)
22. Landolt Bernstein, II Band, 5.Teil, Bandteil a, Springer, Berlin, 1969, p.642
23. F.W.Altena and C.A.Smolders, Chapter 3 of this thesis
24. C.Cohen, G.B.Tanny, and S.Prager, J.Polym.Sci.Polym.Phys. ed., 17,477(1979)
25. G.S.Hartley and J.Crank, Trans.Far.Soc., 45,801(1949)
26. P.J.Flory, Principles of Polymer Chemistry, Cornell UP, Ithaca, 1953, p.548
27. P.M.Fahey and H.E.Grethlein, Desalination, 9,297(1971)
28. C.Lemoyne, C.Friedrich, J.L.Halary, C.Noël, and L.Monnerie, J.Appl.Polym.Sci., 25,1883(1980)
29. to be published
30. K.Kamide, Y.Miyazaki, T.Abe, Polym.J., 11,523(1979),and K.Kamide, T.Terakawa, and Y,Miyazaki, Polym.J., 11,585, (1979)
31. P.J.Flory, Proc.Roy.Soc.London.ser A, 234,60(1956)

32. P.Navard, J.M.Haudin, S.Dayan, and P.Sixou, J.Polym.Sci., Polym.Lett., 19,379(1981)
33. R.Bokhorst, F.W.Altena, and C.A.Smolders, Lecture presented at the IDEA Congress Bahrain, Nov 30 - Dec 3 1981, to be published in Desalination

## 7.7 APPENDIX 1

DIFFUSION OF SOLVENT

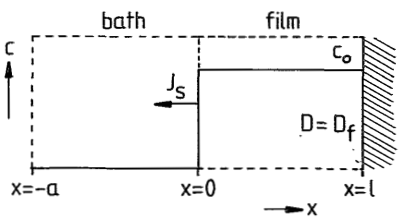


FIG.1. Diffusion of solvent from a sheet with constant diffusion coefficient $D_f$.

Diffusion equation: $\frac{\partial c}{\partial t} = D_f \frac{\partial^2 c}{\partial x^2}$ $0<x<1$

Initial condition: $c(x,0) = c_o$

Boundary condition: $a \frac{\partial c}{\partial t} = D_f \frac{\partial c}{\partial x}$ $x=0,\ t>0$

For short times[17]:

$$\frac{M_t}{M_\infty} = 1 - \sum_{n=1}^{\infty} \frac{2\alpha(1+\alpha)}{1+\alpha+\alpha^2 q_n^2} \exp(-D_f q_n^2 t/l^2)$$

Where $M_t$ and $M_\infty$ are the amounts of solvent in the bath at

time = t and at equilibrium ($t\to\infty$) resp., and $q_n$ are the roots of

$$\tan q_n = - \alpha q_n$$

where $\alpha = a/l$ i.e. the ratio of volumes of bath and polymer solution and l is the film thickness. The number of terms needed in the summation is about 50.

From the mass balance:

$$M_\infty = \frac{l c_o}{1+1/\alpha}$$

Experimental situation: $V_{polym.sol.} = 25 cm^3$, $V_{bath} = 375\ cm^3$,

$l = 0.5$ cm, $\alpha = 15$, so $M_\infty = 0.05$ for $c_o = 0.8$ (weight fraction solvent in solution).

## 7.8 APPENDIX 2

## DIFFUSION OF SOLVENT THROUGH A SKINNED MEMBRANE

The solution of the problem has been given by Crank.[17]

$$\frac{M_t}{(\Delta x)c_o} = 2\left(\frac{D_{sk}t}{\pi(\Delta x)^2}\right)^{\frac{1}{2}} \{1+2\sum_{n=1}^{\infty}\beta^n \exp(-n^2(\Delta x)^2/D_{sk}t)\}$$

$$-4\sum_{n=1}^{\infty} n\beta^n \operatorname{erfc}(n\Delta x/\sqrt{D_{sk}t})$$

with $\beta = (1-k)/(1+k)$

$k = (D_{sk}/D_f)^{\frac{1}{2}}$

The initial conditions are: $c(x,0) = c_o$ for $-l < x < \infty$

$c(x,0) = 0$ for $x < -l$

$M_t$ is the total amount of solvent leaving the medium through unit area of the surface at $x = -l$.

PENETRATION OF NONSOLVENT

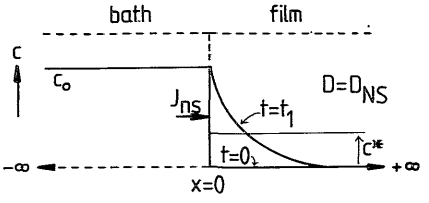


FIG.1. Diffusion of nonsolvent in a sheet with constant diffusion coefficient $D_{NS}$.

Diffusion equation : $\frac{\partial c}{\partial t} = D_{NS} \frac{\partial^2 c}{\partial x^2}$ $\quad t>0;\ x>0$

Initial condition: $c(x,0) = 0 \quad x>0$

Boundary condition: $c(x,t) = c_o = 1 \quad x<0;\ t>0$

The solution is: $c(x,t) = 1-\mathrm{erf}\left(\frac{x}{2\sqrt{D_{NS}t}}\right)$

At $t=t^*$: $c(x,t^*)=c^*$, which is known from the liquid-liquid phase diagram. $c^*$ is the water content at phase separation. The total amount taken up by the film in time t is:

$$M_t = 2(D_{NS}t/\pi)^{\frac{1}{2}}c_o$$

Another approximation has been given by Strathmann[13]: Suppose the precipitation front is at $x^*$ at time $t=t^*$. The nonsolvent flux can be approximated by:

$$J_{NS} = \frac{D_{NS}(1-c^*)\varepsilon}{x^*\tau}$$

$\varepsilon/\tau$ is a geometric factor to correct for the porosity and the totuosity of the precipitated polymer layer. For $\varepsilon>50\%$: $\tau\simeq 2$. The rate of penetration of the coagulation front is proportional to $J_{NS}$:

$$J_{NS} = \left(\frac{1-c^*}{2} + c^*\right)\frac{dx^*}{dt}$$

Combining the above equations leads to:

$$(x^*)^2 = \frac{4D_{NS}\varepsilon(1-c^*)}{\tau(1+c^*)}t$$

# APPENDIX

## APPLICABILITY OF GAS PERMEATION METHODS TO CHARACTERIZE ULTRAFILTRATION OR REVERSE OSMOSIS MEMBRANES.*)

F.W.ALTENA, H.A.M.KNOEF, H.HESKAMP, D.BARGEMAN and C.A.SMOLDERS
Department of Chemical Technology, Twente University of Technology, Enschede, The Netherlands.

SYNOPSIS

The measurement of the gas permeability coefficient as a function of the mean pressure across the membrane can be used to determine a mean pore radius of the membrane. Experiments are performed in the pore size region where both viscous flow and slip flow contribute to the gas flux. This method has been applied by several authors to characterize asymmetric ultrafiltration or hyperfiltration membranes. In this Appendix this method is criticized on two grounds. In the first place, accurate measurements show an unexpected dependence of the mean pore radius of microporous membranes on the type of gas used. Secondly, in the pore size region where ultrafiltration or hyperfiltration membranes have their expected pore radius, the viscous flow contribution to the permeability coefficient cannot be determined with sufficient accuracy. This means that the above-mentioned method cannot be used to determine a mean pore radius.

*) Submitted for publication to Journal of Membranes Science.

## INTRODUCTION

The measurement of the flow rate of a gas through a porous medium can provide a means to determine a mean pore radius of the porous material. In recent years several authors[2-4] have used the method suggested by Yasuda[1] to characterize ultrafiltration or hyperfiltration (reverse osmosis) membranes. The flow rate of the gas can be converted to a gas permeability coefficient, which is a linear function of the mean pressure across the membrane. A mean pore radius is calculated from the coefficients of this functional dependence, using theoretical equations originally given by Carman.[5]

We have several objections against the use of this method. The first objection is that Yasuda's method does not result in an unequivocal pore radius. We have tried to reproduce some of Yasuda's experiments on a Millipore filter with a nominal pore radius of 50 nm. We have found that the pore radius determined depends on the type of gas used. With helium the value found for the pore radius is consistently about half the value obtained with nitrogen or carbon dioxide. Yasuda[1] however obtains approximately the same values for all gases. This discrepancy is, as will be shown in this Appendix, not due to lack of accuracy of the measurements, but is probably caused by the incorrect use of theoretical equations.

The second objection to the use of the method is that only relatively large pores contribute to the convective flow of the gas. The authors who made use of the method of Yasuda did not obtain pore radii below 25 nm.[1-4] For standard ultrafiltration membranes of polysulfone[3] this value is in our opinion not realistic.

Kakuta et al[4] have calculated even smaller values for reverse osmosis membranes of cellulose acetate. A surprisingly low value of the pore radius has been given, viz. 1.5-2 nm. We calculated from their experimental plot of the permeability coefficient versus the mean pressure a pore ra-

dius of about 8 nm (nitrogen). Furthermore their measurements for helium do not seem to be very accurate: a much smaller value for the pore radius would also fit the experimental data for helium.

In this Appendix we describe the experiments which we have performed. We used the same theoretical relations as Yasuda.[1] The calculation of the pore radius from the experimental data has been improved. One of the main conclusions is that insufficient accuracy of the measurement of the pressure decay across the membrane prevents an accurate determination of the pore radius if the pore radius is of the order of 10 nm or smaller. Lowering the pore radius results in a relatively smaller convective contribution to the permeability coefficient. Flow in pores with radii below 10 nm diameter is usually of the Knudsen (non-viscous) type. In this region a pore radius can not be determined with Yasuda's method.

## THEORETICAL CONSIDERATIONS

For the flow of gas through a porous structure Darcy's law takes the following form:[5,6]

$$v_2 = \frac{B_o \bar{p} \Delta p}{\eta p_2 l} \qquad (1)$$

where $v_2$ is the flow velocity of the gas at (outlet) pressure $p_2$, and $\Delta p = p_1 - p_2$ is the pressure difference across the membrane, $\bar{p} = \frac{1}{2}(p_1+p_2)$ is the mean pressure, $B_o$ is the specific permeability coefficient, $\eta$ is the viscosity and $l$ is the thickness of the membrane. For the gas flux through the membrane we can write, if we combine constant factors:

$$J = K\frac{\Delta p}{l} \qquad (2)$$

where K is the permeability coefficient. If the mean pore diameter is comparable in size to the mean free path

(0.01-0.1 μm at room temperature and at atmospheric pressure) K contains another (non-viscous) term. This effect is due to the so-called slip effect, and can be included in K:

$$K = K_o + \frac{B_o}{\eta} \bar{p} \tag{3}$$

$K_o$ and $B_o$ are characteristic of the porous medium and the gas.

The gas flux is measured by the pressure decay in a gas ballast chamber of fixed volume $V_o$ connected to the membrane test cell. Following Yasuda:[1]

$$J = \frac{d(pV)}{dt} = -V_o \frac{d(\Delta p)}{dt} \tag{4}$$

Combining (2), (3) and (4) gives, after deleting constant factors (see below):

$$- \frac{d(\Delta p)}{dt} = (K_o + \frac{B_o}{\eta} \bar{p}) \Delta p \tag{5}$$

with $\bar{p} = \frac{1}{2}(p_1+p_2) = \frac{1}{2}(\Delta p+2p_2)$, where in our case $p_2$ is the atmospheric pressure. Equation (5) becomes:

$$- \frac{d(\Delta p)}{dt} = (K_o + \frac{B_o}{\eta} p_2) \Delta p + \frac{B_o}{2\eta} (\Delta p)^2 \tag{6}$$

The flux equations has been rewritten in a differential equation for the pressure difference across the membrane. For simplicity we write $p = \Delta p$, $a = K_o + \frac{B_o}{\eta} p_2$ and $b = \frac{B_o}{2\eta}$.

Equation (6) becomes:

$$- \frac{dp}{dt} = ap + bp^2 \tag{7}$$

In the foregoing constant terms have been omitted because only the ratio of a and b defines the pore radius to be calculated (see equation (12)).

Yasuda[1], Shimizu[2], Cabasso[3] and Kakuta[4] all follow Carman[5] by putting:

$$B_o = \frac{\varepsilon m^2}{k_o q^2} \tag{8}$$

$$K_o = \frac{4\varepsilon\delta m}{3k_1 q^2}\,\bar{v} \tag{9}$$

where m is the equivalent pore radius, $\varepsilon$ is the porosity, $q^2$ the tortuosityfactor and $k_o$ and $\delta/k_1$ are assumed to be constants(Carman[5] suggested the values of $k_o = 2.5$ and $\delta/k_1 = 0.8$). $\bar{v}$ is the average molecular velocity of the gas with molecular weight M:

$$\bar{v} = \left(\frac{8RT}{\pi M}\right)^{\frac{1}{2}} \tag{10}$$

Combining (8), (9) and (10) gives:

$$m = \left(\frac{B_o}{K_o}\right) \frac{16}{3} \left(\frac{2RT}{\pi M}\right)^{\frac{1}{2}} \tag{11}$$

or when using a and b defined by (7):

$$m = \left(\frac{2\eta b}{a - 2b\, p_{atm}}\right) \frac{16}{3} \left(\frac{2RT}{\pi M}\right)^{\frac{1}{2}} \tag{12}$$

This is the desired pore radius to be calculated from the experiments.

## EVALUATION OF EXPERIMENTAL DATA

In the experiments the pressure decay p = p(t) is measured. Yasuda[1] determines dp/dt from this decay recorded on a strip chart recorder. $K_o$ and $B_o$ can be determined from

equation (5) using the slope and intercept and from equation (11) m can then be calculated.

We have taken a different approach by rewriting equation (7) and intergrating from chosen points of $p = p(t)$, viz. $p_o$ at $t = t_o$ and $p_e$ at $t = t_e$:

$$\int_{p_o}^{p_e} \frac{dp}{ap + bp^2} = -\int_{t_o}^{t_e} dt \qquad (13)$$

It follows:

$$\frac{1}{a}\left[\ln\left(\frac{a+bp_e}{p_e}\right) - \ln\left(\frac{a+bp_o}{p_o}\right)\right] = t_e - t_o \qquad (14)$$

In principle we only need two points $(t_e, p_e)$ at fixed $(t_o, p_o)$ of the pressure decay to solve a and b from nonlineair equations of the type(14). We prefer this method of data analysis to the one used by Yasuda because the pressure itself can be determined more accurately than dp/dt.

In practise it is better to take more points $(t_e(i), p_e(i), i = 2,..n)$ and to evaluate at least 10 (n>10) equations (14) to calculate a and b. This is done by a numerical procedure using a non-linear least squares algorithm which solves n equations simultaneously. The choice of the points on the pressure decay curve could be a source of inaccuracy. We have tried two procedures:

- a fixed $(t_o,p_o)$ is chosen, (0 seconds, 3.5 bar), and n points $(t_e,p_e)$ on the curve are equally spaced in time; n equations(14) are solved for each $(t_e,p_e)$-$(t_o,p_o)$ pair.
- In the second procedure the point $(t_o,p_o)$ is varied; n points are chosen on the pressure decay curve, and equation (14) is solved with pairs $(t_2,p_2)$, $(t_{n/2+1},p_{n/2+1})$ and $(t_2,p_2)$, $(t_{n/2+2},p_{n/2+2})$ etc. (n even>4).

These two procedures do not give different results.

When a and b have been calculated the experimental p = p(t) curve is compared with the calculated one. From equation (14) it follows:

$$p = \frac{a}{\exp\{-a(t_o - t) + C\} - b} \tag{15}$$

$$\text{with } C = \ln\left(\frac{a}{p_o} + b\right) \tag{16}$$

## REQUIRED ACCURACY OF PRESSURE MEASUREMENTS

In the experiments the pressure difference across the membrane p decreases from $p_o$ (about 3.5 bar) to zero. As will be seen below, $b \ll a$. Thus, when p is small, dp/dt is mainly determined by a and a high precision of b cannot be expected (see equation (7)).

In the case of Millipore VM type membranes the following approximate values of a and b have been found (see section results): Helium: a=0.2, b=0.002; Nitrogen: a=0.1, b=0.01. From (7) we see that a relative error $\Delta p/p$ of 0.01 gives a relative error in b and consequently in m (cf. (12)) of $\Delta b/b$ of 0.1 for nitrogen and 0.5 for helium (at p=1 bar; dp/dt held constant). A precise determination of b (or m) can only be expected when $\Delta p/p = 0.0001$. In this case the respective relative errors are 0.01 ($N_2$) and 0.05 (He). We conclude that a very precise measurement of p, the pressure difference across the membrane, is required. Yasuda[1] derives values for the pressure gradient from a strip chart recorder. The reading error thus introduced is of the order of 0.01. No precise determination can be expected. An absolute precision of about 0.003 bar is required to obtain m with sufficient accuracy.

EXPERIMENTAL

The experimental set-up is shown in Figure 1. The pressure decay in the reservoir (0.01 $m^3$) is measured by the pressure transducer (Viatran 304, 0-150 PSIA, 3000 μV FSO). The ballast chamber is pressurized to a pressure of about 5 bar. The valve between gascylinder and ballast chamber is closed, the ball-valve between the ballast chamber and the cell with the membrane is opened and the pressure decay is recorded. In order to avoid an initial transient stage of pressure decay, the chamber is pressurized to a pressure 50% higher than the pressure (3.5 bar) needed in the measurement.[1] The gas is allowed to flow through the membrane before the reading of the pressure is taken. We have used a Millipore filter holder XX 4502500.

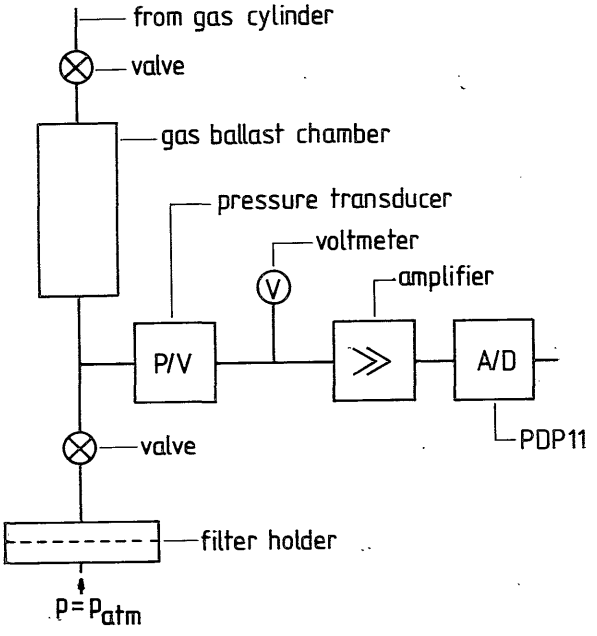


FIG.1. Experimental set-up for gas permeation experiment.

The pressure transducer is coupled on line to the A/D converter of a PDP 11 minicomputer. Amplification of the signal of the pressure transducer was necessary (Tektronix

AM 502,200x). The data of the minicomputer were handled off-line to calculate the equivalent pore radius. Calibration of the A/D readings versus the signal of the pressure transducer (digital voltmeter, HP 3465 A) was performed. The uncertainty in the static pressure measurement appeared to be ± 0.003 bar. The initial pressure decay is about 0.01 bar/s. The A/D converter averages 16 samples of the pressure signal (total time 8 msec), and gives no extra contribution to the uncertainty.

The absolute pressure reading of the pressure transducer is calibrated with an Industrial Air Dead Weight Tester of Barnet, type 3320 (10-1000 PSI), which has a sensitivity of $3.10^{-3}$ bar. The deviation of linearity of the pressure transducer is about this value and well within the specifications of the manufacturer.

The experiments were performed in a thermostated room at T = 20°C. The atmospheric pressure is read from a Lambrecht mercury column manometer, reading error ± $2.10^{-4}$ bar.

## RESULTS AND DISCUSSION

We have performed experiments on a Millipore type VM membrane. This membrane has a nominal pore radius of 50 nm, given by the manufacturer.

Using the procedure described in the section on evaluation of experimental data we calculated values for a and b from the pressure decay curve from 20 or 40 equations of the type (14). We have used three gases: helium, nitrogen and carbon dioxide. The pressure readings were taken at intervals of 0.5 minute, during 20 minutes. The calculated values for a, b and the resulting pore radius m are given in table 1.

| | a | b | m(nm) |
|---|---|---|---|
| helium | 0.237 ± 0.003 | 0.0029 ± 0.001 | 15 ± 5 |
| nitrogen | 0.108 ± 0.002 | 0.0084 ± 0.0007 | 40 ± 4 |
| carbon dioxide | 0.094 ± 0.005 | 0.010 ± 0.001 | 38 ± 4 |

Table 1: Pore radius of a Millipore VM membrane.

The given inaccuracy has been estimated by choosing a and b values such that $F < 5.10^{-4}$, where $F = \sum_{n}^{40} (p_{calc}(t_n)-p_{exp}(t_n))^2$. We have used equations (15) and (16) to determine $p_{calc}(t_n)$. This value of F means that the difference $|p_{calc}(t_n)-p_{exp}(t_n)|$ for each point is about $3.10^{-3}$ bar, the uncertainty in the pressure measurement.

When we started our experiments we considered Yasuda's method a useful tool to characterize porous membranes. Determination of dp/dt from the pressure decay curve seemed to us rather inaccurate. This problem could be circumvented by solving a set of non-linear equations in which the pressure appears itself instead of the derivative. After solving this problem it became evident that very accurate pressure measurements were needed to obtain sufficient accuracy in the equivalent pore radius. Above we have given the results of sufficiently accurate measurements.

Application of the method of Yasuda to characterize porous membranes now appears in our opinion of very limited value because of two major problems. From our experiments we find a much smaller pore radius for helium (15 nm) than for nitrogen or carbon dioxide (about 40 nm). This difference cannot be due to lack of accuracy of the measurements. To obtain a pore radius for helium of about 40 nm one would have to allow for a systematic error in the pressure measurement of as large as 0.03 bar. The expected accuracy is about 10 times better.

Secondly, in using the equations of Carman[5] we assume

that both terms of the permeability coefficient, the viscous flow and the slip contribution, are present. Considering the mean free path of the three gases used (He:270 ; $N_2$:90 and $CO_2$:160 nm at 1 bar and 20°C[7]), we see that the pore diameter is of the order of the mean free path. If there should be a larger number of pores of a much smaller diameter the situation would be different. These pores contribute much less to the viscous flow through the membrane but might contribute a relative higher amount to the non-viscous flow. As we know, the permeability coefficient should be a linear function of the mean pressure. For many porous media K passes through a minimum at small values of $\bar{p}$, when the region of Knudsen flow is reached.[6] This region is reached sooner for helium because of the larger mean free path. The same reasoning applies to K as a function of the pore radius. Therefore, if a large number of small pores is present, then there is a large contribution of these to the non-viscous term of the permeability coefficient, and an apparently smaller pore radius will be found. In this way a complex averaging over the pore size distribution occurs in the gas permeation experiment.

Another reason for the discrepancy of the results could be the fact that the theoretical equations are incorrect, a problem already touched upon by Carman himself.[5] We have no intention to deal with this issue here.

Extending our studies to the pore size region where toplayers of ultrafiltration or even hyperfiltration membranes have their expected pore size, adds another problem. That is: to determine the convective term of the permeability coefficient with sufficient accuracy. Some simple calculations using equation (15) show that we cannot discriminate between pore radii of 2 and 4 nm: as far as the accuracy of the pressure measurement is concerned the convective contribution could be equally well absent. Application of Yasuda's method to determine a pore radius means that an averaging takes place over the relatively large pores. A similar discrepancy as we have seen with the Millipore mem-

branes can be seen from the plots of the permeability coefficient against the mean pressure of Kakuta.[4] A smaller value for helium than for nitrogen might also fit the inaccurate data.

## CONCLUSION

The gaspermeation method as described by Yasuda is inadequate to determine pore radii in microporous or asymmetric ultrafiltration and reverse osmosis membranes.

## AKNOWLEDGEMENT

The authors are grateful to Dr. M. Bos for his help with the on-line pressure measurements.

## REFERENCES

1. H.Yasuda and J.T.Tsai, J.Appl.Polym.Sci., 18,805(1974)
2. Y.Shimizu, H.Akabane, A.Tanioka, K.Miyasaka, and K.Ishikawa, J.Polym.Sci., Polym.Phys.Ed., 17,1495(1979)
3. I.Cabasso, K.Q.Robert, E.Klein and J.K.Smith, J.Appl. Polym.Sci., 21,1883(1979)
4. A.Kakuta, M.Kuramoto, M.Ohno, H.Kushida, A.Tanioka and K.Ishikawa, J.Polym.Sci.Polym.Chem.Ed., 18,3229(1980)
5. P.C.Carman, Flow of gases through porous media, Butterworths, London, 1956, p.2 and 77
6. F.A.L.Dullien, Porous media Fluid transport and Pore Structure, Academic Press, New York, 1979, p.81 and 202
7. Handbook of Chemistry and Physics, table F, CRC Press, Cleveland, 1977

## SUMMARY

In this thesis the relationship between the formation process of asymmetric membranes and phase separation phenomena in polymer solutions is investigated.

Chapter 1 is a general introduction on membrane formation and related problems. A good characterization of the skin of an asymmetric membrane in terms of its thickness and structure and knowledge of the relation of these properties with transport behaviour is desired but not yet available. Most of the work presented in this thesis is performed on the study of the phase separation behaviour of cellulose acetate (CA) solutions. In many commercial membrane filtration installations CA membranes are used. However, improvement of CA membranes is still desirable. Knowledge of the formation mechanism of asymmetric membranes may provide guidelines along which future improvements can be achieved. Some views on membrane formation published in the literature are briefly mentioned. A controversial point is the necessity of an evaporation step in the asymmetric membrane preparation process.

In Chapter 2 a general description of asymmetric membrane formation is given based on theoretical and experimental knowledge of phase separation in concentrated polymer solutions. Gelation and liquid-liquid phase separation are responsible for the formation of the dense skinlayer and the porous supporting layer, respectively. The description is thought to be applicable to several ultrafiltration and reverse osmosis membrane materials: cellulose acetate, polyacrylonitrile, polyphenyleneoxide and polysulfone. The formation of macrovoids in the sublayer receives special attention.

In Chapter 3 the nature and the kinetics of phase changes in a specific polymer/solvent/nonsolvent ternary system, viz. CA/dioxane/water, are investigated. The techniques used were turbidimetry (cloud points), Differential Scanning Ca-

lorimetry and Pulse Induced Critical Scattering. Liquid-liquid phase separation occurs at low to medium polymer concentration and high nonsolvent content, whereas gelation occurs at high polymer concentration and low nonsolvent content.

In Chapter 4 DSC measurements on gelation are extended. Gelation is discussed in terms of local crystallization. The melting points of the gels as a function of the composition of the ternary system can be described by the Flory melting point depression equation for a polymer in a mixed solvent/nonsolvent. Kinetic effects are discussed.

In Chapter 5 a numerical method to calculate the binodal in a ternary system of a polymer in a solvent/nonsolvent mixture is presented. The Flory-Huggins theory for three components is applied to the membrane forming polymers: cellulose acetate and polysulfone. Concentration dependent solvent/nonsolvent interaction parameters are taken into account. It is shown that, when the solvent is varied, the value of the solvent/nonsolvent interaction parameter primarily determines the location of the miscibility gap in cellulose acetate systems. For polysulfone the large polymer/nonsolvent interaction parameter overwhelms the influence of the other interaction parameters.

The knowledge of interaction parameters is rather poor. With osmometric measurements, described in Chapter 6, the osmotic pressure and the preferential sorption can be determined in moderately concentrated CA solutions of up to 10% polymer. Binary polymer/solvent and ternary interaction parameters are calculated from the experimental quantities using the Flory-Huggins equations. As known variables we take the polymer/solvent parameter (determined from separate experiments) and the solvent/nonsolvent parameter (taken from the literature). With the calculated interaction parameters the composition at liquid-liquid phase separation can be predicted, but this is not yet in accordance with experimental information.

In Chapter 7 some aspects of diffusion during membrane

formation are studied. Measurements of outdiffusion of solvent indicate that the nascent skin is not a substantial barrier for solvent transport. Separate diffusion coefficient measurements in ternary CA/solvent/water systems are performed. The local composition in the precipitating film can be related in a model description to the gradients of the chemical potentials of nonsolvent in the film. The ratio of nonsolvent and solvent fluxes determines the direction of the composition path in the ternary diagram. The differences in the phase separation behaviour of membrane forming systems with acetone and dioxane as the solvents are discussed. In the precipitating film from the acetone solution the nascent skin apparently discriminates between nonsolvent and solvent flow. The nonsolvent flux is much smaller than with dioxane as the solvent.

Finally, in an Appendix a gaspermeation method published in the literature is critically evaluated. It is shown that the method cannot be applied to determine a mean pore radius of ultrafiltration or reverse osmosis membranes.

## SAMENVATTING

In dit proefschrift wordt het verband tussen het vormingsproces van asymmetrische membranen en fasescheidings verschijnselen in polymeeroplossingen onderzocht.

Hoofdstuk 1 vormt een algemene inleiding tot het onderwerp. Een factor van belang is dat de precieze struktuur en de dikte van de toplaag en het verband tussen deze eigenschappen en het transport gedrag van het vervaardigde membraan nog nader vastgesteld dienen te worden. Het experimentele werk in dit proefschrift is geconcentreerd op de bestudering van ontmengprocessen in cellulose acetaat oplossingen. Cellulose acetaat (CA) membranen worden veel gebruikt in commerciële membraan filtratie installaties. Verbetering van de membranen is echter gewenst. Kennis van het vormingsmechanisme van asymmetrische membranen kan ons een richtsnoer verschaffen waarlangs verbeteringen in de toekomst bereikt kunnen worden. Enkele benaderingen die in de literatuur gegeven zijn voor de membraanvorming worden aangestipt. Een controversieel punt is de noodzaak van een verdampingsstap in het membraan vervaardigings procédé.

Een algemene beschrijving van de vorming van asymmetrische membranen wordt gegeven in Hoofdstuk 2. Zij is gebaseerd op theoretische en experimentele kennis van faseschеiding in geconcentreerde polymeer oplossingen. Gelering en vloeistof-vloeistof ontmenging zijn verantwoordelijk voor de vorming van respectievelijk de dichte toplaag en de poreuze ondersteunende laag. De beschrijving is toepasbaar op verscheidene polymeren waarvan ultrafiltratie en hyperfiltratie membranen vervaardigd worden: cellulose acetaat, polyacrylonitril, polyphenelyeneoxide and polysulfon. De vorming van peervormige holten in de onderlaag krijgt bijzondere aandacht.

In Hoofdstuk 3 worden de aard en de kinetiek van fasescheidingsprocessen in een bepaald polymeer/oplosmiddel/niet-

oplosmiddel systeem nl. CA/dioxaan/water onderzocht. De gebruikte technieken zijn troebelingspunt bepalingen,Differentiele Scanning Calorimetrie en Pulse Induced Critical Scattering.
Bij niet al te hoge polymeer concentratie en een hoog gehalte aan niet-oplosmiddel wordt vloeistof-vloeistof ontmenging waargenomen. Gelering treedt op bij hoge polymeerconcentratie en lage waterconcentratie in het systeem.

In Hoofdstuk 4 wordt gerapporteerd over de smeltpuntbepalingen met DSC aan gelen van CA in dioxaan/water mengsels. De gelering wordt toegeschreven aan kristallisatie op lokale schaal. Het blijkt mogelijk te zijn de afhankelijkheid van het smeltpunt van de polymeerconcentratie en de samenstelling van het oplosmiddel/niet-oplosmiddel mengsel te beschrijven met de theorie van Flory voor de smeltpuntsverlaging. Kinetische aspecten worden onderzocht.

In Hoofdstuk 5 is een numerieke methode beschreven voor de berekening van de binodaal in een ternair systeem polymeer/oplosmiddel/niet-oplosmiddel. Gebruik is gemaakt van de Flory-Huggins theorie voor drie componenten. Het ontmenggebied wordt berekend voor twee membraanmaterialen nl. cellulose acetaat en polysulfon. In de berekening wordt een concentratie afhankelijke oplosmiddel/niet-oplosmiddel interactieparameter meegenomen. De grootte van deze parameter bepaalt voornamelijk de plaats van het ontmenggebied in het systeem CA/oplosmiddel/water. In het systeem met polysulfon blijkt de grote waarde van de polymeer/niet-oplosmiddel parameter de invloed van verandering in de andere interactieparameters te overheersen.

Er is niet veel bekend over de grootte van de interactieparameters in systemen met drie componenten. Met behulp van osmometrie worden in Hoofdstuk 6 de osmotische druk en de preferentiele adsorptie bepaald van matig geconcentreerde CA oplossingen in mengsels van dioxaan en water. De polymeer/niet-oplosmiddel en de ternaire interactie parameters worden berekend uit de vergelijking van waarden van experimentele

grootheden en de voorspelling hiervan met de Flory-Huggins theorie. De oplosmiddel/niet-oplosmiddel parameter (uit de literatuur gegevens afgeleid) en de polymeer/oplosmiddel interactie parameter (uit een afzonderlijk experiment bepaald) worden bekend verondersteld. Met de berekende interactie parameters is getracht het ontmenggebied te voorspellen. Het gevonden gebied is niet in overeenstemming met experimentele gegevens uit Hoofdstuk 3.

In Hoofdstuk 7 wordt de diffusie van oplosmiddel en niet-oplosmiddel tijdens membraanvorming nader onderzocht. Metingen van de oplosmiddel diffusiestroom geven aan dat de huid in wording geen grote barrière vormt voor het oplosmiddel transport uit de precipiterende film. Diffusiecoefficienten in ternaire CA/oplosmiddel/water systemen zijn afzonderlijk bepaald. In een modelbeschrijving wordt de verandering van de plaatselijke samenstelling in de film in verband gebracht met de gradienten in de chemische potentialen van oplosmiddel en niet-oplosmiddel. Het quotient van de water- en oplosmiddelstroom bepaalt de richting van de verandering van de lokale samenstelling in het ternaire diagram. De verschillen in het faseschеidings gedrag van CA in oplosmiddelen acetone en dioxaan in relatie tot membraanvorming worden besproken. De waterstroom bij membraanvorming uit een CA oplossing in acetone blijkt veel kleiner te zijn dan bij een oplossing in dioxaan. De zich vormende huid van het membraan uit de CA/acetone oplossing gedraagt zich kennelijk selectief ten opzichte van oplosmiddel- en watertransport.

Tot slot wordt in een Appendix ingegaan op een gaspermeatie methode, gepubliceerd in de literatuur, waarmee een gemiddelde poriestraal van een membraan bepaald zou kunnen worden. Er wordt aangetoond dat de methode niet gebruikt kan worden voor ultrafiltratie en omgekeerde osmose membranen.

## LEVENSBESCHRIJVING

Franciscus Willibrordus Altena werd op 23 juli 1953 geboren te Bloemendaal. Hij behaalde in 1970 zijn HBS-B diploma aan het Pius X College te Almelo. In datzelfde jaar begon hij zijn studie in de Technische Natuurkunde aan de Technische Hogeschool Twente te Enschede.

De baccalaureaatsstudie werd in 1974 afgerond met als hoofdrichting Lage Temperaturen. In januari 1978 werd het doctoraalexamen Technische Natuurkunde afgelegd met als hoofdrichting Reologie bij de vakgroep Overdrachtsverschijnselen.

In december 1977 trad hij in dienst als wetenschappelijk assistent bij de vakgroep Macromoleculaire Chemie en Materiaalkunde van de afdeling Chemische Technologie van de T.H.Twente. In de periode tot 1 december 1981 is het onderzoek verricht dat in dit proefschrift beschreven is.

Vanaf 1 februari 1982 zal hij gedurende een jaar onderzoek verrichten naar het vervuilingsmechanisme van membranen bij het Rensselaer Polytechnic Institute, Troy, N.Y., U.S.A. Voor dit onderzoek is een beurs toegekend door de Nederlandse Organisatie voor Zuiver Wetenschappelijk Onderzoek (ZWO).

SPOOKBEELD VAN MEMBRAANTECHNOLOGEN

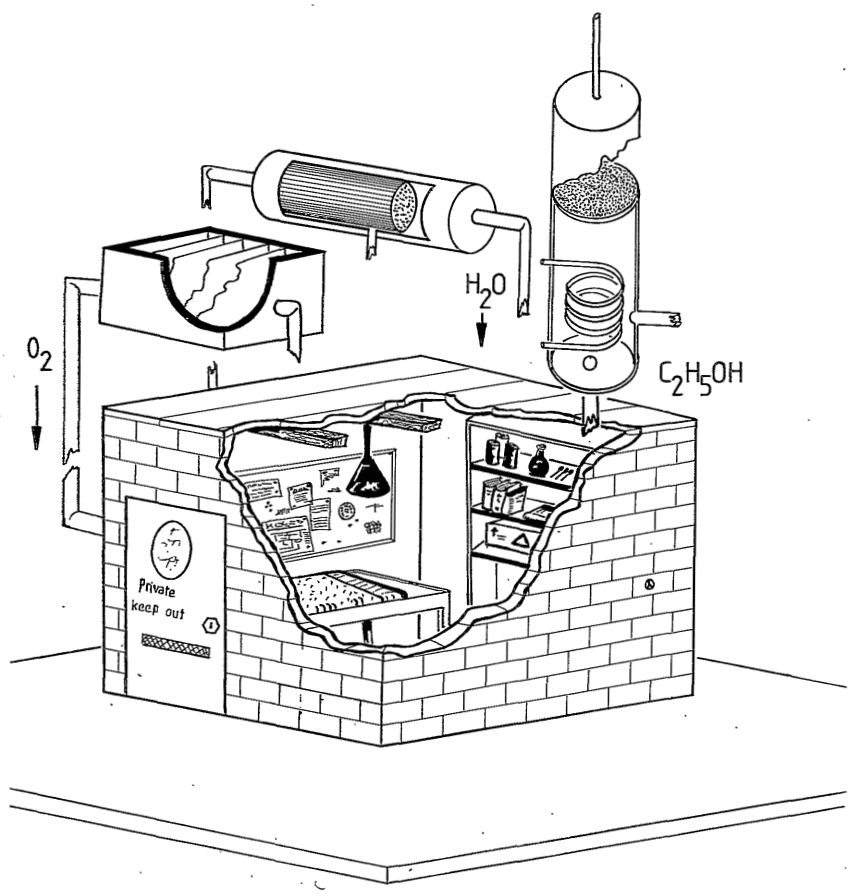


Atoomvrije schuilkelder: Hyperfiltratie, gasscheiding en pervaporatie.